Effects of deleterious opsin gene variants on cone photoreceptor structure, function, and viability

Scott H. Greenwald

A dissertation submitted in partial fulfillment
of the requirements for the degree of

Doctor of Philosophy

University of Washington

2013

Reading Committee:
Maureen Neitz, Chair
Greg Horwitz
Jay Neitz

Program Authorized to Offer Degree:
Neurobiology & Behavior

University of Washington

Abstract

Effects of deleterious opsin gene variants on cone photoreceptor structure, function, and viability

Scott H. Greenwald

Chair of the Supervisory Committee:
Maureen Neitz
Department of Ophthalmology

Specific L/M-opsin interchange variants have recently been linked to a variety of eye disorders that include diminished ERGs, color blindness, and pathologically high myopia. One disease-causing variant, designated LVAVA according to its defining amino acid sequence, has been linked to two distinct vision disorders. Males with LVAVA in one of the first two positions in the X-chromosome opsin gene array develop pathologically high myopia and have abnormal ERGs, while those with an LVAVA variant as their only X-chromosome opsin gene have extreme and uncorrectable vision loss. In this dissertation, retinal function was measured by ERG in two men with the latter, non-syndromic disease. While cones expressing the LVAVA opsin were physiologically compromised, residual function was maintained into adulthood. Furthermore, these cones disrupted the function of neighboring S cones that did not harbor the toxic variant. In order to directly test the relationship between the LVAVA variant and pathology, the non-syndromic disease was modeled in a targeted gene replacement mouse in which the endogenous *Opn1mw* gene was exchanged for an engineered *Opn1lw*$^{\mathrm{LVAVA}}$ gene. Because the presence of S-opsin in coexpressing mouse cones could interfere with the experiments, the *Opn1sw* genes were knocked out of both the LVAVA mice and the control mice

that expressed a functional human opsin (LIAIS). ERG and histological experiments demonstrated that the mouse model faithfully recapitulated functional and morphological retinal defects associated with the human disease. Another variant, referred to as LIAVA, completely and selectively disrupts the function of cones that express it. Retinal function was evaluated by ERG in a subject who was previously reported to express an LIAVA variant in all of his L/M cones. The human data were compared to ERG and retinal morphology data collected from an *Opn1lw*^{LIAVA} *Opn1sw*$^{-/-}$ mouse model that exhibited a late-onset and relatively mild phenotype. While the results from mice demonstrated that the LIAVA amino acid sequence is directly harmful to cones, the source of dysfunction in human cones likely arises from aberrant splicing of the LIAVA messenger RNA due to the nucleotide haplotype of exon 3 associated with this amino acid combination. The S-opsin knockout mouse line that provided the genetic background for all mice used in the LVAVA and LIAVA studies was generated using targeted gene replacement technology, and the effects of removing S-opsin from cones that would otherwise coexpress both S and M/L-opsins were investigated. In addition to making the interpretation of data collected from the disease models more straightforward, characterizing the *Opn1mw Opn1sw*$^{-/-}$ mice and the *Opn1lw*^{LIAIS} *Opn1sw*$^{-/-}$ mice provided insights into issues relating to visual adaptation, regulation of opsin gene expression, and cone viability.

Table of Contents

This dissertation is dedicated to my uncle, Richard Gutnick, who taught me to expect the value of what I get out of [. . .] to be commensurate with the effort that I have put in.

Acknowledgments

This dissertation is the product of many remarkable people who I have had the good fortune to have in my life. Maureen and Jay Neitz have been thoroughly outstanding mentors. They have guided my education with great care and patience, while providing me with many opportunities to grow as a scientist both in their laboratory and at meetings/workshops across the globe. Jim Kuchenbecker contributed intellectually and technically to the ERG component in each chapter of this dissertation. Dan Roberson initiated the work on the S-opsin knockout mouse and graciously allowed me to pick up where he left off. Jing Huang and Dan Possin have taught me nearly everything that I know about doing histology from immunolabeling to microscopy, and they have given me a wealth of guidance and technical assistance. Netta Smith has taught me a multitude of experimental techniques, and she has done a tremendous amount of administrative work on my behalf. Her assistance at the bench and her willingness to share mouse colony maintenance responsibilities, along with Amielle Moreno and Mark-Joseph Torres, permitted my projects to move forward much faster. Candice Davidoff provided valuable feedback during discussions throughout my dissertation and, like Jessica Rowlan, was always willing to lend a hand at the bench. I am also grateful to other members of the Neitz Lab, including Mike Manookin, Christian Puller, Toni Haun, Brian Schmidt, and Katie Mancuso, for their support over the years. I appreciate that Jack Saari and Anita Hendrickson were always happy to share their expertise when I encountered challenges with my experiments. As members of my thesis committee, Greg Horwitz and Leo Pallanck provided wonderful feedback throughout my dissertation and made sure that I stayed on track. I would like to thank the Program in Neurobiology & Behavior, and specifically Lucia Wisdom and Ann Wilkinson who helped me navigate the system. I am tremendously grateful to my family (especially Herbert, Anita, Hal, and Anna Greenwald) and friends (including all people mentioned above) for their ongoing support throughout the many twists and turns of graduate school.

List of Figures

List of Tables

Chapter 1

Genetically engineered mice for investigating the consequences of variation in the human *OPN1LW* and *OPN1MW* genes

Abstract

Specific variants of human long-wavelength (L) and middle-wavelength (M) cone opsin genes have recently been associated with a variety of vision disorders caused by cone malfunction, including red-green color vision deficiency, blue cone monochromacy, myopia, and cone dystrophy. Strikingly, most of the cone opsin alleles that are associated with vision disorders do not have deleterious point mutations, as is the case for disease-causing mutations in rhodopsin. Instead, specific combinations of normal polymorphisms that arose by genetic recombination in exon 3 between the genes encoding L and M opsins appear to cause disease. Knockout/knock-in mice promise to make it possible to study how these deleterious human cone opsin variants affect the structure, function, and viability of the cone photoreceptors. However, it must be first established that wildtype human cone photopigments function normally when they replace the endogenous mouse photopigment and that the interpretation of the results are not compromised by co-expression of short-wavelength (S) opsin in the cones expressing the mutant. Here, the creation and validation of two lines of genetically engineered mice that can be used to study disease-causing variants of human L/M-opsins, *in vivo*, are described. One line has a knockout of the mouse S-opsin gene, and the other has a recombinant L-opsin gene associated with normal vision. The two lines of mice were crossed to generate double mutant mice, and the structure and function of their cone photoreceptors were characterized. In addition to providing a testbed for mutant opsins, the results have provided insight into functional differences between human versus mouse cone photopigments and into how cones are affected when the majority of opsin expression is lost.

Introduction

In the human population, there is a high frequency of variant cone opsins in which amino acids have been interchanged between ancestral long- (L) and middle- (M) wavelength opsins by a high rate of recombination between the respective genes. A subset of these cone opsin "interchange" variants have been linked to a growing number of human eye disorders (Carroll *et al*., 2012; Carroll *et al.,* 2004; McClements *et al*., 2013a; Mizrahi-Meissonnier *et al.,* 2010; Neitz *et al*., 2004). Thus far, understanding opsin interchange variants and their role in vision defects has come from the study of human subjects or cell lines carrying mutant opsin genes *in vitro*. It would be beneficial to have an *in vivo* system that could be used to understand the disease at a mechanistic level and to evaluate potential therapies. With this goal in mind, the purpose of the present study was to characterize a mutant mouse that carries a targeted gene replacement of the mouse endogenous X-chromosome cone opsin gene with a human L-opsin cDNA. However, mice naturally co-express their short wavelength (S) opsin in the majority of their M cones (Applebury *et al*., 2000; Röhlich, van Veen, & Szél, 1994; Szél *et al*., 1993). In order for the human L-opsin mouse to be used in studies that examine the effects of L- or M-opsin variants associated with vision abnormalities on cone structure, function, and viability, the interpretation of results must not be compromised by the co-expression of wildtype S-opsin in the cones expressing the human gene. Thus, a knockout of the mouse short-wavelength (S) opsin gene was also generated and crossed with the human L-opsin mouse.

The *OPN1LW* and *OPN1MW* genes each have six exons. The first and sixth exons do not normally vary. Exon 5 specifies nine amino acid positions that differ in a stereotyped manner between L and M cone photopigments, and two of these positions (277 and 285) are responsible for the majority of the separation in peak sensitivity of the L and M cones. Exons 2, 3 and 4 together specify eleven amino acid positions that vary because of recombination between the ancestral L and M genes (for recent review, see (Neitz & Neitz, 2011)).

Dimorphisms at amino acid positions 116, 180, 230 and 233 are known to shift the tuning of the absorption spectra of the photopigments (Asenjo, Rim, & Oprian, 1994; Merbs & Nathans, 1993; J. Neitz, Neitz, & Jacobs, 1989; M. Neitz, Neitz, & Jacobs, 1991). Until recently, these four residues were assumed only to affect spectral tuning, while all other variable amino acid positions were believed to be without consequences for cone function or vision. However, several recent studies have identified combinations of the polymorphic amino acid positions encoded by exon 3 as being deleterious (Carroll, *et al*., 2012; Carroll, *et al.*, 2004; Crognale *et al*., 2004; McClements, *et al*., 2013b; Mizrahi-Meissonnier, *et al.*, 2010; M. Neitz, *et al*., 2004). The amino acids at the dimorphic positions encoded by exon 3 are as follows: 153 is methionine (M) or leucine (L), 171 is either valine (V) or isoleucine (I), 174 is either alanine (A) or valine, position 178 is either valine or isoleucine, and position 180 is either alanine or serine (S). One deleterious variant has the amino acids Leucine, Isoleucine, Alanine, Valine, and Alanine at amino acid positions 153, 171, 174, 178 and 180, respectively, and is abbreviated LIAVA. This variant has been associated with a complete absence of cone photoreceptors function. A second variant that differs from LIAVA only at position 171, where it has Valine instead of Isoleucine (LVAVA), has been associated with high myopia, cone dysfunction, and cone dystrophy (Carroll, *et al.*, 2012; McClements, *et al*., 2013b). Here, the knock-in gene that replaces the wildtype M cone opsin to become the sole photopigment in cone photoreceptors of mice encodes an LIAIS variant of human L-opsin, designated *Opn1lw*$^{\text{LIAIS}}$, which is known to have normal function.

Materials and methods

Animals

All experiments using animals conformed to the principles regarding the care and use of animals adopted by the American Physiological Society and the Society for Neuroscience, and was approved by the Animal Care and Use Committee at the University of Washington.

Two lines of genetically modified mice were created by Ozgene, Inc. (Perth, Australia) using targeting constructs according to our specifications. One construct was designed to replace the endogenous mouse *Opn1mw* gene with a human cDNA encoding a normal L cone opsin with following amino acids at the polymorphic positions encoded by exon 2, 3 and 4: T65, I111, S116, L153, I171, A174, I178, S180, I230, A233, and M233. The modified locus in mice in this study was $Opn1lw^{LIAIS/LIAIS}$ for females or $Opn1lw^{LIAIS/Y}$ for males, but for simplicity, here the locus is referred to as $Opn1lw^{LIAIS}$. The second construct was designed to create a large deletion within the mouse *Opn1sw* gene, thereby creating an S-opsin knockout mouse, designated $Opn1sw^{-/-}$. The modified loci were confirmed by direct sequencing of genomic DNA and sequencing of cDNA derived from retinal messenger RNA (mRNA).

Mice used in this study were C57BL/6. Mice that were wildtype at both the M and S-opsin gene loci are designated $Opn1mw^{+/+}$ $Opn1sw^{+/+}$, and the corresponding S-opsin knockout mice are designated *Opn1mw* $Opn1sw^{-/-}$. The L-opsin gene replacement mice are designated $Opn1lw^{LIAIS}$ $Opn1sw^{+/+}$, and the corresponding S-opsin knockout mice are designated $Opn1lw^{LIAIS}$ $Opn1sw^{-/-}$. Genetically modified opsin loci were confirmed to be correct by direct sequencing in all founder animals. The genotypes of all animals used in this study were confirmed using the polymerase chain reaction (PCR).

Targeted replacement of the Opn1mw gene

A targeting vector was created to replace the endogenous mouse *Opn1mw* gene on the X-chromosome with a human L-opsin cDNA via homologous recombination. Recombination was mediated by a 5' homology arm that was 11.9 kilobase pairs (kb) in length, and a 3' homology arm that was 2.8 kb. The 5' arm extended from nucleotide position 71,366,218, which is upstream of the *Opn1mw* gene on mouse X-chromosome, through codon 65 in exon 2 of the mouse *Opn1mw* gene (nucleotide position 71,378,135 July 2007 version of mouse genome assembly). The Quick Change site directed mutagenesis kit (Stratagene, La Jolla, CA) was used to alter mouse codons 58, 62, and 65 to encode the same amino acids as the corresponding codons in human *OPN1LW*. Amino acids 58 and 62 do not vary among human *OPN1LW* genes but codon 65 does, and in our construct, this codon specifies threonine (T65). Mouse codon 58 was changed from ACC to GTC, mouse codon 62 was changed from CTT to TTT, and mouse codon 65 was changed from GTT to ACT. The 3' homology arm extended from mouse X-chromosome nucleotide 71,389,460 to 71,392,250 which lies within intron 5 of the mouse *Opn1mw* gene. Between the 5' and 3' homology arms in the targeting construct was a segment of the human cDNA from plasmid hs7 (Nathans, Thomas, & Hogness, 1986b) extending from codon 66 through the polyadenylation signal. A PGK-NEO cassette flanked by loxP sites was positioned between the human cDNA fragment and the 3' homology arm, which was deleted by Cre-mediated recombination in the final modified locus. The endogenous mouse *Opn1mw* locus and the targeted replacement locus are illustrated in **Figure 1A** and **B**. The opsin encoded by the final modified locus retained the amino acids specified by mouse exon 1, but the amino acids specified by exon 2 through 6 corresponded to those encoded by a human L-opsin that is abbreviated LIAIS according to the previously described convention. The exon 2 encoded dimorphic positions were T65, I111, S116, and the exon 4 encoded dimorphic positions were I230, A233, M236.

Figure 1. **Schematic of the *Opn1sw* gene in the *Opn1sw*$^{+/+}$ mouse and the *Opn1sw*$^{-/-}$ mouse.** Rectangles indicate the exons and the black lines indicate the introns and non-exonic DNA flanking the loci. The first and last exons include the 5' and 3' untranslated regions, respectively, in addition to the protein coding regions. The locations of the ATG start codon, TGA stop codon, and the polyadenlyation signals are marked. (**A**) The endogenous *Opn1mw* gene. (**B**) A targeting construct containing human cDNA encoding exons 2 through 6 replaced the entire *Opn1mw* gene, except for exon 1, intron 1, and part of exon 2. Exon 2 is a mouse/human hybrid gene (boundary denoted by dashed line), although the three codons in the mouse sequence encoding amino acids inconsistent with the human L/M-opsin were changed by site directed mutagenesis to the human specifications. Three versions this *Opn1lw*$^{\text{LIAIS}}$ targeting vector have been made, each encoding the amino acid sequence, LIAIS, LIAVA, or LVAVA. (**C**) The wildtype *Opn1sw* gene. (**D**) The targeted locus carries a 1324 base pair deletion between introns 2 and 4. In generating the knockout gene, an intermediate construct was generated (not shown) in which a neomycin selectable marker, flanked by one loxP site was integrated by homologous recombination into intron 4 and a second loxP site was introduced into intron 2. Mice carrying the intermediate locus were crossed to mice carrying the gene for Cre-recombinase. Offspring in which the neomycin resistance marker and exons 2 through 4 of the *Opn1sw* locus were deleted by Cre-mediated recombination were bred to homozygosity. These mice were homozygous for the *Opn1sw* knockout gene, which was confirmed by complete sequencing of the locus. The removal of the neomycin selectable marker via Cre-recombinase left a loxP site in what is left of intron 2, and its location is labeled.

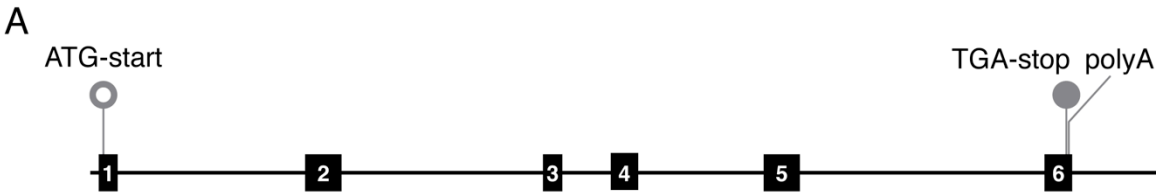
A
ATG-start
TGA-stop
polyA
1
2
3
4
5
6

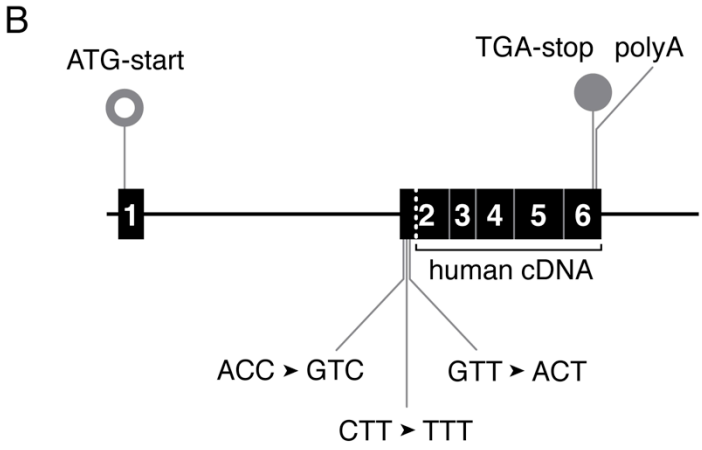
B
ATG-start
TGA-stop
polyA
1
2
3
4
5
6
human cDNA
ACC ➤ GTC
GTT ➤ ACT
CTT ➤ TTT


C
ATG-start
TGA-stop
polyA
1
2
3
4
5

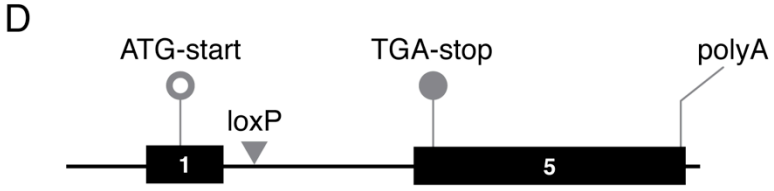
D
ATG-start
TGA-stop
polyA
loxP
1
5

Opn1sw knockout

A targeting construct was designed to delete exons 2, 3, and 4 of the *Opn1sw* gene on mouse chromosome 6 in order to create an S-opsin knockout. Deletion of exons 2 through 4 was achieved by homologous recombination between the targeting vector and the endogenous *Opn1sw* locus. The 5' homology arm extended from within intron 1 of the mouse *Opn1sw* gene upstream by 3.9 kb and the 3' homology arm extended from within intron 4 to 3.6 kb downstream. The endogenous *Opn1sw* gene and the knockout are illustrated in **Figure 1C** and **D**.

Genotyping

DNA was isolated from each mouse and PCR performed to determine the genotype for both the S-opsin and M-opsin gene loci. All PCRs were performed on an ABI Model 2700 or Veriti Thermal Cycler. For the *Opn1sw* locus, primer pair 1 (**Table 1**) was used with the iTaq kit (Biorad, Hercules, CA). Reaction volumes were 10 µl with a final concentration of 20 nanomolar (nM) each for the forward and reverse primers, 100 nM for each of the dNTPs (dATP, dGTP, dTTP, and dCTP), and 2 millimolar (mM) $MgCl_2$. A 0.9 kilobase pair (kb) PCR product was expected from the knockout locus, and a 2.2 kb product was expected from the intact locus. Both products were expected from heterozygous animals; however, the 2.2 kb product was not reliably detected in heterozygotes, presumably because the shorter product was preferentially made. An additional PCR assay with primer pair 2 (Table 1, lower case letters correspond to intron sequences and upper case letter correspond to exon sequences) was used to reliably distinguish between *Opn1sw*$^{+/-}$ versus *Opn1sw*$^{-/-}$ mice. For all mice in which a 0.9 kb PCR product was observed from PCRs with primer pair 1, PCR was done with primer pair 2 using the ABI AmpliTaq Gold kit with reaction volumes of 10 µl and a final concentration of 300 nM for each primer, 100 nM for each of the dNTPs, and 2 mM for $MgCl_2$. PCR products were subjected to agarose gel electrophoresis. PCR assays performed using primer pair 2 do not give a product

in *Opn1sw*$^{-/-}$ mice because both primers correspond to the deleted region. However, for heterozygotes, the intron 2/exon 3 primer pair gives a 0.2 kb PCR product.

PCR was used to determine whether the opsin gene present on the X-chromosome(s) of the mice was the endogenous *Opn1mw* or *Opn1lw*^{LIAIS} gene using primer pairs 3 and 4 (Table 1). The primer pair designed to amplify the *Opn1mw* gene used a forward primer that crossed the intron 2/exon 3 boundary and a reverse primer that crossed the exon 3/intron 3 boundary. Primer pair 4 was designed to amplify the *Opn1lw*^{LIAIS} gene. These primer sets were used with the AmpliTaq Gold kit (ABI) at a concentration of 300nM each. The dNTP concentrations were each 100nM. PCR products were analyzed by agarose gel electrophoresis. The 196 bp *Opn1mw* PCR product was only observed in mice with that gene intact and not in mice with only *Opn1lw*^{LIAIS} gene. Likewise, the 169 bp *Opn1lw*^{LIAIS} PCR product was observed in the knock-in mice but not in mice with only the wildtype locus. Together, these PCR reactions detected heterozygous animals that arose in intermediate generations in the breeding scheme used to generate the double mutant mice *Opn1lw*$^{LIAIS/LIAIS}$ *Opn1sw*$^{-/-}$ (females) and *Opn1lw*$^{LIAIS/Y}$ *Opn1sw*$^{-/-}$ (males).

Table 1. **PCR primers and thermal cycling conditions**.

Primer pair	Primer sequence	Primer location	Thermal cycling
1	5'TGTCACGGATACTTCCTCTTTGGTC 5'GAGGGCCAACTTTGCTAGAAGAGAC	*Opn1sw* exon 1 *Opn1sw* exon 5	94°C for 3 min; 35 cycles of 94°C for 30 sec, 68°C for 1.5 min; 72°C for 10 min
2	5'ttcttccagttctggaatgaatgtttg 5'AGTCCTCAGCAACTGGGAGTAGGAGAAG	*Opn1sw* intron 2 *Opn1sw* exon 3	95°C for 9 min; 38 cycles of 94°C for 30 sec, 61.5°C for 40 sec; 72°C for 10 min
3	5'tctcttcttccgtgtagGAATCACAGG 5'acacccttacCTGCTCCAACCAAAG	*Opn1mw* intron 2/exon 3 *Opn1mw* intron 3/exon 2	95°C for 9 min; 8 cycles of 94°C for 45 sec, 65°C for 45 sec; 32 cycles of 94°C for 1 min, 65°C for 45 sec; 72°C for 10 min
4	5'GGATCACAGGTCTCTGGTCTC 5'CTGCTCCAACCAAAGATGG	*Opn1lw*^{LIAIS} exon 3 *Opn1lw*^{LIAIS} exon 3	95°C for 9 min; 8 cycles of 94°C for 45 sec, 59°C for 45 sec; 32 cycles of 94°C for 1 min, 59°C for 45 sec; 72°C for 10 min
5	5'cttctttgccacacttggagGTGAAATC 5'GCCATGATCCAGGTGAAGACCACAC	*Rho* intron 1/exon 2 *Rho* exon 2	94°C for 3 min; 35 cycles of 94°C for 30 sec, 68°C for 1.5 min; 72°C for 10 min

Reverse transcriptase (RT) PCR on opsin mRNA

Animals were euthanized, retinas were immediately isolated and stored in RNALater (Ambion, Austin, TX), and subsequently retinal RNA was isolated using the RNeasy kit (Qiagen, Gaithersburg, Maryland). Retinas of five *Opn1sw*$^{-/-}$ mice were pooled and retinas from four *Opn1sw*$^{+/+}$ mice were pooled. Reverse transcriptase (RT) PCR was performed using the RNA PCR kit (ABI), and RNA samples were not treated with DNAse I. For the *Opn1sw*$^{+/+}$ mice, reactions using primer pair 1 (Table 1) yielded a 2.2 kb product from genomic DNA and a 0.6 kb product from cDNA. For the *Opn1sw*$^{-/-}$ mice, these primers yielded a 0.9 kb product from genomic DNA, and a 0.2 kb product is expected from the modified locus if it is transcribed. As a negative control, reactions without the addition of reverse transcriptase enzyme were carried out, and in this condition, only a product from genomic DNA is expected. As a second positive control, primers to mouse rhodopsin cDNA (primer pair 5, Table 1) were used in reverse transcriptase PCR using RNA from the retinas of *Opn1sw*$^{-/-}$ and *Opn1sw*$^{+/+}$ mice. The forward primer spanned the exon 1/2 splice junction so that only cDNA is amplified, and the reverse primer corresponded to sequences in exon 2. Because both the *Opn1sw*$^{-/-}$ and *Opn1sw*$^{+/+}$ mice have intact rhodopsin genes, a PCR product of 0.15 kb is expected with these primers.

Quantification of M-opsin transcription

Mice were euthanized and eyes were marked with permanent ink to mark the cornea/sclera to label orientation prior to enucleation. Eyes were placed on a pad of sterile paper tissues soaked in RNase-free phosphate buffered saline (PBS). Under a stereomicroscope, the temporal-nasal meridian was marked. A very small puncture hole was made in the cornea with a needle, and the eye was immediately submerged in a dish of ice-cold, RNase-free PBS. The cornea and lens were removed, and the eye was cut along the temporal-nasal meridian. The ventral hemi-retina was teased from the RPE and immediately placed in RNALater. Ventral retinas of both eyes were combined for each animal. The mRNA was extracted and DNA removed by treating with

DNase I. Synthesis of cDNA was competed with a kit according the manufacturers recommendations (Invitrogen, Carlsbad, CA) and an aliquot of the product was diluted to ~12.5ng/µL for real time PCR. Each sample was amplified in quadruplicate according the standard protocol provided by Applied Biosystems for their custom designed Taqman assay for mouse M-opsin cDNA(Applied Biosystems, Mm01193546_m1) and mouse beta-actin cDNA (Applied Biosystems, Mm00607939_s1). M-opsin cDNA quantitation was normalized to beta-actin cDNA.

Immunocytochemistry

Mice were euthanized with a lethal dose of sodium pentobarbital and tissues fixed via cardiac perfusion first with 0.13 M phosphate buffered saline (PBS) pH 7.2-7.4 containing 2 units of heparin per mL, followed by 4% paraformaldehyde (PFA) in PBS, followed by 4% paraformaldehyde plus 1% glutaraldehyde in PBS. Glutaraldehyde served to keep the neural retina attached to the RPE so that the cone outer segments would remain intact. Each solution was warmed to ~37°C just prior to administration and ~35-40mL of perfusate was delivered at each stage. Once the perfusion was stopped, the mouse was wrapped in a moist paper towel and left to further fix for 2-3 hours before enucleation and dissection.

Permanent ink was used to mark the orientation of the eye, the anterior segment was removed, and the eye-cup was fixed in 4% PFA overnight at 4°C and then stored in PBS at 4°C. Retinal whole-mounts were made by flattening the dissected retina between tissues soaked in 4% PFA for two hours and then transferring them to a culture plate for 6 more hours of fixation. Afterward, the PFA was replaced with PBS containing 0.03% sodium azide (Sigma).

For sections, eyecups were drained of PBS, imbedded in low gelling temperature agarose (Type XI, Sigma, 8% in PBS). A small agar block surrounding the eyecup was cut out with a razor

blade and oriented. The specimen block was mounted to the sectioning plate with cyanoacrylic adhesive. To help keep the RPE from separating from the retina and breaking the cone outer segments, sections were kept relatively thick (100μm). Sagittal slices containing both dorsal and ventral retina were produced. Sections from within 100 μm of the optic nerve head were transferred to a culture plate containing PBS with 0.03% sodium azide.

Antibody labeling was carried out on a rotating table shaker. Sections were incubated with 1% sodium borohydride in PBS for 30 minutes at room temperature to quench glutaraldehyde autofluorescence and then washed thoroughly in PBS. To block non-specific labeling, whole mounts or sections were incubated overnight at 4°C with a solution containing 5% donkey serum (Jackson ImmunoResearch, Cat #004-000-120), 1mg/ml BSA (Jackson ImmunoResearch, Cat #001-000-161), and 0.03% Triton X-100 in PBS (pH 7.4). The primary antibodies used in this study were rabbit anti red-green opsin diluted 1:200 (Millipore, Cat # AB405) and goat anti-S-opsin (Santa Cruz Biotechnology, Cat # sc-14365) diluted 1:100. Primary antibodies were incubated at 4°C for at least 3 days for sections and 2 days for whole mount tissue. Specimens were washed in PBS 3 times for 30 minutes each, then incubated at 4°C overnight with DAPI (4',6-diamidino-2-phenylindole,dihydrochloride 1:10,000; Invitrogen, Cat # D-21490) plus secondary antibodies. The secondary antibody for the L/M-opsin antibody was Alexa Fluor 488 labeled donkey anti-rabbit IgG(H+L) diluted 1:200 in antibody dilution buffer (Invitrogen, Cat # A21206) and the secondary for S-opsin antibody was Alexa Fluor 633 labeled donkey anti-goat IgG(H+L) diluted 1:200 (Invitrogen, Cat # A21082). This was followed by three 30 minute PBS washes, 30 minutes of post-fixation with 4% paraformaldehyde, and three more 30 minute PBS washes. Finally, the retinal slices were placed on slides with 2% DABCO in glycerol and covered with cover slips.

Microscopy

Widefield images were acquired using a Nikon Eclipse E1000 with a 20x (open-air) objective and camera set with a 1.5x optical zoom. For each specimen, 50 optical sections were taken 0.5 μm apart and the M-opsin Z-stack was reconstructed in ImageJ. The Z-stack was oriented so that the lengths of the outer segments were in plane, and the distance between where antibody staining began and ended was measured as an estimate of the length of the outer segments. Further, a 3D projection of the Z-stack was generated and the number of cones with visible M-opsin in the outer segment could be quantified.

Confocal image slices were acquired using an Olympus FluoViewTM FV1000. Sections were imaged using a 20X oil immersion lens (40 images taken 0.5 μm apart) and the Z-stacks were reconstructed in ImageJ. Channel exposure levels were balanced within and across images using Adobe Photoshop. For the retinal whole mounts, images were taken using a 10x open-air lens and mosaics were constructed with Adobe Photoshop's native mosaic construction software.

ON-OFF (long-flash) electroretinogram (ERG)

Mice were anesthetized with an intraperitoneal injection of ketamine (110.25 mg/kg) and xylazine (11.025 mg/kg) diluted in sterile saline. The eye was dilated by topical application of 1.0% atropine sulfate. Each animal was positioned on a water-heated, laminate platform with the head stabilized via a bite bar. The active lead was a custom, platinum-coated wire-ring electrode placed parallel to the surface of one eye, encircling the perimeter of the cornea and making a flat connection. The reference lead was a custom platinum-coated wire electrode bent to match the curvature of the back of the eye and was inserted between the bottom eyelid and sclera where it was proximal to the optic nerve.

A Roland Consult (Brandenburg, Germany) Q400 Ganzfeld ERG system was modified to hold 26 ultraviolet (UV) LEDs (Nichia NSHU591B, 365 nanometer (nm) peak) and 26 green LEDs (Nichia NSP6510S LEDs, 520 nm peak). Custom circuitry controlled intensities of the LEDs with pulse width modulation, providing a linear intensity response with no shift in peak wavelength. The same circuitry was also used to synchronize the light stimulus with the Roland Consult Retiport software. Each LED was independently adjustable, allowing S or M cone photopigment specific stimuli to be generated via the method of silent substitution. The light stimulus was flashed at 1 Hz with a 50% duty cycle. During the first 500 milliseconds (ms) of each cycle (Phase 1), quantal catch was high for the specific photopigment isolating stimulus (S or M), while in the final 500 ms (Phase 2), the quantal catch was low for the specific photopigment isolating stimulus. Specifically, a 520 nm light was used to isolate the M-opsin response, and a 365 nm light was alternated with a 520 nm light in a silent substitution paradigm to isolate the S-opsin response. All ERGs were performed in the photopic light range with background lights adjusted to suppress rod activity. Data were reported as the averages of 20 ERG records and the size of the ERG corresponds to the b-wave amplitude, which is measured as the absolute voltage change from the a-wave trough to the b-wave peak. The b-wave is generated by the depolarization of ON-bipolar cells (Bush & Sieving, 1996) and therefore can be used as an indirect indicator of the photoreceptor response.

Results

We created a line of mice in which exons 2-4 of the mouse *Opn1sw* gene have been deleted, with the goal of creating a null mutant. A second line of genetically engineered mice in which the mouse *Opn1mw* gene was replaced with a recombinant gene that encoded a normal variant of a human *OPN1LW* gene was created by fusing a human L-opsin cDNA extending from codon 66 in exon 2 to the polyadenylation signal following exon 6. This created a recombinant X-chromosome opsin gene locus that encoded an L-opsin with the N-terminal 33 amino acids encoded by exon 1 of the endogenous mouse gene, and the remainder of the protein corresponded to the amino acids specified by codons 66 through 364 of a human L-opsin gene. The combination of amino acids L153, I171, A174, I178, and S180 (abbreviated LIAIS) was specifically chosen because it is the combination of exon 3 encoded polymorphisms that gives a normal functioning pigment with the fewest amino acid differences compared to the LIAVA variant, which has been associated with complete absence of cone function (Carroll, et al., 2004). The advantage of the design of the knock-in locus is that it allows gene expression to be controlled by the endogenous mouse regulatory DNA sequences. However, the disadvantage is the potential for the exon 1 encoded amino acid differences between mouse and human (shown in **Figure 2**) to interfere with normal function of the photopigment.

Figure 2. **Alignment of human and mouse exon 1.** The single letter amino acid code is used. Residues that differ between mouse and human are underlined and bolded. The human sequence is 5 amino acids longer than mouse due to the absence of residues corresponding to human amino acid residues 4-8 in mouse.

Hum M A Q **Q** **W** **S** **L** **Q** R L **A** G **R** **H** **P** **Q** D **S** Y E D S T **Q** **S** S I F T Y T N S N S T **R**
Mus M A Q R L **T** G **E** **Q** **T** **L** D **H** Y E D S T **H** **A** S I F T Y T N S N S T **K**

Both genetically modified loci were confirmed by direct sequencing of all founder animals (data not shown), and in addition, breeders and experimental animals were genotyped. The genotype assays for the *Opn1mw* versus *Opn1lw*^{LIAIS} loci reliably gave bands of different sizes for the endogenous versus modified locus, even in heterozygous females (data not shown); however, two assays were needed to reliably distinguish between the wildtype and knockout *Opn1sw* loci. An example of the genotyping results for the *Opn1sw*$^{-/-}$, *Opn1sw*$^{+/-}$, and *Opn1sw*$^{+/+}$ animals is shown in **Figure 3**. A 2.2 kb PCR product is obtained from the wildtype *Opn1sw* locus when primer pair 1 (Table 1) is used, whereas a 0.9 kb band is obtained from the knockout (**Figure 3A**). Heterozygotes were expected to show both bands but as shown in Figure 3A, the assay reliably detects homozygotes but not heterozygotes. Specifically, the 2.2 kb band from the intact locus was not always detected. Thus, for all mice in which the knockout locus was detected, DNA was used in a second reaction with primer pair 2 (Table 1, **Figure 3B**). The forward primer corresponds to intronic sequences which are only present in the intact *Opn1sw* locus. If transcribed, the *Opn1sw*$^{-/-}$ locus would have exon 1 spliced to exon 5 which would produce a frame shift starting at codon 116 and introduce a transcriptional termination signal at codon 134. The mRNA is expected to be 0.2 kb.

Retinal mRNA from *Opn1sw*$^{-/-}$ and *Opn1sw*$^{+/+}$ mice was isolated and used in reverse transcriptase PCR to determine whether the knockout locus was transcribed at a detectable level. As a positive control, we showed that rhodopsin mRNA is readily detectable using the same reverse transcriptase reactions with a forward primer that corresponded to the exon 1/exon 2 junction of the mouse rhodopsin gene (**Figure 3C**). The mRNA extracts were not treated with DNase I and the PCR primer pair 1 (Table 1) can amplify either *Opn1sw* genomic DNA or complimentary DNA (cDNA). For animals with the intact *Opn1sw* locus, a band of the size expected from the cDNA was observed when the RT enzyme was added, and only a band of the size expected from genomic DNA was observed in the absence of the RT enzyme (**Figure 3D**). In contrast, for

animals with the knockout locus, a band of the size expected from genomic DNA was observed both in the presence and absence of the RT enzyme; however, in the presence of the RT enzyme, a very faint band of the size expected for cDNA derived from the knockout locus was observed (**Figure 3D**).

Figure 3. **PCR and RT-PCR genotyping assays to confirm *Opn1sw* gene knockout. (A)** A 1.5% agarose gel showing results obtained from DNA isolated from *Opn1sw*$^{+/+}$, *Opn1sw*$^{-/-}$, and *Opn1sw*$^{+/-}$ mice, as indicated by labels above each lane. MW is the molecular weight marker. A 2.2 kb fragment is obtained from the wildtype locus from PCR using primers to exons 1 and 5, a 0.9 kb fragment is obtained from the knockout mouse, and both the 2.2 and 0.9 kb bands are expected from the heterozygous animals, although the 2.2 kb band often is not detectable due to preferential amplification of the smaller product. **(B)** PCR products from amplification with primers to intron 2 and exon 3 to distinguish between *Opn1sw*$^{-/-}$ and *Opn1sw*$^{+/-}$ mice, as labeled above the lanes. A 0.2 kb band is observed in heterozygous animals, but no band is observed in S-opsin knockout mice because intron 2 and exon 3 have been deleted. **(C)** As described in the methods, reverse transcriptase (RT) PCR using rhodopsin cDNA primers on RNA isolated from retinas of *Opn1sw*$^{+/+}$ mice and *Opn1sw*$^{-/-}$ were used as positive controls to demonstrate that RNA could be isolated and amplified from both experimental and control mouse retinas. The expected 0.15 kb band can be clearly seen for both mouse lines. **(D)** Reverse transcriptase PCR using cDNA primers on isolated RNA from *Opn1sw*$^{+/+}$ mice and *Opn1sw*$^{-/-}$ mice (as labeled) were used. The lanes without reverse transcriptase (labeled RT -) show just one band each, amplifying only genomic DNA, yielding 2.2 kb and 0.9 kb products for *Opn1sw*$^{+/+}$ and *Opn1sw*$^{-/-}$ retinas respectively (as described in the methods). The *Opn1sw*$^{+/+}$ reaction with reverse transcriptase (labeled RT +) has the capacity to amplify both the smaller RNA and the genomic DNA, yet due to preferential amplification of the smaller and more numerous RNA, only the smaller 0.6 kb band is visible. Unlike the *Opn1sw*$^{+/+}$ RT PCR, the *Opn1sw*$^{-/-}$ lane with RT + has 2 bands: One bright band of amplified genomic DNA and a much fainter band (arrowhead) at the 0.2 kb mark. This indicates that RNA for the truncated gene is produced but appears to be present in very low quantities. Most likely, the truncated mRNA is being degraded before it can be translated; however, at least a small amount of transcription is occurring.

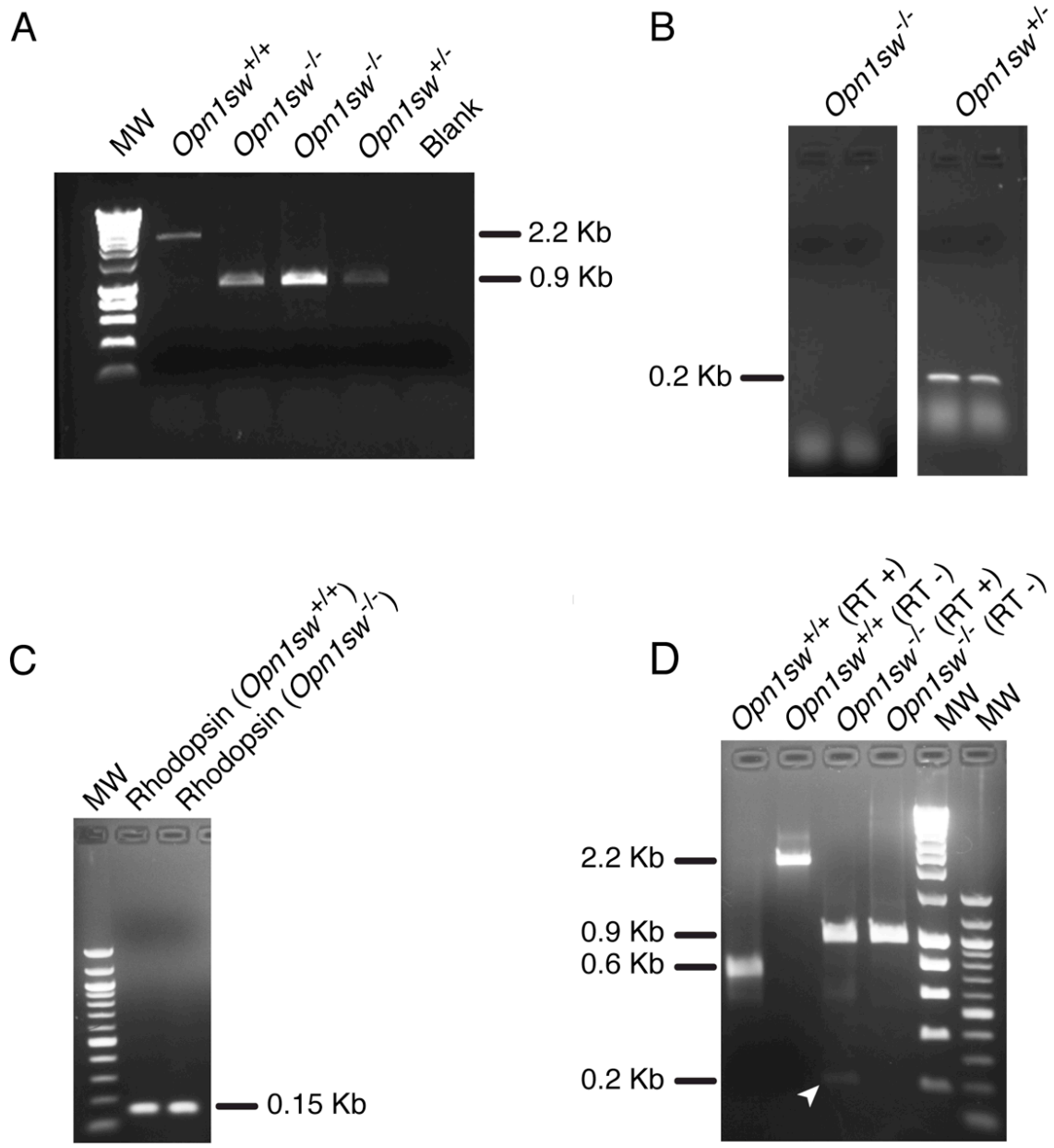
A
MW
Opn1sw+/+
Opn1sw-/-
Opn1sw-/-
Opn1sw+/-
Blank
2.2 Kb
0.9 Kb
B
Opn1sw-/-
Opn1sw+/-
0.2 Kb
C
MW
Rhodopsin (Opn1sw+/+)
Rhodopsin (Opn1sw-/-)
0.15 Kb
D
Opn1sw+/+ (RT +)
Opn1sw+/+ (RT -)
Opn1sw-/- (RT +)
Opn1sw-/- (RT -)
MW
MW
2.2 Kb
0.9 Kb
0.6 Kb
0.2 Kb

Whole-mounted retinas from *Opn1sw*$^{+/+}$ animals immunolabeled with antibodies to L/M- and S-opsin revealed an expression pattern (**Figure 4)** in which the majority of cones expressed both L- and S-opsin, and they showed a dorsal-to-ventral gradient of increasing co-expression. The whole mount shown is from a 15-month-old *Opn1lw*^{LIAVA} *Opn1sw*$^{+/+}$ mouse. The same antibodies were applied to sections of retina from *Opn1lw*^{LIAIS} *Opn1sw*$^{+/+}$ and *Opn1lw*^{LIAIS} *Opn1sw*$^{-/-}$ mice. In the ventral retinas shown in **Figure 5**, while the *Opn1lw*^{LIAIS} *Opn1sw*$^{+/+}$ mouse showed strong immunolabeling with the antibody to S-opsin, this signal was absent in the *Opn1lw*^{LIAIS} *Opn1sw*$^{-/-}$ mice, as expected if the S-opsin gene was successfully knocked out. This result is consistent with the absence of S cone function, described below.

Figure 4. **L/M- and S-opsin labeling in whole mounted retina from a 15-month-old *Opn1sw*$^{+/+}$ mouse.** Confocal images were acquired from a dorsal-ventral strip going down the center of the retina (arrowhead indicates location of optic nerve head). M-opsin labeling (**left panel**, red label) is strong in both the dorsal and ventral retina, while S-opsin labeling (**middle panel**, green label) is sparse in the dorsal retina and strong in the ventral retina. The merged image (**right panel**) shows that while majority of cones co-express both M and S-opsin, the cones in the far dorsal retina overwhelming express M-opsin; co-localized labeling appears yellow or orange, depending on the relative quantities of each opsin present. In the right panel, the scale bar represents 250 μm. Insets from the dorsal and ventral retina are enlarged ~5x, and the scale bar represents 100 μm.

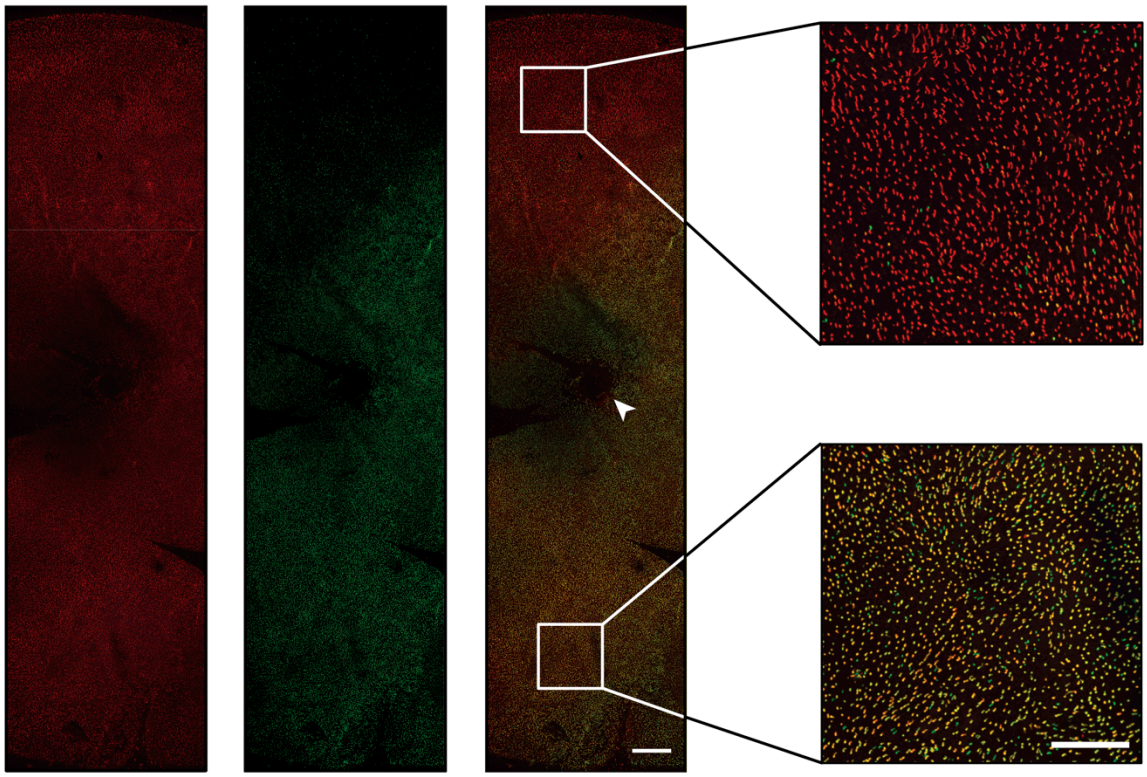
M-opsin
S-opsin
merge

Figure 5. **Immunohistochemistry using antibodies against M- and S-opsins.** Images acquired from the ventral retinas of an *Opn1lw*^{LIAIS} *Opn1sw*$^{+/+}$ mouse (left column) and an *Opn1lw*^{LIAIS} *Opn1sw*$^{-/-}$ mouse **(right column)** incubated with antibodies against both M-opsin (red) and S-opsin (green). M-opsin is labeled in both lines of mice **(top row)**, whereas S-opsin labeling is only observed in the *Opn1sw*$^{-/-}$ mouse **(middle row)**. Double labeling is evident (yellow cones) in the merged image for the *Opn1sw*$^{+/+}$ mouse, but not in the *Opn1sw*$^{-/-}$ mouse **(bottom row)**. Scale bar represents 50 μm.

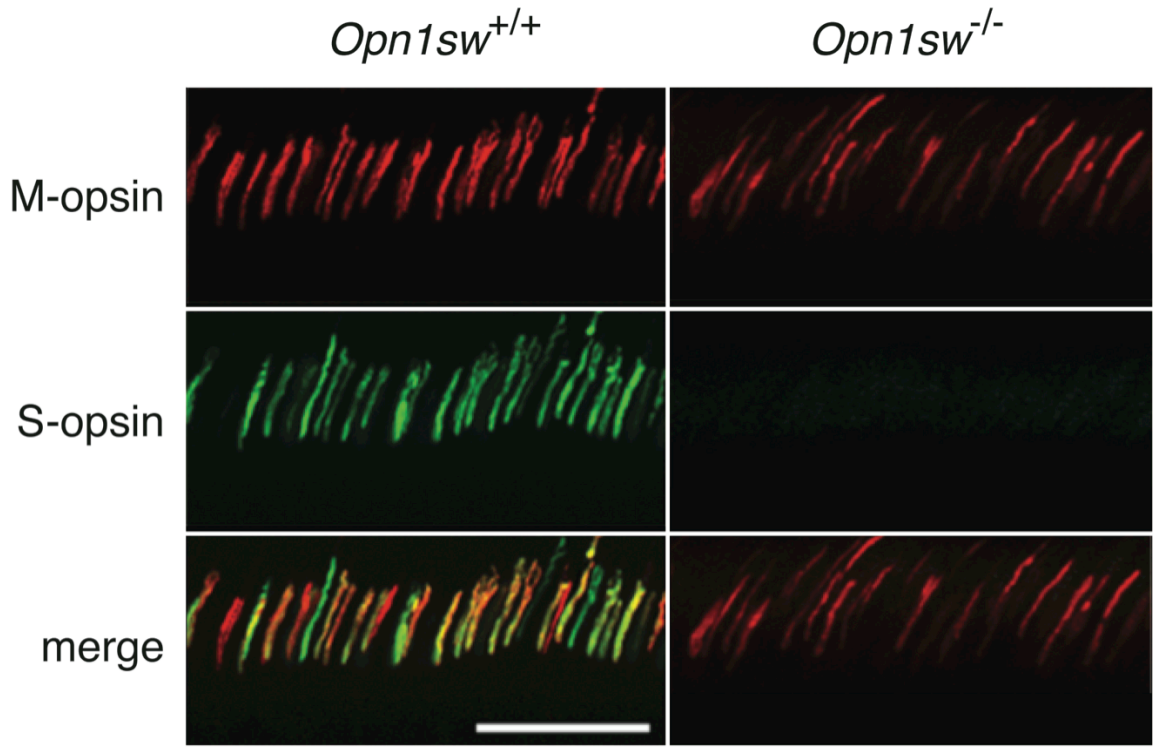
Opn1sw+/+
Opn1sw-/-
M-opsin
S-opsin
merge

Absence of S-opsin changes the M-opsin mediated light response

On-Off ERGs were performed with three-month-old *Opn1mw Opn1sw*$^{+/+}$ mice (n=10) and age-matched *Opn1mw Opn1sw*$^{-/-}$ mice (n=9) using a light to specifically stimulate the S cone photopigment. The S-photopigment response was absent in *Opn1mw Opn1sw*$^{-/-}$ mice (**Figure 6**), which is consistent with there being no functional S-opsin. In contrast, a robust response to the same stimulus was observed in *Opn1mw Opn1sw*$^{+/+}$ mice. Both the *Opn1mw Opn1sw*$^{+/+}$ and *Opn1mw Opn1sw*$^{-/-}$ mice generated strong ERGs in response to the M-photopigment isolating stimulus. Together, these results validated the S-isolating stimulus condition and confirmed the absence of functional S-opsin in the *Opn1mw Opn1sw*$^{-/-}$ mice.

The ERG waveforms produced in response to the M-photopigment-isolating stimulus by the *Opn1mw Opn1sw*$^{+/+}$ and the *Opn1mw Opn1sw*$^{-/-}$ mice have consistently distinct temporal profiles. Within the On-phase of the response, the b-wave peaked sooner and was faster to return to baseline for *Opn1mw Opn1sw*$^{+/+}$ mice, as compared to *Opn1mw Opn1sw*$^{-/-}$ mice (**Table 2**). Because the amplitude of the b-wave varied across animals and because the voltage did not necessarily return to baseline prior to the start of the Off-phase of the stimulus, the On-response decay time was calculated as the time required for the maximum On-response signal to diminish by 80%. **Figure 7** shows aggregate ERG waveforms from three-month-old *Opn1mw Opn1sw*$^{+/+}$ (n=9, black trace) and *Opn1mw Opn1sw*$^{-/-}$ (n=10, gray trace) mice. Moreover, the presence of S-opsin in dually expressing cones, without any S cone pigment stimulation, affects the amplitude of the M response. For both *Opn1mw Opn1sw*$^{+/+}$ and *Opn1mw Opn1sw*$^{-/-}$ mice, responses to a series (0.2 $\mu W/mm^2$ to 11.8 $\mu W/mm^2$) of M-opsin isolating lights increased logarithmically with intensity (**Figure 8)**; however, the slope of the function is shifted in the S-opsin knockout mice (n=10 per line). Compared to *Opn1mw Opn1sw*$^{+/+}$ mice, the *Opn1mw Opn1sw*$^{-/-}$ mice show higher sensitivity at lower light levels, but there is little difference at the highest light levels that produce near maximal responses.

Figure 6. **S-opsin responses from *Opn1sw*$^{+/+}$ and *Opn1sw*$^{-/-}$ mice.** The *Opn1mw Opn1sw*$^{+/+}$ mice (n=10) exhibit a robust response (black trace) to the S cone pigment-isolating stimulus, whereas this response is entirely absent in the *Opn1mw Opn1sw*$^{-/-}$ mice (n=9; gray trace). The bar at the top of the figure represents the timing of the On-Off light stimulus. For the S-isolating condition, the 365 nm LED was on exclusively during Phase 1, and a 520 nm light was on during Phase 2 to counterbalance any response resulting from the absorption of short wavelength light by the M-photopigment. Error bars represent the SEM.

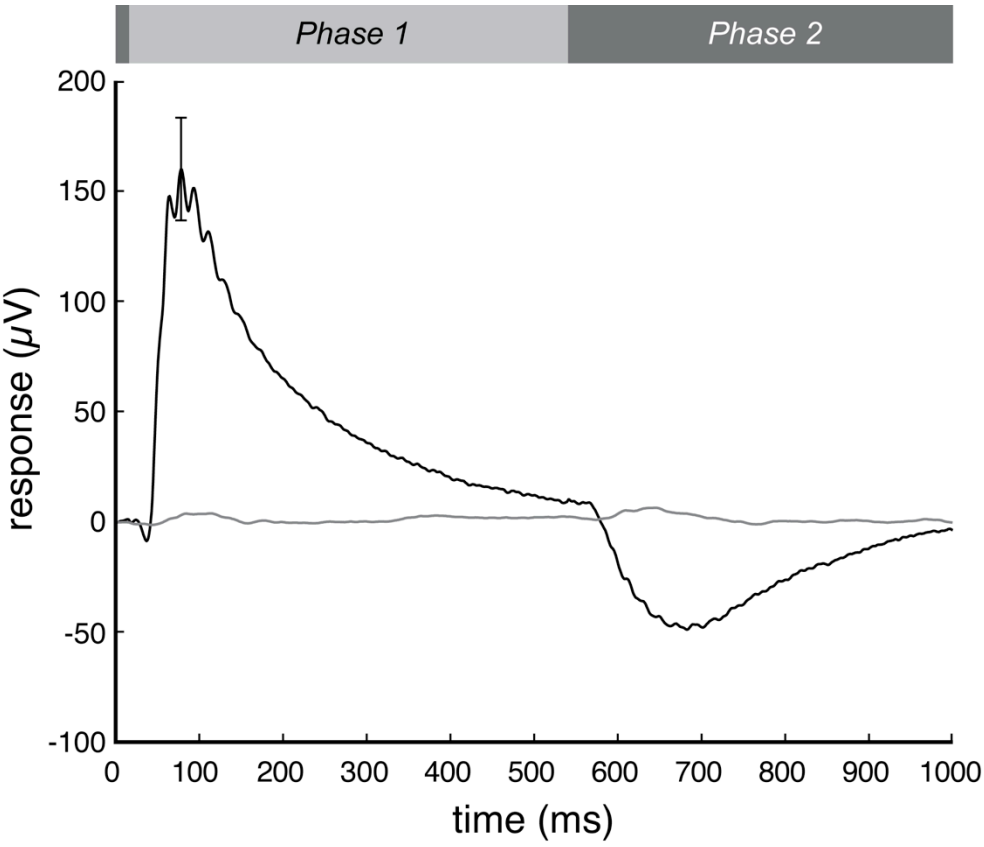
Phase 1
Phase 2
200
150
100
50
0
-50
-100
response (μV)
0
100
200
300
400
500
600
700
800
900
1000
time (ms)

Table 2. **ON-response timing profiles of wildtype and *Opn1mw Opn1sw*$^{-/-}$ mice in response to 520 nm light**. The latency for the voltage to maximally increase (b-wave) following the downward deflection at light-onset (a-wave) was measured (On-response time). Further, the amount of time necessary for the b-wave to decay by 80% was measured (On-decay time). Differences (abbreviated as differ) between the wildtype and *Opn1mw Opn1sw*$^{-/-}$ mice for these two ERG components were calculated at time-points across 16 months in the same mice.

Mouse Line	Age (m)	# of mice	On-response time (ms)	SEM	Differ (ms)	p-value	On-decay time (ms)	SEM	Differ (ms)	p-value
Opn1mw/Opn1sw$^{+/+}$	1.5	9	67.2	1.8	-5.2	0.07	181.9	3.9	30.3	0.003
Opn1mw/Opn1sw$^{-/-}$	1.5	10	62.0	2.0			212.2	7.6		
Opn1mw/Opn1sw$^{+/+}$	3	9	66.0	0.8	24.0	0.002	165.6	3.5	109.9	3.0×10^{-6}
Opn1mw/Opn1sw$^{-/-}$	3	10	90.0	6.0			275.5	14.9		
Opn1mw/Opn1sw$^{+/+}$	6	9	65.8	0.8	8.2	0.03	176.2	6.3	72.8	2.9×10^{-6}
Opn1mw/Opn1sw$^{-/-}$	6	10	73.9	3.1			249.0	8.3		
Opn1mw/Opn1sw$^{+/+}$	9	10	70.1	3.0	6.5	0.3	196.7	15.5	86.2	0.0001
Opn1mw/Opn1sw$^{-/-}$	9	10	76.6	5.1			282.9	15.5		
Opn1mw/Opn1sw$^{+/+}$	12	10	64.1	1.4	15.3	4.9×10^{-5}	175.9	14.1	80.7	0.0001
Opn1mw/Opn1sw$^{-/-}$	12	10	79.4	2.5			256.6	8.9		
Opn1mw/Opn1sw$^{+/+}$	16	10	66.5	1.3	-0.8	0.8	153.0	5.1	122.5	0.0004
Opn1mw/Opn1sw$^{-/-}$	16	10	65.7	3.1			275.5	20.5		

Figure 7. **The absence of the S photopigment alters the temporal profile of mouse M-isolated ERG.** Aggregate ERG waveforms from three-month-old *Opn1mw Opn1sw*$^{+/+}$ (n=9, black trace) and *Opn1mw Opn1sw*$^{-/-}$ (n=10, gray trace) mice. All responses have been normalized by b-wave amplitude so that the temporal signatures can be directly compared. Error bars represent SEM. Because the amplitude of the b-wave varies across animals and the voltage does not necessarily return to zero prior the start of the OFF-phase of the stimulus, the "On-decay time" was calculated as the time required for the maximum ON-response signal to decay by 80% (denoted by arrowheads).

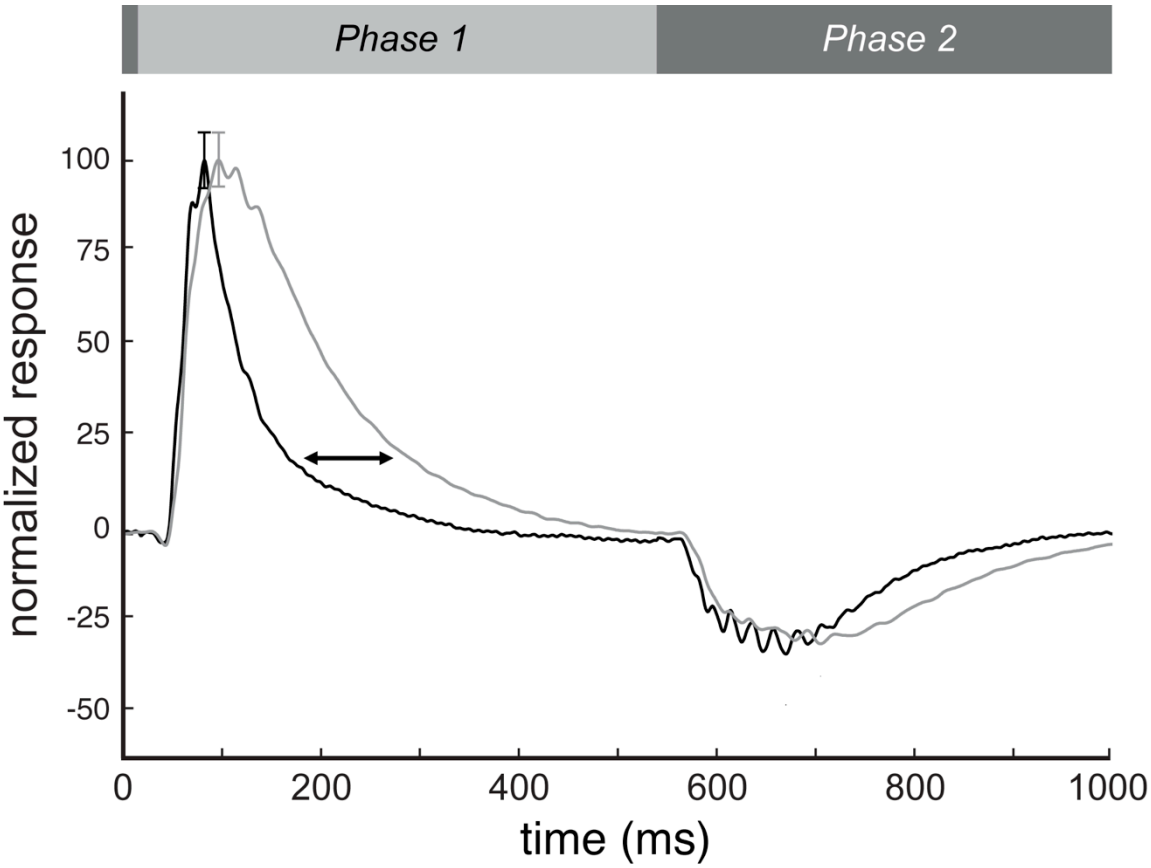
Phase 1
Phase 2
normalized response
100
75
50
25
0
-25
-50
0
200
400
600
800
1000
time (ms)

Figure 8. **The intensity response function for M-opsin stimuli has a steeper slope for wildtype mice than S-opsin knockout mice.** Responses to an M-isolating (520nm light) intensity response series (0.2 μW/mm^2 to 11.8 μW/mm^2) in three-month-old *Opn1mw Opn1sw*$^{+/+}$ (black symbols, n=10) and *Opn1mw Opn1sw*$^{-/-}$ (gray symbols, n=10) mice. Light intensity values are shown on a log scale. Error bars represent the SEM; the dashed lines are best linear fits to the data.

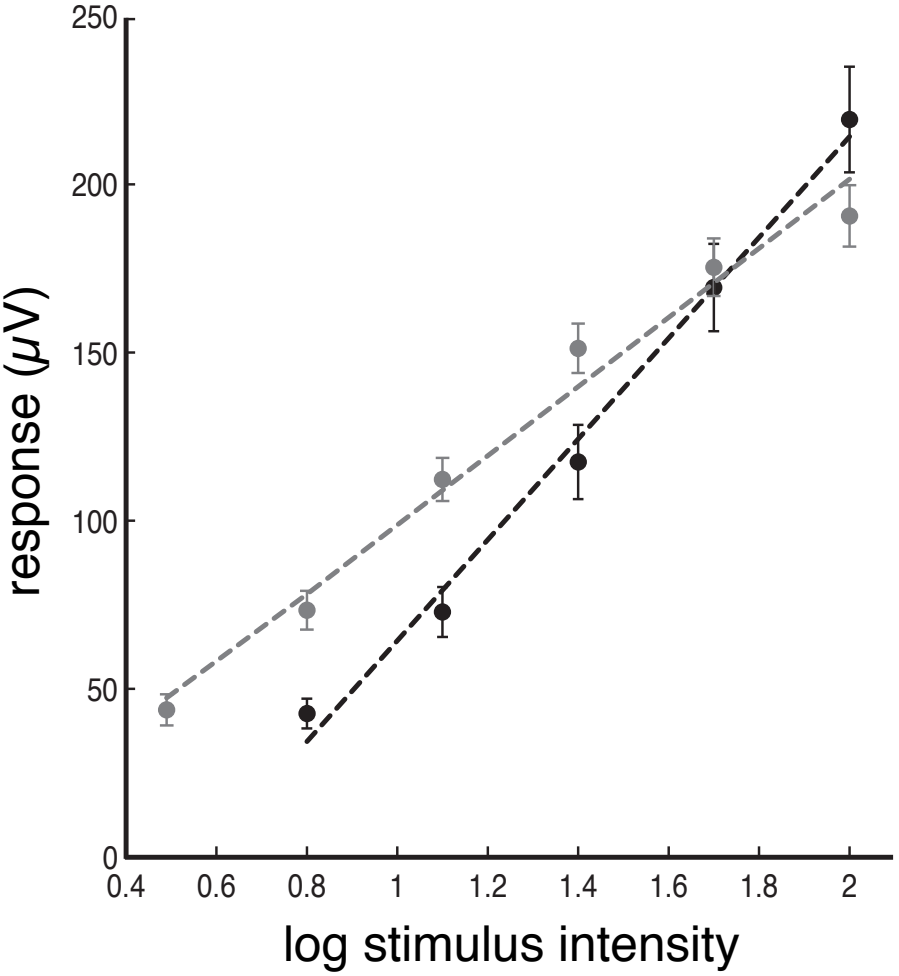
250
200
150
100
50
0
response (μV)
0.4
0.6
0.8
1
1.2
1.4
1.6
1.8
2
log stimulus intensity

ERGs generated in response to two intensities (3.0 μW/mm^2 and 11.8 μW/mm^2) of the M-opsin isolating stimulus were collected from the same *Opn1mw Opn1sw*$^{+/+}$ and *Opn1mw Opn1sw*$^{-/-}$ mice across the first 16 months of life. In this longitudinal study, M-opsin mediated ERG response amplitudes to brighter lights decreased substantially with age in the *Opn1mw Opn1sw*$^{-/-}$ line, whereas the responses remained more stable over time in the *Opn1mw Opn1sw*$^{+/+}$ line (**Figure 9A**). The mild age-dependent decrease in ERG b-wave amplitude in the *Opn1mw Opn1sw*$^{+/+}$ mice was consistent with previous reports (Williams & Jacobs, 2007). Interestingly, even though there was a dramatic decrease in M-opsin mediated ERG amplitudes with age for the S-opsin knockout mice, the ERG amplitudes were initially increased above those of the wildtype mice at the earliest time points in response to the lower intensity (3.0 μW/mm^2) stimulus.

Strikingly, there was less of an age-dependent decrease in L/M-opsin mediated ERG b-wave amplitudes in S-opsin knockout mice in which the human L-opsin replaced the wildtype mouse M-opsin. The ERG amplitudes and slopes of the fitting functions were similar between the *Opn1lw*^{LIAIS} *Opn1sw*$^{+/+}$ mice and the *Opn1mw Opn1sw*$^{+/+}$ mice at both stimulus intensities. In **Figure 9B**, the slopes of the regressions fitting the *Opn1lw*^{LIAIS} *Opn1sw*$^{-/-}$ data for each intensity were quite similar to those of the *Opn1lw*^{LIAIS} *Opn1sw*$^{+/+}$ mice. At the higher stimulus intensity, the *Opn1lw*^{LIAIS} *Opn1sw*$^{-/-}$ mice did not have as robust a response as the *Opn1lw*^{LIAIS} *Opn1sw*$^{+/+}$. However, at the lower stimulus intensity, the response amplitudes of the *Opn1lw*^{LIAIS} *Opn1sw*$^{-/-}$ and *Opn1lw*^{LIAIS} *Opn1sw*$^{+/+}$ lines were not statistically different at any time-point, except 16 months.

***Figure 9*. Progressive cone dysfunction occurs in mice when the *Opn1sw* gene is knocked out.** M-photopigment isolated ERGs were collected from **(A)** *Opn1mw Opn1sw*$^{+/+}$ (filled black symbols), *Opn1mw Opn1sw*$^{-/-}$ (filled gray symbols), **(B)** *Opn1lw*^{LIAIS} *Opn1sw*$^{+/+}$ (open black symbols), and *Opn1lw*^{LIAIS} *Opn1sw*$^{-/-}$ (open gray symbols) mice across 16 months using a 520nm light at intensities of 3.0 μW/mm^2 (**left panels**) and 11.8 μW/mm^2 (**right panels**). Error bars represent the SEM and data is fit using logarithmic functions (dashed traces). For most data points, n=10; however, in the remaining instances, the sample size was reduced (as low as n=7 in one case) due to natural mortality or technical issues. Color-coded arrowheads in panel B denote where data from the corresponding set in panel A would be if superimposed.

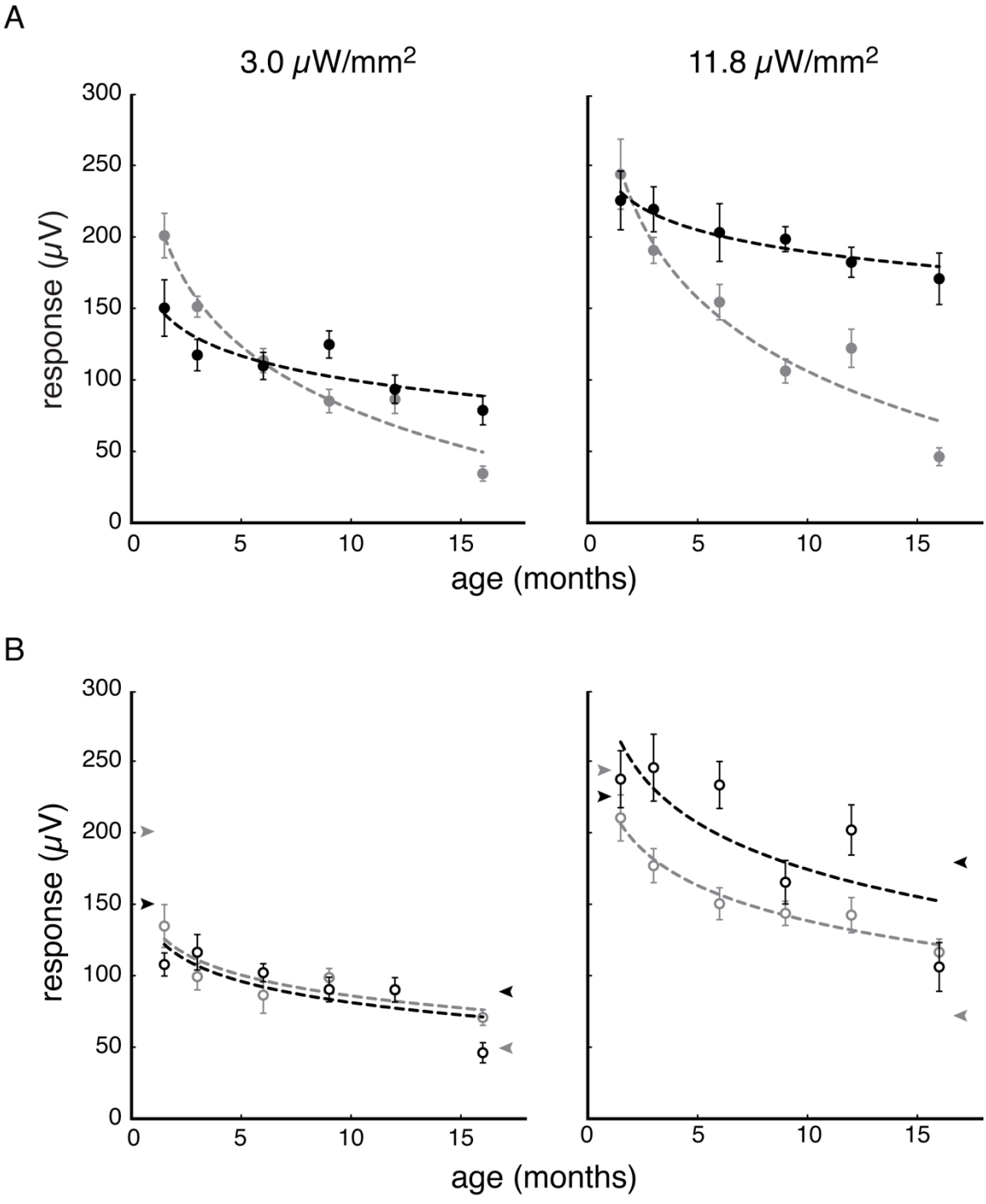
A
3.0 μW/mm2
11.8 μW/mm2
response (μV)
age (months)
B
response (μV)
age (months)

M-opsin expression profiles in Opn1lw^{LIAIS} Opn1sw$^{+/+}$ versus Opn1mw Opn1sw$^{-/-}$ cones

One possible explanation for the decline in M-opsin mediated ERG amplitudes with age is that M-opsin expression declines with age in the absence of S-opsin. To investigate this, real time quantitative RT-PCR was used to measure M-opsin mRNA and beta-actin mRNA in retinas from 12-month-old *Opn1mw Opn1sw*$^{+/+}$ mice and age-matched *Opn1mw Opn1sw*$^{-/-}$ knockout mice. RNA was extracted from ventral hemi-retinas because this was where S-opsin expression would have been most abundant under normal conditions (Applebury, et al., 2000; Haverkamp et al., 2005). At this age, the amount of M-opsin mRNA was 44% lower (p-value = 0.001) in the *Opn1sw*$^{-/-}$ mice (**Figure 10**). Based on this finding, experiments were conducted to determine whether this decrease in M-opsin transcription produced the predicted morphological and physiological consequences.

***Figure 10*. Quantitation of M-opsin in *Opn1mw Opn1sw*$^{+/+}$ vs *Opn1mw Opn1sw*$^{-/-}$ mice by qPCR.** At an age of 12 months, the retina of the *Opn1mw Opn1sw*$^{-/-}$ mouse (n=4) had 44% less M-opsin mRNA than the wildtype mouse (n=4). Error bars represent the SEM.

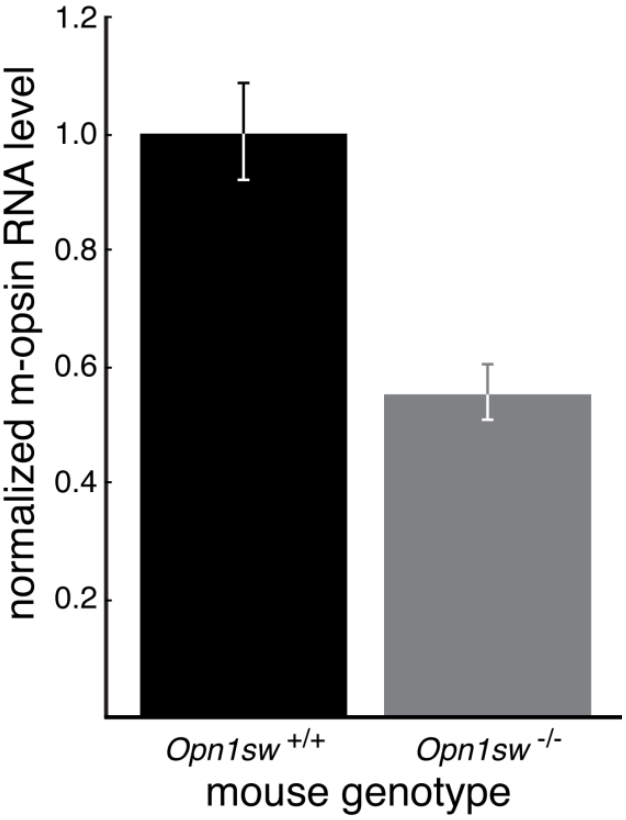
1.2
1.0
0.8
0.6
0.4
0.2
normalized m-opsin RNA level
Opn1sw +/+
Opn1sw -/-
mouse genotype

Absence of S-opsin leads to outer segment retraction

Widefield images of immunolabeled, dorsal-to-ventral sections were acquired from 16-month-old mice from each of the four lines (n=5 per line, except n=3 for the *Opn1mw Opn1sw*$^{+/+}$ line). Individual outer segment lengths were measured in a 5.7 mm^2 field, and the number of visible cone outer segments in a 2.8 mm^2 subfield was counted. All analyses were performed with the S-opsin channel turned off to avoid inflating the results from the two *Opn1sw*$^{+/+}$ mouse lines. Representative confocal images were taken for each mouse line at the dorsal and ventral retina (**Figure 11**).

The number of cone outer segments in dorsal retina from *Opn1mw Opn1sw*$^{+/+}$, *Opn1mw Opn1sw*$^{-/-}$, *Opn1lw*^{LIAIS} *Opn1sw*$^{+/+}$, and *Opn1lw*^{LIAIS} *Opn1sw*$^{-/-}$ mice did not differ significantly (**Figure 12A**). However, the number of cone outer segments in ventral retina was significantly reduced for both lines of *Opn1sw*$^{-/-}$ mice compared to the corresponding lines of *Opn1sw*$^{+/+}$ mice; *Opn1mw Opn1sw*$^{-/-}$ mice had 97% ($p = 3.2x10^{-7}$) fewer cone outer segments compared to *Opn1mw Opn1sw*$^{+/+}$ mice, and *Opn1lw*^{LIAIS} *Opn1sw*$^{-/-}$ mice had 59% fewer cone outer segments compared to *Opn1lw*^{LIAIS} *Opn1sw*$^{+/+}$ mice ($p<0.005$). Although there was no difference in the number of outer segments in ventral retina for wildtype versus *Opn1lw*^{LIAIS} *Opn1sw*$^{+/+}$ mice, there was a significant difference in the number of cone outer segments that could be visualized in the corresponding S-opsin knockout mice; there were 14 times more cones with outer segments that were visibly stained in the ventral retina from *Opn1lw*^{LIAIS} *Opn1sw*$^{-/-}$ mice compared to *Opn1mw Opn1sw*$^{-/-}$ mice (**Figure 12A**).

Measurements of the outer segments were averaged for each line of mice (**Figure 12B**). In dorsal retina, there was no statistically significant difference in outer segment length among the different lines; however, there was a trend for the *Opn1mw Opn1sw*$^{-/-}$ mice to have shorter outer segments than the *Opn1mw Opn1sw*$^{+/+}$ mice (-15%, p=0.09). In the ventral retina, the outer segments in the

Opn1mw Opn1sw$^{-/-}$ mouse were 4.2x shorter than in the *Opn1mw Opn1sw*$^{+/+}$ mice ($p=6.7x10^{-5}$) and 3.5x shorter than in the *Opn1lw*^{LIAIS} *Opn1sw*$^{-/-}$ mice ($p<0.002$). Measurements in the ventral retina also showed that outer segments tended to be shorter in *Opn1lw*^{LIAIS} *Opn1sw*$^{-/-}$ mice than in *Opn1lw*^{LIAIS} *Opn1sw*$^{+/+}$ mice (-16%, p=0.075).

***Figure 11. Opn1sw* gene knockout results in morphological changes.** Confocal image sections acquired at the far dorsal **(left column)** and far ventral **(right column)** retina for each mouse line. 19.5 µm deep z-stacks (0.5 µm spacing) were acquired with a 20x oil immersion objective. M-opsin (red), cone sheaths (green/PNA), and nucleic acid (blue/DAPI) are labeled. Images show that M-opsin staining is abnormally low in the ventral retina of both *Opn1sw*$^{-/-}$ lines, but the effect is most dramatic in the *Opn1mw Opn1sw*$^{-/-}$ mouse. Despite the *Opn1mw Opn1sw*$^{-/-}$ mouse being virtually devoid of outer segments, the cones appear to remain viable, as the cone sheaths and nuclei are present. Scale bar represents 100 µm.

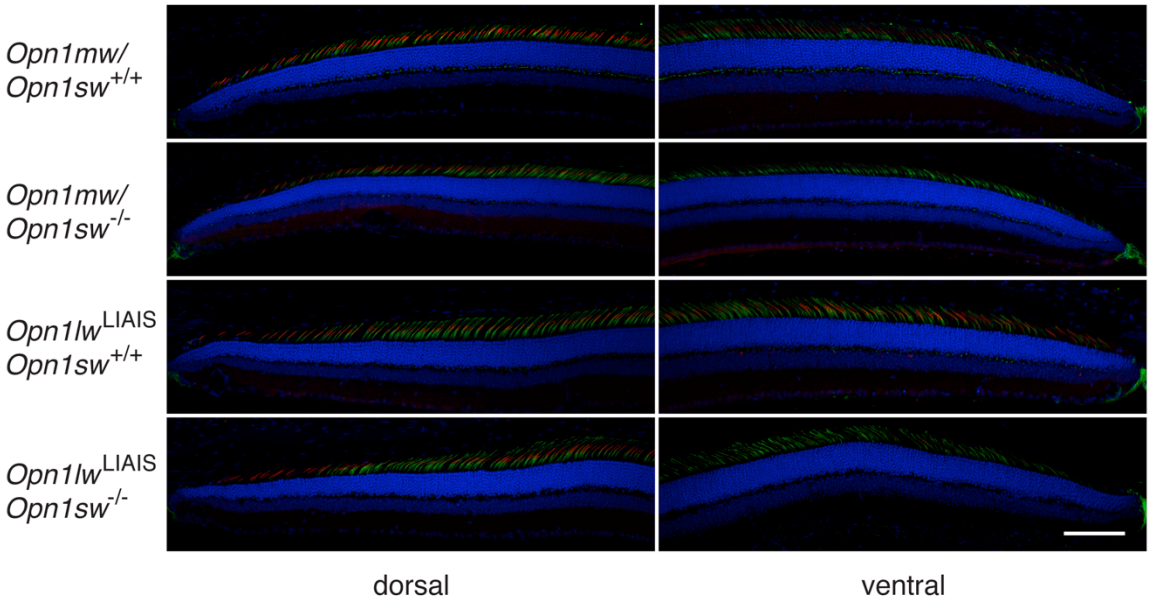
Opn1mw/
Opn1sw+/+
Opn1mw/
Opn1sw-/-
Opn1lwLIAIS
Opn1sw+/+
Opn1lwLIAIS
Opn1sw-/-
dorsal
ventral

***Figure 12*. Outer segment length measurements and cone counts in 16-month-old mice.** Immunolabeled sections from 16-month-old wildtype (n=5, black bars), *Opn1mw Opn1sw*$^{-/-}$ (n=5, gray bars), *Opn1lw*^{LIAIS} *Opn1sw*$^{+/+}$ (n=3, textured black bars), and *Opn1lw*^{LIAIS} *Opn1sw*$^{-/-}$ (n=5, textured gray bars) mice were imaged by widefield microscopy. **(A)** The number of cone outer segments with M/L-opsin labeling was counted in 2.8 mm^2 regions of the dorsal and ventral retina. **(B)** The lengths of the outer segments of cones remaining in 5.7 mm^2 regions within the dorsal and ventral retina were measured, and the average is reported for each line. Error bars represent the SEM.

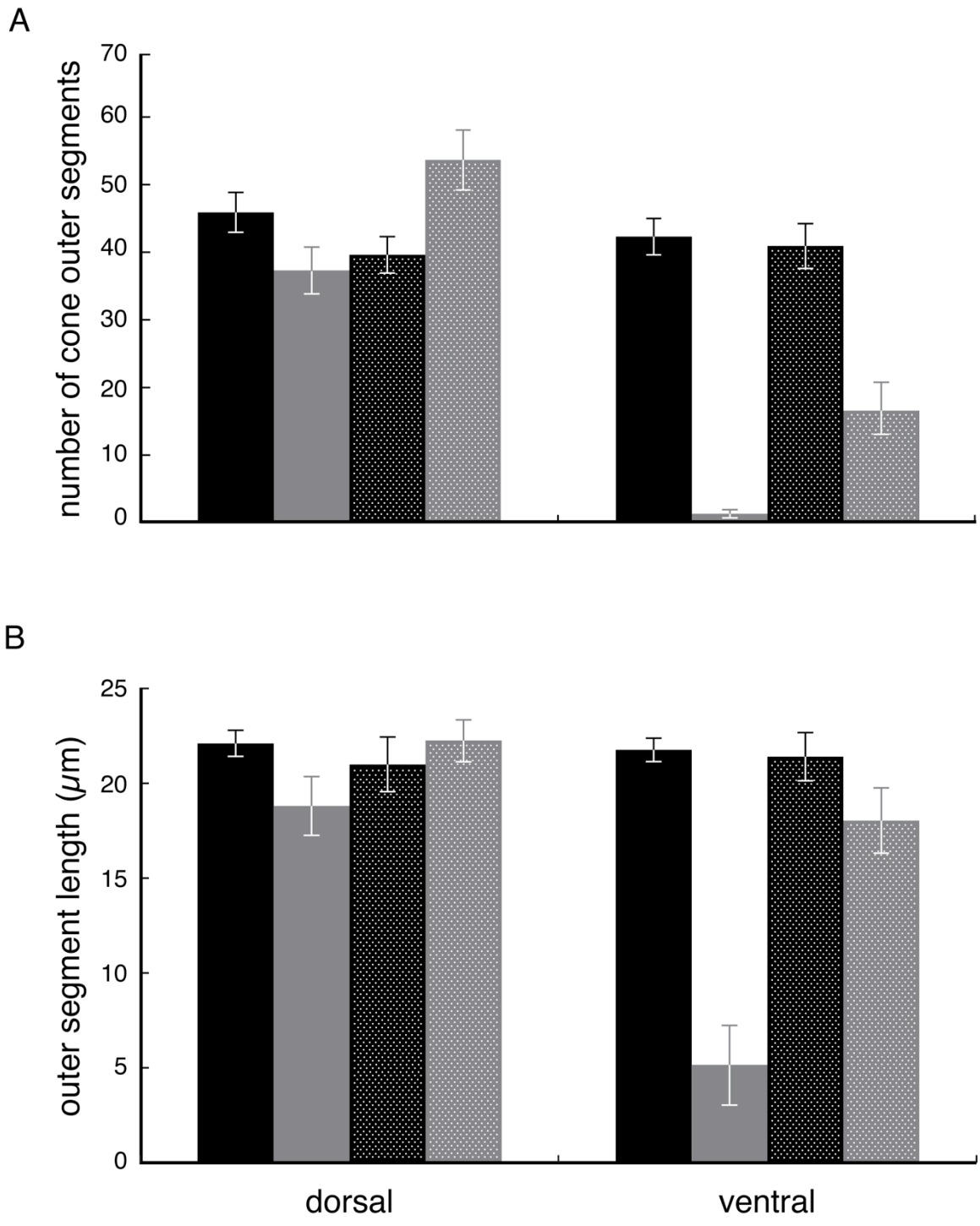
A
number of cone outer segments
70
60
50
40
30
20
10
0
B
outer segment length (μm)
25
20
15
10
5
0
dorsal
ventral

Discussion

The majority of cones in the wildtype mouse express both S- and M-opsin. One goal of the experiments described here was to create an S-opsin knockout mouse to be used for studying deleterious variants of human L- and M-opsin in isolation. The S-opsin mouse we constructed has no detectible response to lights that only modulate quantal catches in S photopigment. There was also no S-opsin detected at the protein level, and the fact that only a very faint band was observed in reverse transcriptase PCR from the *Opn1sw*$^{-/-}$ locus created here (Figure 3D) makes it most likely that any mRNA produced by remnants of the S-opsin gene is highly unstable and decays rapidly. Thus, the construction of the S-opsin mouse was successful.

Characterization of the S-opsin knockout illuminated important consequences of a decrease in opsin expression for cone structure and viability. Earlier, Daniele *et al.* (2011) inadvertently created a hypomorphic S-opsin mouse line by targeted integration of a Neomycin resistance gene within the *Opn1sw* gene, whereby the transcription of the Neomycin resistance gene presumably disrupted the expression of the S-opsin. Daniele and colleagues pooled data from mice ages 1.5 to 8 months and noted that the absence of S-opsin expression in their mouse line gave rise to increased M-opsin expression. An increase in M-opsin could be consistent with the ERG results reported here for mice younger than 6 months (Figure 9A); however, for mice over 8 months, our M-opsin mediated ERG amplitudes show a decline that is consistent a decrease in M-opsin. In addition, quantitative real-time reverse transcriptase PCR using 12-month-old mice indicate that M-opsin expression is ultimately reduced in the *Opn1sw*$^{-/-}$ mice compared to *Opn1sw*$^{+/+}$ mice (Figure 10).

In immunolabeling experiments, cones were observed in which there was no detectable opsin (M or S). We cannot determine whether apparently "empty" cones are indeed empty or whether they contain a an undetectably small amount of M-opsin, and likewise, it is unclear whether the "true

blue" cones that must be empty have degenerated. Nonetheless, taken together, the results support the conclusion that, over the long term, the *Opn1sw*$^{-/-}$ background leads to disruption of the cone outer segments.

Only a small fraction of the opsin expressed in most ventral cones is M-opsin. It is possible that, in young mice, the absence of competition with S-opsin transcripts for translational machinery allows for an increase in M-opsin production. This up-regulation could explain the initial increase in the M-opsin mediated ERG b-wave amplitudes that we observed in the *Opn1mw Opn1sw*$^{-/-}$ mice. However, if the normal amount of M-opsin expression in the ventral cones is only about 5-20% of the total and the increase in expression doubled that amount, most of these cones in the S-opsin knockout mouse would still have less than half the normal amount of opsin. The opsin protein is known to be an important structural component of the photoreceptor outer segment (Papermaster & Dreyer, 1974; Wald, Brown & Gibbons, 1963; Fliesler & Basinger., 1985) and those with insufficient opsin may be unstable and degenerate over the long term (Lem *et al*., 1999).

The two most engaging observations related to the loss of outer segments in the S-opsin knockout mice are 1) the human L-opsin appears to be more stable in the S-opsin knockout mouse than the wildtype mouse M-opsin and 2) the loss of the outer segment does not appear to affect the viability of the cone. Even in the ventral retinas, where the loss of outer segments is greatest, the retinas have normal numbers of cone nuclei. This latter observation may be a testament to how robust the cones are. One implication is that in some human vision disorders involving dysfunction of the opsin, the cones may remain viable and amenable to gene therapy.

Finally, an overarching goal was to develop an *in vivo* system to characterize the effects of variant L/M-opsin on the structure, function, and viability of the cones in order to understand the

diseases at a mechanistic level and to evaluate potential therapies. The outer segment damage produced by the S-opsin knockout was most pronounced in the ventral retina, where opsin co-expression is high in the wildtype mouse. In spite of this observation, the S-opsin knockout mice should serve the intended purpose of providing a testbed for studying mutant L and M opsins as long as the studies are restricted to the dorsal retina. Moreover, the problem seems even less of a concern since disruption of the cone outer segments was more apparent in the *Opn1mw Opn1sw*$^{-/-}$ than in the *Opn1lw*$^{\text{LIAIS}}$ *Opn1sw*$^{-/-}$ mouse, and it appears that in the absence of S-opsin, the human L-opsin is better able to stabilize the cone outer segment.

Chapter 2

Characterization of the effects on cone structure and function for a cone opsin variant that is associated with high myopia or cone dystrophy depending on the genetic background

Abstract

Successive occurrences of unequal meiotic recombination between the long (*OPN1LW*) and middle (*OPN1MW*) wavelength opsin genes have produced variant haplotypes that are increasingly being associated with eye diseases. One such L/M-opsin interchange variant, designated LVAVA to denote the amino acids encoded at positions 153, 171, 174, 178, and 180, has been linked to two distinct vision disorders. Males with LVAVA in one of the first two positions in the X-chromosome opsin gene array have high myopia, while those who have an LVAVA variant as their only X-chromosome opsin gene have cone dysfunction and cone dystrophy leading to extreme, uncorrectable vision loss. In the present study, loss of retinal function was measured by ERG in two men with the latter, non-syndromic disease. While cones expressing the LVAVA opsin were physiologically compromised, residual function was maintained into adulthood. Furthermore, these cones disrupted the function of neighboring S cones that did not harbor the toxic variant. In order to directly test the relationship between the LVAVA variant and pathology, the non-syndromic disease was modeled in a targeted gene replacement mouse in which the endogenous *Opn1mw* gene was exchanged for an engineered *Opn1lw*$^{\mathrm{LVAVA}}$ gene. ERG and histological experiments demonstrated that the mouse model faithfully recapitulated functional and morphological retinal defects associated with the human disease.

Introduction

Recently it was discovered that commonly occurring variants of human long (L) and middle (M) wavelength cone opsins are associated with high-grade myopia (MYP1) and with cone dystrophy (Carroll *et al.*, 2012; McClements *et al.*, 2013b). The L and M opsins are dimorphic at eighteen amino acid positions (for recent review, see Neitz & Neitz, 2011). Differences encoded by exon 5 of the genes distinguish L from M opsins in a stereotyped manner for the majority of humans (Neitz, Neitz & Kainz, 1996; Neitz & Neitz, 2011); exons 1 and 6 do not typically differ between L and M genes (Nathans, Thomas & Hogness, 1986b), and exons 2, 3 and 4 together specify 11 positions that are dimorphic among L, among M, and between L and M opsins. Exon 3 encodes five dimorphic positions: 153, 171, 174, 178 and 180. L- or M-opsin variants with the combination of exon 3 encoded dimorphisms of Leucine 153, Valine 171, Alanine 174, Valine 178 and Alanine 180 (abbreviated LVAVA) are associated with high-grade myopia (MYP1) (McClements *et al.*, 2013b) or with cone dystrophy (Carroll *et al.*, 2012), depending on the genetic background at the X-chromosome cone opsin locus.

The discovery that LVAVA cone opsin variants are deleterious was largely due to the fact that they are also associated with a rare syndrome, termed Bornholm Eye Disease (BED), that includes abnormal photopic ERGs and high-grade myopia (Haim, Fledelius & Skarsholm, 1988; McClements *et al.*, 2013b). All affected members of the original BED family were red-green color vision deficient males. Another family was identified as having symptoms nearly identical to that of the original BED family, except that the affected males had a different form of red-green color vision deficiency (Young *et al.*, 2004). This finding ultimately allowed the locus involved in BED, MYP1, to be mapped to Xq28 (Schwartz, Haims & Skarsholm, 1990; Young *et al.*, 2004), which is where the L and M cone opsin genes reside (official gene designations are *OPN1LW* and *OPN1MW*, respectively).

Rearrangement of the Xq28 opsin gene locus is the major cause of red-green color vision deficiency (Nathans *et al.*, 1986a), and likewise, this mechanism was responsible for the color vision defects observed in the affected members of both BED families (Young *et al.*, 2004). In a separate family identified with symptoms similar to BED, the disorder was also mapped to Xq28; however, those affected did not present with a color vision deficiency (Radhakrishna *et al.*, 2005; Ratnamala *et al.*, 2011). Sequencing of the *OPN1LW* and *OPN1MW* genes in the affected members of all three families revealed that the first gene in the array encodes an LVAVA variant, followed by a gene encoding another L or M variant. Thus, the affected males express the LVAVA variant in one submosaic of L/M cones and the variant encoded by the second gene in the array in another submosaic (McClements *et al.*, 2013a). Another characteristic reported for the BED phenotype was an abnormal cone ERG (Young *et al.*, 2004).

Two additional men were identified as having dichromatic color vision because of gene rearrangements at the Xq28 opsin gene locus that left just a single cone opsin gene in each case. Both men were diagnosed as having cone dystrophy, but not high-grade myopia, and their cone opsin genes were found to encode LVAVA variants (Carroll *et al.*, 2012). In these individuals, every L/M cone expressed the LVAVA variant. Thus, males who express an LVAVA opsin variant in a subset of L/M cones and a variant in the remaining L/M cones have high-grade myopia, whereas individuals who express an LVAVA opsin variant in all of their L/M cones have cone dystrophy. In order to understand how LVAVA variants contribute to myopia and to cone dystrophy, we must first understand the effects of LVAVA variants on cone photoreceptor structure and function. To this end, we examined the function of cones expressing an LVAVA variant in human subjects who express the LVAVA variant in all of their L/M cones. Furthermore, we examined the effects of the LVAVA variant on cone structure and function in genetically engineered mice in which the S-opsin gene was knocked-out and the endogenous

mouse M-opsin gene on the X-chromosome had been replaced either with a human LVAVA L-opsin variant or by a control normal human L-opsin variant.

Materials and methods

Human subjects

Two male subjects each had a single opsin gene on the X-chromosome, and in both cases, the gene encoded an LVAVA variant. Results from genetic analysis and retinal imaging studies were reported previously for these subjects (Carroll *et al.*, 2012). One subject (subject JC_0347) had only an L-opsin gene on his X-chromosome, while the other subject (subject JC_0564) had only an M-opsin gene (Carroll *et al.*, 2012). At the time of our experiments, JC_0347 was 33 years old and JC_0564 was 45 years old. Both subjects exhibited nystagmus. For comparison, the same experiments were conducted on five control subjects (mean age 27 years; age range 22-33 years). Experiments on human subjects were approved by the Institutional Review Board at the University of Washington and were conducted in accordance with the principles embodied in the Declaration of Helsinki.

Mice

Animal experimentation conformed to the principles regarding the care and use of animals adopted by the American Physiological Society and the Society for Neuroscience. Animal experimentation conducted here was approved by the Animal Care and Use Committee at the University of Washington. Three lines of genetically modified mice were created by Ozgene, Inc. (Perth, Australia). The general design of the modified X-chromosome opsin gene locus used in two of these mouse lines is described elsewhere (Smallwood *et al.*, 2003; Greenwald, *manuscript in preparation*, and Chapter 1). For this locus, one construct was designed to replace the endogenous mouse *Opn1mw* gene with a human cDNA encoding a normal L cone opsin with the following amino acids at the polymorphic positions encoded by exon 2, 3 and 4: threonine 65, isoleucine 111, serine 116, Leucine 153, isoleucine 171, alanine 174, isoleucine 178, serine 180, isoleucine 230, alanine 233, and methionine 236, and abbreviated LIAIS according to positions 153, 171, 174, 178, and 180. The corresponding modified locus is *Opn1lw*$^{LIAIS/LIAIS}$ for

females or *Opn1lw*$^{LIAIS/Y}$ for males. Males and females were used interchangeably in this study, and for simplicity, the control locus is referred to as *Opn1lw*^{LIAIS}. The second construct was designed to replace the endogenous mouse *Opn1mw* gene with an LVAVA variant that was identical in all respects to the *Opn1lw*^{LIAIS} control, except for the codons encoding the amino acids at positions 171 and 180. Consistent with the *Opn1lw*^{LIAIS} mice, both males and females were used in experiments and are collectively referred to as *Opn1lw*^{LVAVA}. The third construct was designed to delete a region of the mouse *Opn1sw* gene extending from within intron 1 to intron 4, thereby creating an S-opsin knockout mouse, designated *Opn1sw*$^{-/-}$. All three modified loci were confirmed by direct sequencing of genomic DNA and of cDNA derived from retinal messenger RNA (mRNA) for the *Opn1lw*^{LIAIS} and *Opn1lw*^{LVAVA} mice. The different lines of mice were bred to create two double mutant lines: *Opn1lw*^{LIAIS} *Opn1sw*$^{-/-}$ and *Opn1lw*^{LVAVA} *Opn1sw*$^{-/-}$ so that the LVAVA variant could be investigated in isolation of other photopigments. This was necessary because mouse cone photoreceptors normally co-express S- and L/M-opsin, whereas human cone photoreceptors do not. All mice used in experiments described here were verified by genotyping using the polymerase chain reaction as previously described in detail (Young *et al.*, 2004). The *Opn1sw*$^{-/-}$ and *Opn1lw*^{LIAIS} *Opn1sw*$^{-/-}$ lines were previously validated and that has been published elsewhere (Greenwald, *manuscript in preparation*, and Chapter 1).

Electroretinogram (ERG)

Cone photoreceptor function was examined using the ON-OFF (long-flash) ERG. Dilation, electrodes, and electrode placement were as described previously for humans (Carroll *et al.*, 2000), and for mice (Greenwald, *manuscript in preparation*, and Chapter 1). Mice were anesthetized with an intraperitoneal injection of ketamine (110.25 mg/kg) and xylazine (11.025 mg/kg) diluted in sterile saline.

For human subjects, a Roland Consult (Brandenburg, Germany) Q450 Ganzfeld system was modified to hold ten 1 Watt (W) LEDs that peak at 414 nanometers (nm). The Q450 also had built in LEDs that peak at 525 nm, 594 nm, and 641 nm. For mice, a Roland Consult Q400 was modified to hold twenty-six LEDs that peak at 520 nm and 26 LEDs that peak at 365 nm (Nichia NSHU590A).

Custom circuitry controlled the LED intensities with pulse-width modulation, which provided a linear intensity response with no shift in peak wavelength. Frame sync pulses from the software controlled the timing of the LEDs, and the light stimulus flashed at approximately 1 Hz with a 50% duty cycle. During the first 500 ms of each cycle (Phase 1), quantal catch increased for the specific photopigment-isolating stimulus (S or M/L), while in the final 500 ms (Phase 2), the quantal catch decreased. A silent substitution paradigm was used to hold the non-targeted photopigment(s) constant over both phases. ON and OFF responses were generated at the interfaces between the two phases, and the duration of each phase was set so that retinal activity would return to baseline. Additionally, a 20 Hz–100 Hz band-pass filter was used to reject non-retinal signals that can occur during the 1s interval while still allowing the main ERG components to pass.

The technique used to calculate the quantal catch of each photopigment has been described previously (Pauers *et al.*, 2012), with an added estimate for the yellowing of the lens as a function of age (Pokorny, Smith & Lutze 1987). Light intensity values for human M/L cone ERGs were calculated such that M- and L-cones were modulated together with the same quantal increase. Assuming M- and L-cones contribute linearly to the ERG waveform, this method yields equal ERG amplitudes despite variations in cone ratio. For the S photopigment-isolating condition, light intensities were modulated with a larger quantal increase. This increase in quantal modulation was done because, compared to (M+L) cone isolation, the S cone signal-to-noise ratio

is relatively low given that S cones comprise only ~6% of the cone photoreceptor population (Carroll *et al.*, 2004).

Humans and mice were light adapted under standard fluorescent room lighting. In both species, ERGs were performed under photopic conditions with background lights adjusted to suppress rod activity. For human ERGs, the number of stimulation cycles contributing to a single trial was variable; each trial was terminated when additional cycles did not appreciably change the averaged waveform. For instance, taking the average of ~100 cycles was often necessary for measuring S cone-isolated ERGs. For mouse ERGs, all waveforms represent the average of 20 stimulation cycles. Retinal function was assessed by the amplitude of the ERG b-wave, which was measured as the absolute voltage change between the a-wave and b-wave peaks. In the photopic ERG a-, b- and d-waves are considered to be generated by cones/OFF-bipolar, ON-bipolar, and OFF-bipolar cells respectively (Bush & Sieving, 1996). Because there is no specific S-OFF bipolar cell (Dacey & Packer, 2003), the S cone ERG was considered to be properly isolated when no d-wave was present in the waveform.

Immunocytochemistry & image acquisition in mice

Mice were euthanized with a lethal dose of sodium pentobarbital (Nembutal 50mg/mL) at 3 months (n=4 per line), 10 months (n=1 per line), and 16 months (n=5 per line) of age. Tissue was fixed via a dual stage intracardial perfusion of 4% paraformaldehyde followed by a cocktail of 4% paraformaldehyde + 1% glutaraldehyde. The eyes were dissected and 100 µm thick sagittal sections were made using a vibratome so that each specimen contained the dorsal and ventral retina. Sections were incubated with 1% sodium borohydride in PBS for 30 minutes at room temperature (RT) and then washed thoroughly in PBS. Sections were incubated overnight at 4°C with a solution containing 5% donkey serum (Jackson ImmunoResearch, Cat #004-000-120), 1mg/ml BSA (Jackson ImmunoResearch, Cat #001-000-161), and 0.03% Triton X-100 in PBS

(pH 7.4). A rabbit anti-M/L-opsin primary antibody was used at a dilution of 1:200 (Millipore, Cat # AB405) and goat anti-S-opsin primary antibody (Santa Cruz Biotechnology, Cat # sc-14365) was used at a dilution of 1:100. Primary antibodies were incubated at 4°C for at least 3 days for sections and 2 days for whole mount tissue. Specimens were washed in PBS 3 times for 30 minutes each, and incubated overnight at 4°C with DAPI (4',6-diamidino-2-phenylindole,dihydrochloride 1:10,000; Invitrogen, Cat # D-21490) plus secondary antibodies. The secondary antibody for the L/M-opsin antibody was Alexa Fluor 488 labeled donkey anti-rabbit IgG (H+L) diluted 1:200 in antibody dilution buffer (Invitrogen, Cat # A21206) and the secondary antibody for the S-opsin antibody was Alexa Fluor 633 labeled donkey anti-goat IgG(H+L) diluted 1:200 (Invitrogen, Cat # A21082). This was followed by three 30 minute PBS washes, 30 minutes of post-fixation with 4% paraformaldehyde, and three more 30 minute PBS washes. Finally, the retina slices were placed on slides with 2% DABCO in glycerol and cover-slipped. Nuclei and cone sheaths were labeled with DAPI and PNA, respectively. 30x widefield images were acquired from the dorsal retina and L-opsin labeled outer segments were individually counted and measured in length. All images, 292.5 µm in width, were taken ~200 µm ventral to the ora serrata. The depth of the z-stack used for measuring outer segment lengths was 19.5 µm and a 9.5 µm substack was generated for the outer segment counts. Confocal images were acquired using an Olympus FluoViewTM FV1000 confocal microscope with a 20x or 60x oil-immersion lens. Z-stacks were combined using Image J software (Schneider *et al.*, 2012) and channel exposure levels were balanced within and across images using Adobe Photoshop.

Results

ERG defects in human subjects with all L/M cones containing an LVAVA opsin

In response to an L/M cone-isolating stimulus (525 nm), the average b-wave amplitude from the single-gene subjects (n=2) was 88.4% ($p<0.01$) lower compared to that of the normal subjects (n=5) (**Figure 13A**). As illustrated in **figure 13B**, scaling the data five-fold for the LVAVA subjects revealed characteristic ERG a-, b-, and d-waves, with timing consistent with the normal waveform. We tested the hypothesis that this low-level function in the subjects' LVAVA cones might be due to S cone contribution to the ERG as a result of imperfect L/M cone-isolating conditions. This experiment was carried out by measuring the retinal responses in each subject to the 525 nm stimulus versus the 641nm stimulus (LED intensities were equated to account for L and M cone luminosity functions). The two stimuli elicited equivalent responses (2.5 μV each) from L cones in the *OPN1LW*^{LVAVA} subject (**Figure 14A**). However, for the subject with only *OPN1MW*^{LVAVA} gene, the 525 nm light would be expected to more strongly activate the photopigment than the 641nm light. Correspondingly, this subject produced a larger amplitude ERG in response to the 525 nm stimulus (6.4 μV versus 2.6 μV, respectively) **(Figure 14B)**. Together, these results indicate that the ERGs shown in Figure 13 were generated by the M or L cones with little or no contribution from S cones.

Furthermore, in order to determine whether the effects of an LVAVA opsin variant were confined to the cones expressing it or whether nearby photoreceptors were also affected, S cone ERGs were collected from the same single-gene LVAVA subjects and normal subjects (**Figure 15**). Deflections that occurred just after light onset in the single-gene LVAVA subjects' averaged waveform were consistent with ERG a- and b-waves. However, the signal was small compared to normal, and the timing of the putative b-wave wave was inconsistent with the normal S cone ERG. The ERG amplitude was 57.3% ($p=0.01$) lower compared to the normal subjects, and the peak of the b-wave was accelerated by 5.0 ms ($p<0.05$). Signal artifacts in the single-gene

LVAVA subjects' ERGs were attributed to eye blinks and eye movements/nystagmus (e.g. deflection peaking at 173 ms in Figure 14b).

***Figure 13*. Human LVAVA cones have decreased function.** (**A**) Retinal responses to a 525 nm light stimulus in LVAVA subjects (n=2, gray trace) were weaker than in normal subjects (n=5, black trace). (**B**) Vertically scaling the LVAVA subjects' waveform by 5x showed that genuine ERGs were generated. Characteristic features of the ERG were present at light onset and light offset, including the a-, b-, and d-waves (labeled).

A

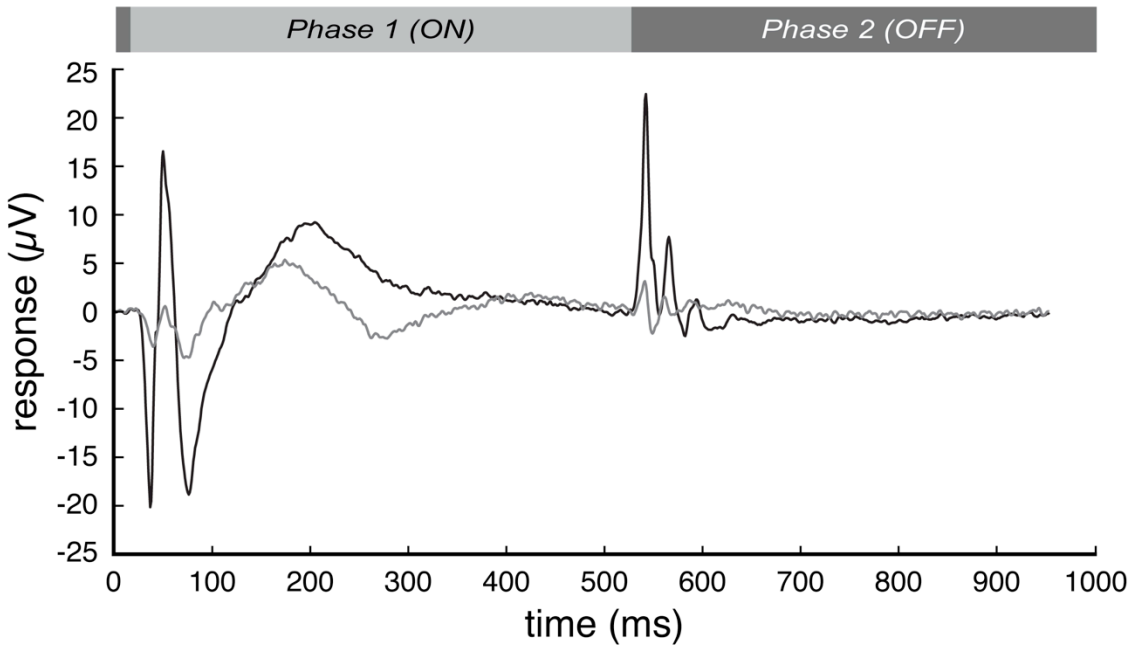
Phase 1 (ON)
Phase 2 (OFF)
response (μV)
time (ms)

B

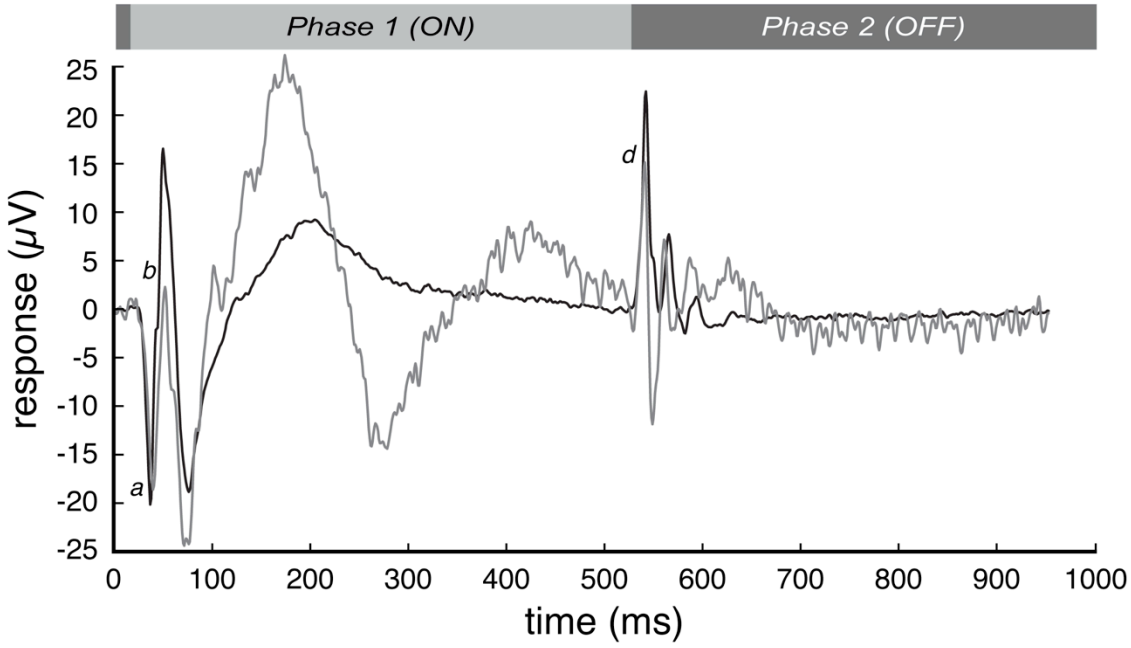
Phase 1 (ON)
Phase 2 (OFF)
a
b
d
response (μV)
time (ms)

***Figure 14*. S cone activation does not account for ERGs detected in human LVAVA cones.** ERGs in response to a 525 nm stimulus (black traces) and a 641 nm stimulus (gray traces) were collected from two LVAVA subjects. (**A**) For the subject with only the *OPN1LW*^{LVAVA} gene, the responses to both stimuli were equivalent. (**B**) The M cone responses to the 641 nm stimulus were comparatively weaker than to the 525 nm stimulus in the *OPN1MW*^{LVAVA} subject. If S cones mediated these subjects' M/L ERGs, then the 641 μV stimulus would have generated weaker ERGs than the 525 nm stimulus in both cases.

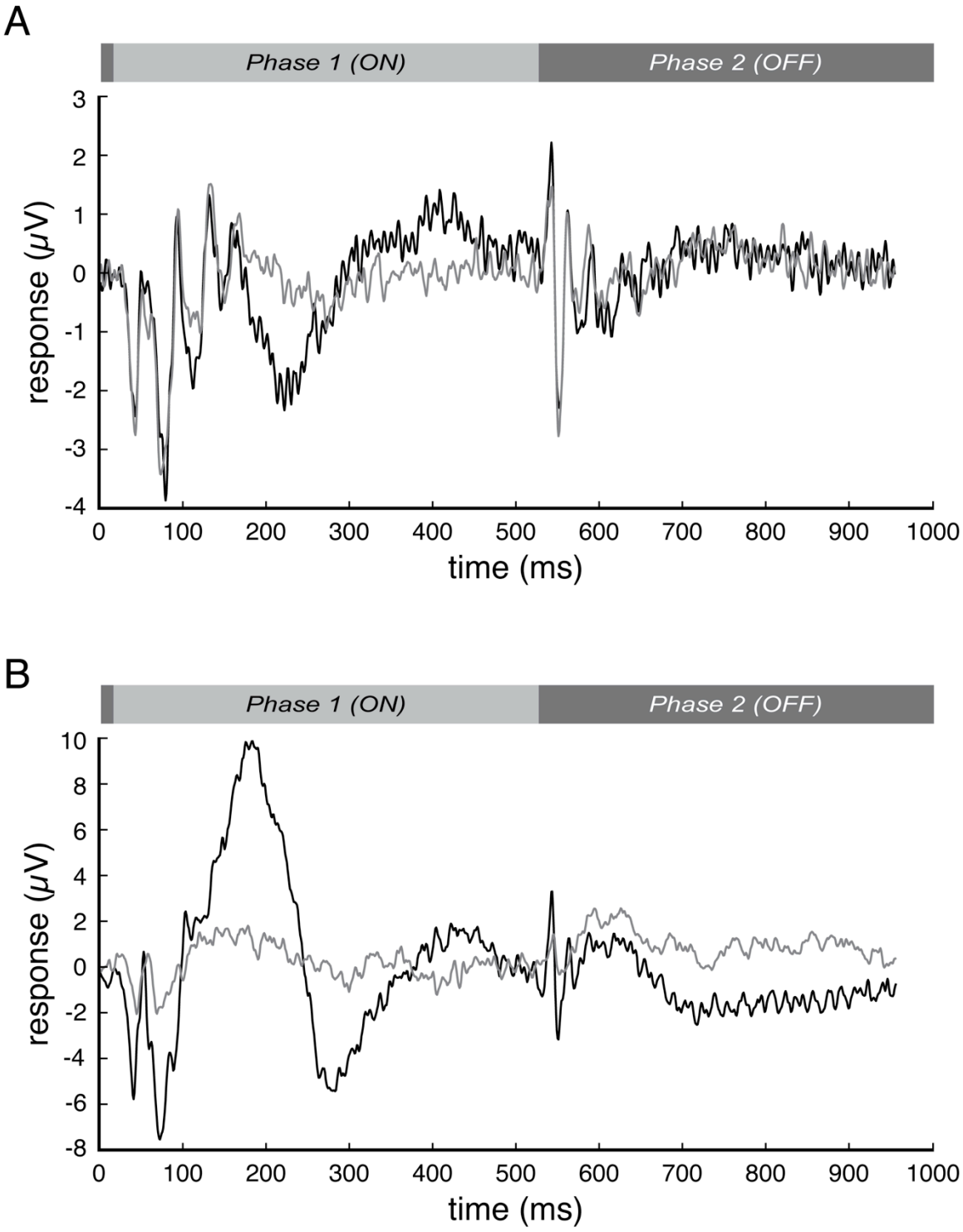
A
Phase 1 (ON)
Phase 2 (OFF)
response (μV)
time (ms)
B
Phase 1 (ON)
Phase 2 (OFF)
response (μV)
time (ms)

***Figure 15*. LVAVA cones cause non-cell autonomous dysfunction in S cones.** S cone isolated ERGs were recorded from *OPN1LW*^{LVAVA} (n=2, gray trace) and normal (n=5, black trace) subjects. The S cone-mediated retinal responses were not only 57.3% weaker than normal in the *OPN1LW*^{LVAVA} subjects ($p=0.01$), but the timing of the b-waves were accelerated by 5.0 ms ($p<0.05$). These results suggest that the *OPN1LW*^{LVAVA} gene conveys toxicity to neighboring photoreceptors.

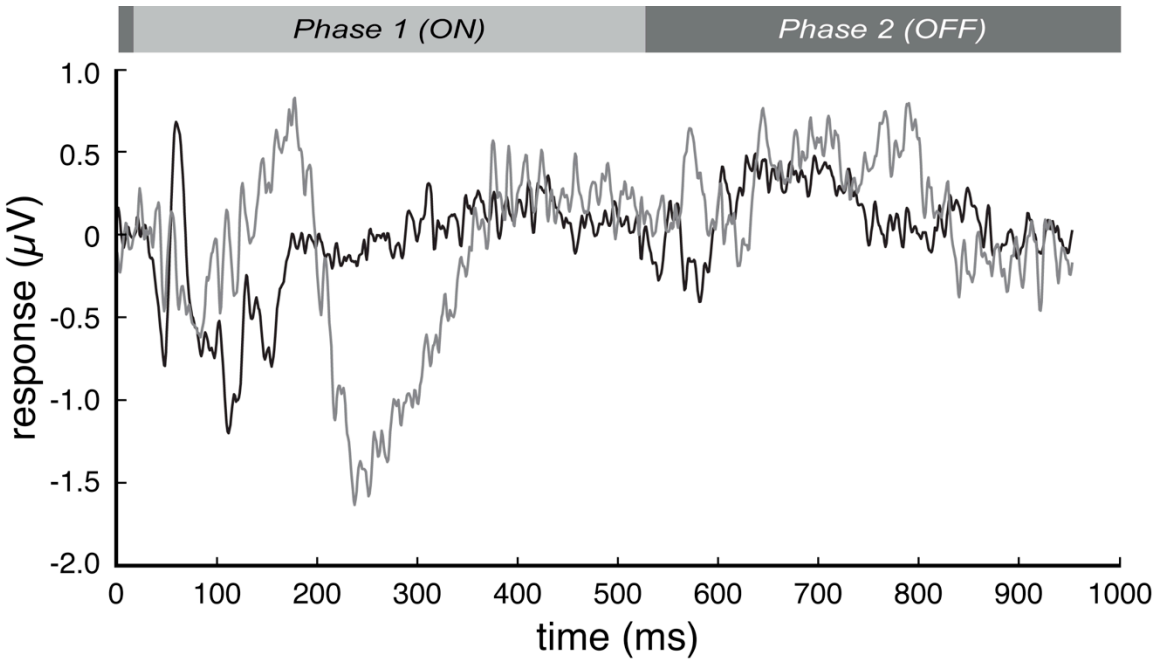
Phase 1 (ON)
Phase 2 (OFF)
1.0
0.5
0
-0.5
-1.0
-1.5
-2.0
response (μV)
0
100
200
300
400
500
600
700
800
900
1000
time (ms)

Decreased retinal function in LVAVA mice

L cone ERGs were measured in *Opn1lw*^{LVAVA} mice across the first sixteen months of life. Due to natural age-related mortality and occasional technical issues with the preparation, there were fewer animals for some data points **(Table 3)**. Using a 520 nm light stimulus (3.0 μW/mm^2 stimulus), retinal responses were collected in the same mice from four months through sixteen months of age and in a separate set of mice at six weeks of age (**Figure 16A**). While an age-dependent decrease in amplitude was observed in both lines, as expected from previous studies of aging mice (Williams & Jacobs, 2007), the *Opn1lw*^{LVAVA} *Opn1sw*$^{-/-}$ mice generated significantly weaker L cone responses than the *Opn1lw*^{LIAIS} *Opn1sw*$^{-/-}$ mice at each time point tested (Table 3). On average, the b-wave amplitudes in the *Opn1lw*^{LVAVA} *Opn1sw*$^{-/-}$ mice were diminished by 24.6 μV ± 4.0, and the effect was maintained across a broad range of light levels. For example, at the twelve-month time point, the *Opn1lw*^{LVAVA} *Opn1sw*$^{-/-}$ mouse exhibited weaker sensitivity than the control mouse at each light level tested in an intensity response series, ranging from 0.4 μW/mm^2 to 11.8 μW/mm^2 with statistical significance observed from 0.4 μW/mm^2 to 3.0 μW/mm^2 (**Figure 16B**, **Table 4**). The dotted lines in Figure 16B illustrate that approximately twice the level of stimulation intensity would be necessary to generate a 60 μV ERG in the *Opn1lw*^{LVAVA} *Opn1sw*$^{-/-}$ mice versus the *Opn1lw*^{LIAIS} *Opn1sw*$^{-/-}$ mice.

Table 3. **L cone ERGs collected across 16 months in *Opn1lw*^{LVAVA} and *Opn1lw*^{LIAIS} mice.**

Mouse Line	Age (m)	# of mice	b-wave (μV)	SEM	p-value
Opn1lw^{LIAIS}	1.5	15	149.4	13.3	0.026
Opn1lw^{LVAVA}	1.5	15	114.4	6.6	
Opn1lw^{LIAIS}	4	9	123.4	10.2	0.015
Opn1lw^{LVAVA}	4	14	93.3	6.3	
Opn1lw^{LIAIS}	6.5	4	78.4	3.5	0.029
Opn1lw^{LVAVA}	6.5	13	53.6	5.5	
Opn1lw^{LIAIS}	9	10	60.3	8.0	0.0035
Opn1lw^{LVAVA}	9	13	35.5	2.6	
Opn1lw^{LIAIS}	12	9	60.0	9.5	0.0078
Opn1lw^{LVAVA}	12	13	34.2	3.2	
Opn1lw^{LIAIS}	16	9	67.7	8.1	0.00013
Opn1lw^{LVAVA}	16	12	31.5	2.6	

***Figure 16*. Mouse *Opn1lw*^{LVAVA} cones have decreased function**. L cone ERGs were collected from *Opn1lw*^{LIAIS} (black symbols) and *Opn1lw*^{LVAVA} (gray symbols) across 16 months. (**A**) Using a 520 nm light stimulus (3.0 μW/mm^2), retinal responses were measured in the same mice from 4 months through 16 months of age (closed circles) and in a separate set of mice at 6 weeks of age (open diamonds). The *Opn1lw*^{LVAVA} mice had significantly weaker responses at each time point. (**B**) Retinal responses to an intensity series (0.4 μW/mm2 to 11.8 μW/mm^2) are shown for the mice at 12 months of age. The *Opn1lw*^{LVAVA} mice had weaker responses at each time point, with statistical significance from 0.4 μW/mm^2 to 3.0 μW/mm^2. The dotted lines illustrate that approximately twice the light intensity would be needed to generate a 60 μV ERG from the *Opn1lw*^{LVAVA} mice as from the *Opn1lw*^{LVAVA} mice. Error bars represent the SEM and data were fit using a cumulative normal function (dashed traces).

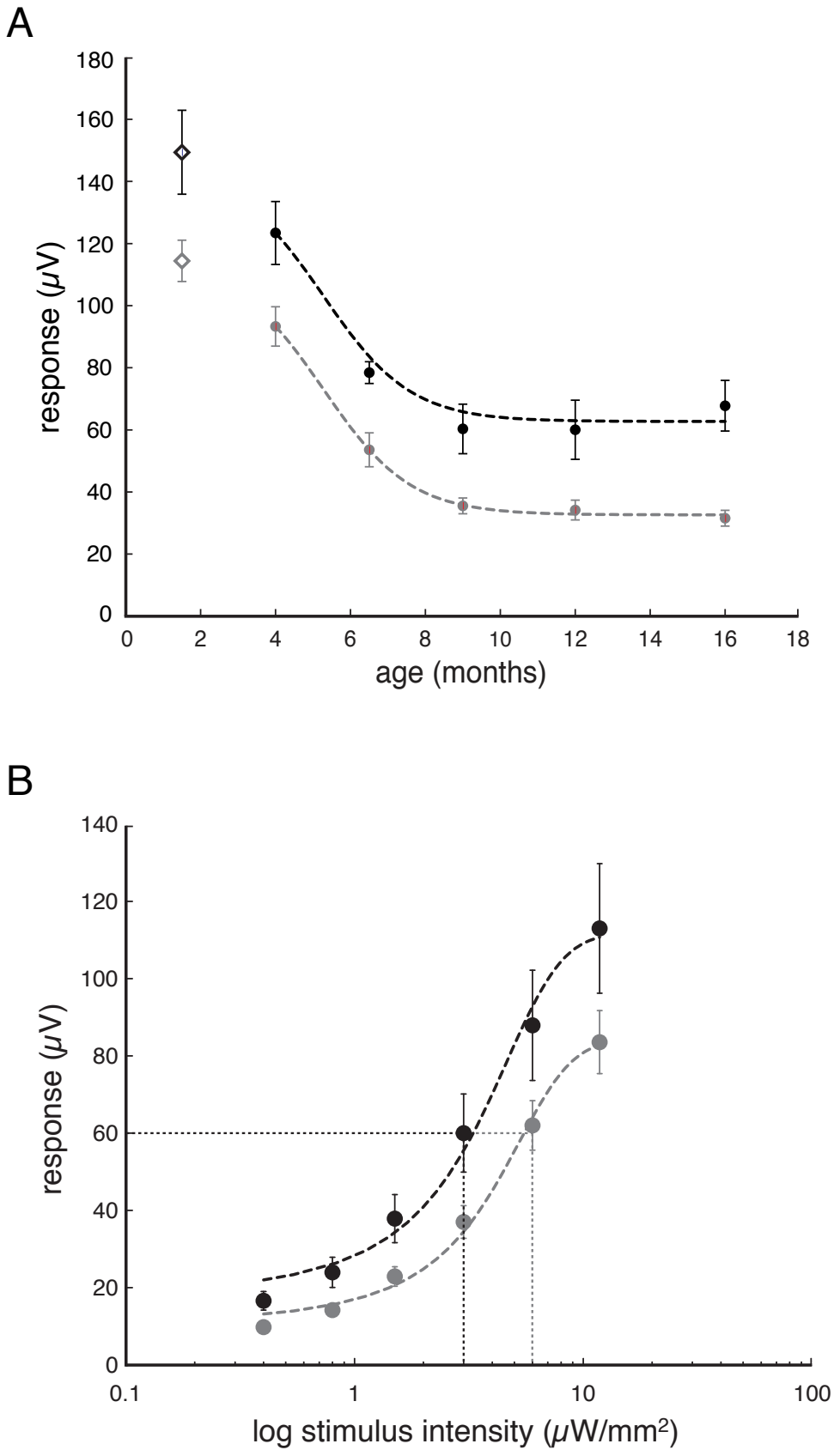
A
180
160
140
120
100
80
60
40
20
0
response (μV)
0
2
4
6
8
10
12
14
16
18
age (months)
B
140
120
100
80
60
40
20
0
response (μV)
0.1
1
10
100
log stimulus intensity (μW/mm²)

***Table 4*. Intensity response series collected in 16-month-old *Opn1lw*^{LVAVA} and *Opn1lw*^{LIAIS} mice.**

Mouse Line	# of mice	Stimulus (μW/mm^2)	b-wave (μV)	SEM	p-value
Opn1lw^{LIAIS}	9	0.4	16.6	2.4	0.0043
Opn1lw^{LVAVA}	14	0.4	9.8	1.0	
Opn1lw^{LIAIS}	9	0.8	24.0	3.9	0.010
Opn1lw^{LVAVA}	13	0.8	14.2	1.3	
Opn1lw^{LIAIS}	9	1.5	37.9	6.2	0.014
Opn1lw^{LVAVA}	14	1.5	22.9	2.5	
Opn1lw^{LIAIS}	9	3.0	60.0	10.1	0.020
Opn1lw^{LVAVA}	14	3.0	37.0	4.2	
Opn1lw^{LIAIS}	9	6.0	87.9	14.3	0.063
Opn1lw^{LVAVA}	14	6.0	62.0	6.4	
Opn1lw^{LIAIS}	9	11.8	113.0	16.8	0.079
Opn1lw^{LVAVA}	14	11.8	83.6	8.2	

Cone outer segment retraction in the LVAVA mouse

The distribution of L-opsin immunoreactivity showed evidence of cone outer segment retraction in the *Opn1lw*^{LVAVA} mouse model beginning early in life, as compared to the *Opn1lw*^{LIAIS} *Opn1sw*$^{-/-}$ control mouse. In images acquired by widefield microscopy, cone outer segments were measured in length and individually counted within the dorsal retinas of three-month-old (n=4 per line) and 16-month-old (n=5 per line) mice. The lengths of the *Opn1lw*^{LVAVA} *Opn1sw*$^{-/-}$ cone outer segments in the dorsal retina were 16.1% ($p<0.03$) shorter than control at three months of age and 23.2% ($p=0.02$) shorter at sixteen months. There was no significant change in outer segment length over time within either mouse line (**Figure 17A**). Furthermore, no significant difference in the number of visible outer segments was observed between the two mouse lines at either the three or sixteen month time point, although the counts tended to be reduced in the *Opn1lw*^{LVAVA} *Opn1sw*$^{-/-}$ mouse (**Figure 17B**). Representative specimens that were analyzed for Figure 16 were re-imaged by confocal microscopy at 20x magnification (**Figure 18A**), and additional confocal images were acquired from the dorsal retina of mice at an intermediate age of ten months (**Figure 18B**). Images reacquired at the outlined regions of the 20x images (top row) at 60x magnification (bottom row) in 10-month-old mice are shown.

***Figure 17*. Outer segment length measurements and cone counts in 3 and 16-month-old mice.** Immunolabeled sections from 3-month-old (n=4 per line) and 16-month-old (n=5 per line) *Opn1lw*^{LIAIS} (black bars) and *Opn1lw*^{LVAVA} (gray bars) mice were imaged by widefield microscopy (30x). For each specimen, (**A**) the lengths of L-opsin labeled cone outer segments within a 5.7 mm^2 region of the dorsal retina were measured, and (**B**) the number outer segments remaining in a 2.8 mm^2 subregion were tallied. Error bars represent the SEM.

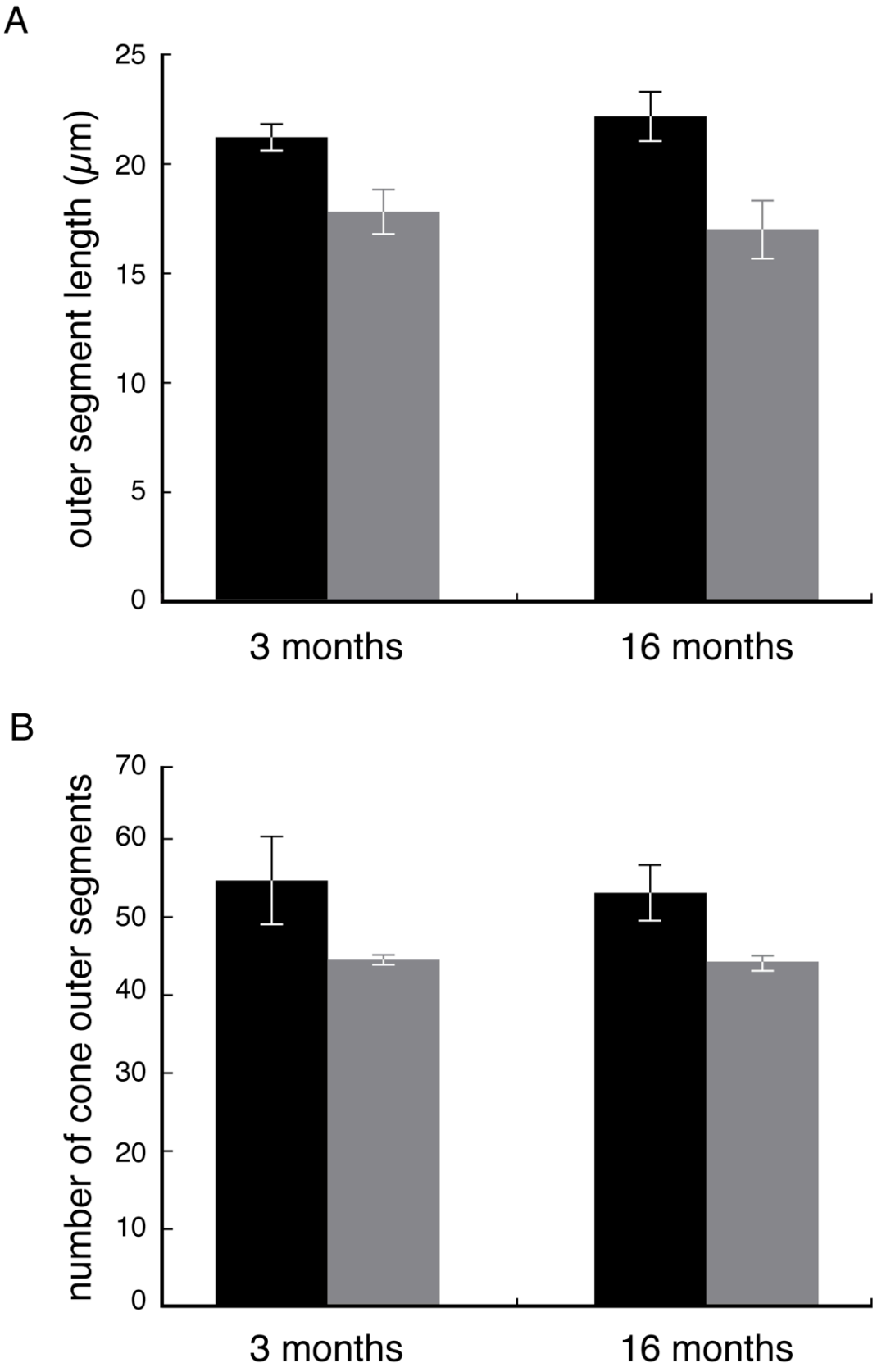
A
outer segment length (μm)
25
20
15
10
5
0
3 months
16 months
B
number of cone outer segments
70
60
50
40
30
20
10
0
3 months
16 months

***Figure 18*. Mouse *Opn1lw*^{LVAVA} cones are morphologically compromised**. Confocal images of sections were acquired at the far dorsal retina. M-opsin (red), cone sheaths (green/PNA), and nucleic acid (blue/DAPI) were labeled. 19.5 µm z-stacks (0.5 µm spacing) were imaged at 20x magnification, and 13.8 µm z-stacks (0.35 µm spacing) were imaged at 60x magnification. (**A**) In comparison to age-matched *Opn1lw*^{LIAIS} mice (top row), cone outer segments were foreshortened and withered in 3-month-old (left column) and 16-month-old (right column) *Opn1lw*^{LVAVA} mice (bottom row) (**B**) The region contained within each dotted box from the 20x images (top row) of 10-month-old *Opn1lw*^{LIAIS} (**left column**) and *Opn1lw*^{LVAVA} (right column) mice was re-imaged at 60x (**bottom row**). Scale bar represents 100 µm for 20x images and 33.3 µm for 60x images.

A

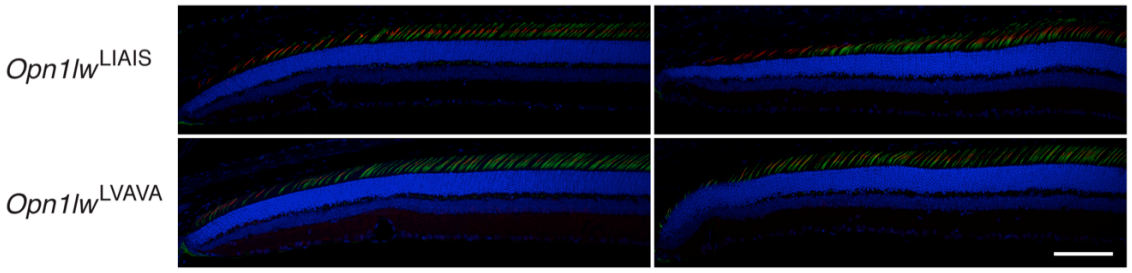
Opn1lw^LIAIS
Opn1lw^LVAVA
3 months
16 months

B

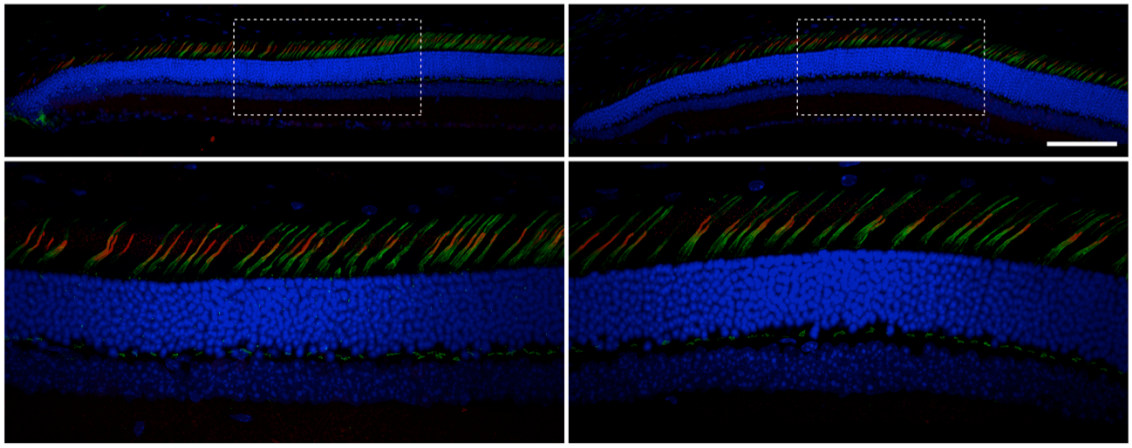
Opn1lw^LIAIS
Opn1lw^LVAVA

Discussion

This study provides direct evidence that an L/M-opsin interchange variant causes cone dysfunction. Here, cone-isolating stimuli were used to directly probe the activity of the cones containing an LVAVA opsin variant both in humans and mice. The fact that the human subjects with *OPN1LW*^{LVAVA} or *OPN1MW*^{LVAVA} as the only opsin gene on the X-chromosome and the *Opn1lw*^{LVAVA} *Opn1sw*$^{-/-}$ mice all exhibited abnormal cone ERGs, while the *Opn1lw*^{LVAVA} *Opn1sw*$^{-/-}$ mice did not, provide direct evidence that the LVAVA opsin variant is responsible for the ERG phenotype.

The distribution of L-opsin in the dorsal retina in three-, ten-, and sixteen-month-old mice indicated outer segment retraction. This is consistent with previous OCT data from single-gene LVAVA patients (Carroll *et al.*, 2012). The degree of outer segment retraction did not differ significantly between mice at three and sixteen months of age, but this defect was associated with decreased cone function as ERGs revealed weakened responses to light by six weeks; however, this decrement remained stable across sixteen months of testing in comparison to the control mice. Moreover, ERGs in *Opn1lw*^{LVAVA} *Opn1sw*$^{-/-}$ mice were weaker than control animals regardless of the intensity of the L-photopigment activating light.

Recently, the results of *in vitro* experiments were reported for an LVAVA variant of the L-opsin gene. The study provides evidence that the nucleotide substitutions associated with the amino acid combination of LVAVA, plus two silent substitutions specified by exon 3, causes an error in exon definition that results in the production of a mixture of full-length mRNA and a truncated mRNA in which exon 3 is skipped (Ueyama *et al.*, 2012). Those authors contend that vision deficits are entirely due to faulty splicing and completely independent of the amino acid sequence. However, both the *Opn1lw*^{LVAVA} mice and the control *Opn1lw*^{LIAIS} mice created here only have to join exons 1 and 2 by splicing out intron 1, while all the other exons are "pre-

spliced" as a consequence of the structure of the knock-in loci. Thus, the cone function abnormalities in *Opn1lw*^{LVAVA} *Opn1sw*$^{-/-}$ mice, compared to the control mice, are attributable to the amino acid sequence of the L cone opsin. These results provide direct evidence that the LVAVA amino acid combination is deleterious. Ueyama and colleagues also reported that several other variants gave mixtures of normally and abnormally spliced transcripts, including exon 3 haplotypes commonly found in non-Japanese populations that are not associated cone dystrophy or severe myopia (e.g. LIAIS and MVVVA). The minigene experiments of Ueyama et al. showed that some aberrantly spliced minigenes skipped exon 2 and some skipped exons 2 and 3. Thus, it is possible that some of the aberrant splicing was an artifact of the *in vitro* experiments. What the experiments reported here make clear is that the combination of amino acids specified by exon 3, LVAVA, causes abnormal function at the level of the amino acid sequence.

As in the mice, L/M cone-isolated ERGs measured in single-gene human subjects demonstrated that LVAVA cone function was diminished in comparison to normal subjects. Based on this result, it was unclear whether the subjects had a full complement of cones that function poorly or if many cones within this population were incapable of transducing light. In mice, the remaining LVAVA cone function was associated with a normal number of outer segments, but these outer segments were abnormally short. Therefore, while LVAVA cones are structurally and functionally defective, it appears that they remain alive and weakly responsive to light. The finding that LVAVA cones remain viable, albeit dysfunctional, suggests that rescuing vision by gene therapy across a wide range of ages may be feasible.

The single-gene human subjects also produced S cone ERGs that were abnormal in amplitude and temporal profile. They also had visual acuities of 20/150 to 20/200, which is worse than for blue cone monochromats who typically have acuities of 20/80 (Green, 1972). Together these findings

indicate that toxicity of the LVAVA variant was not confined to the class of cone that harbored the variant opsin. Using mice to confirm whether LVAVA cones disrupt neighboring cones was not possible because the mice used here only expressed LVAVA L-opsin in their cones and because mice with intact *Opn1sw* genes co-express LVAVA and S-opsin in the majority of cones.

The most severe consequence in terms of the effects of the LVAVA variant on retinal function are exhibited by individuals in whom all L/M cones (94% of the cone photoreceptors) express the LVAVA variant. We report evidence that this causes the adjacent S cones to deteriorate in function, implying an effect on their health and viability. In males who have an LVAVA variant in one submosaic of L/M cones and a normal variant in the other submosaic, the LVAVA variant appears to interfere with visually guided signals for the appropriate cessation of eye growth, resulting in high-grade myopia. The submosaic of L/M cones expressing a normal opsin appears to rescue the more severe cone dystrophy seen in patients with all L/M cones expressing the LVAVA variant, but its interference with visually guided signals during emmetropization leads to a dramatic over-elongation of the eye causing myopia and vision loss from the stresses of the over-elongated eye. Differences in the severity of the myopia across affected males may be a consequence of differences in cone ratio, with milder myopia associated with more skewed cone ratios and more severe myopia associated with cone ratios nearer 1:1. Female carriers of LVAVA have been reported to have much milder myopia than affected males (Young *et al.*, 2004); this would be expected given that they express three or four X-chromosome cone opsin genes in which only one encodes the LVAVA variant.

Chapter 3

An L/M-opsin gene variant specifying LIAVA causes cone photoreceptor defects

Abstract

The intermixing of the long wavelength (*OPN1LW*) and middle wavelength (*OPN1MW*) genes, due to multigenerational episodes of unequal crossover during meiotic recombination, has led to the emergence of many variant haplotypes. While the majority of these variants appear benign, an increasing number of them are being associated with vision disorders, such as uncorrectable vision loss, colorblindness, and pathologically high myopia. One of these variants, referred to as LIAVA according to the single letter amino acid code, completely and selectively disrupts the function of cones that express it. High resolution imaging in human subjects has previously shown that affected cones do not waveguide light, but these cells appear to remain viable and appropriately positioned in the photoreceptor mosaic. Retinal function was evaluated in the present study by ERG in a subject who was previously reported to express an LIAVA variant in all of his L/M cones. Data from this subject were compared to ERG and retinal morphology data collected from a targeted knock-in/knockout LIAVA mouse model that exhibited a late-onset and relatively mild phenotype. While the results from mice demonstrated that the LIAVA amino acid sequence is directly harmful to cones, the source of dysfunction in human cones likely arises from aberrant splicing of the LIAVA messenger RNA due to the nucleotide haplotype of exon 3 associated with this amino acid combination.

Introduction

Human long- (L) and middle- (M) wavelength cone opsin genes, designated *OPN1LW* and *OPN1MW*, respectively, lie in tandem on the X-chromosome at Xq28 (Nathans, Thomas & Hogness, 1986b). Rearrangements of these genes during meiosis, via unequal non-homologous recombination, are the main cause of inherited red-green color vision deficiencies (Nathans *et al.*, 1986a; Drummond-Borg, Deeb & Motulsky, 1989; Neitz & Neitz, 2011). In the United States, one in twelve males and one in 230 females suffers from some form of inherited red-green color vision deficiency. In addition, about 1 in 16 females is a carrier of a red-green color vision defect. Presumably, successive generations of unequal homologous recombination in females has generated the very high degree of nucleotide sequence diversity in the human *OPN1LW* and *OPN1MW* genes, which has in turn given rise to tremendous variability in the corresponding protein sequences (Winderickx *et al.*, 1993; Neitz *et al.*, 1995; Verrelli & Tishkoff, 2004; Neitz & Neitz, 2011).

The *OPN1LW* and *OPN1MW* genes each have six exons. The first and sixth exons do not typically differ among the X-chromosome cone opsin genes. Exon 5 encodes amino acid positions that produce about 21 nm of the nearly 30 nm difference in peak absorption of the L and M cone photopigments (Neitz *et al.*, 1991) and thus can be used to define a gene as encoding an L or an M pigment (Neitz *et al.*, 1996; Kainz, Neitz & Neitz, 1997). Exons 2, 3, and 4 together specify 11 polymorphic amino acid positions, of which only 3 are involved in spectral tuning. Until recently, the remaining eight polymorphic positions have been assumed to have no functional consequences. However, L or M opsins with the combination of amino acids specified by exon 3 of Leucine at position 153, Isoleucine at position 171, Alanine at position 174, Valine at position 178 and Alanine at position 180 (abbreviated LIAVA with the single letter amino acid code) have been associated with the absence of cone function (Carroll *et al.*, 2004: Crognale, 2004; Neitz *et al.*, 2004; Mizrahi-Meissonnier *et al.*, 2010; McClements *et al.*, 2013a).

The Neitz labs have identified twenty-nine males from seven unrelated families who have at least one gene encoding an LIAVA opsin variant in one of the first two positions (5' end) of the X-chromosome opsin gene array (Carroll *et al.*, 2004; Crognale *et al.*, 2004; Neitz *et al.*, 2004; unpublished results). Genes downstream of position two in the array are typically not expressed (Winderickx *et al.*, 1992; Yamaguchi, Motulsky & Deeb, 1997). Every subject tested thus far has exhibited vision deficits that were consistent with the identity of the gene(s) coding for the LIAVA variant. Specifically, people with LIAVA specified by exon 3 of their *OPN1LW* gene had deuteranopia, those with LIAVA specified by their *OPN1MW* gene had protanopia, and those with a single gene on the X-chromosome and therefore LIAVA opsin variant expressed in all of their L/M cones had S cone monochromacy (Crognale et al., 2004). Since S cones represent only ~6% of the cone mosaic (Hofer *et al.*, 2005), S cone monochromacy is associated with significantly reduced photopic vision (Green, 1972).

Previously published, high-resolution retinal imaging data has provided anatomical evidence that cones expressing an LIAVA opsin develop structurally and complete the post-mitotic packing in the fovea. Adaptive optics images acquired from 1.25 degrees eccentric from the fovea in a deuteranope (no M cone contribution to vision) with a normal *OPN1LW* gene and an $OPN1MW^{\mathrm{LIAVA}}$ gene showed large gaps distributed throughout the mosaic that contained no visible cones. Retinal densitometry identified that the wave-guiding cones in this subject were S and L, and statistical analysis predicted the dark areas to be of the correct geometry to have been filled by cones, presumably nonfunctional M cones (Carroll et al., 2004). Simulating the presence of M cones in these regions illustrated that these cones would have been appropriately interleaved with L and S cones throughout the retina. These "place-holders" in the cone mosaic suggest that M cones developed and were positioned in a manner consistent with a normal retina (Wagner-Schuman et al., 2010).

Recently, the haplotypes of exon 3 associated with *OPN1LW* and *OPN1MW* variants that specify the LIAVA combination were shown by *in vitro* minigene experiments to interfere with normal splicing of exon 3 (Ueyama *et al.*, 2012). The splicing pattern observed in HEK 293 cells for a minigene that contained a human L-opsin cDNA, in which a BbsI restriction site extended from within exon 2 to within exon 4, was exchanged for the corresponding DNA fragment from genomic DNA from individuals with the LIAVA variant or with a normal variant. The LIAVA minigene gave rise to a truncated mRNA transcript in which exon 3 was excluded, whereas the normal L-opsin minigenes gave rise to a normal full-length transcript as well as a truncated transcript in which exon 3 was excluded. Another minigene that differed from the LIAVA variant in having Valine specified at position 171 instead of Isoleucine (LVAVA) was shown to give rise to a mixture of full-length and exon 3 skipped mRNA. The LVAVA variant was recently shown to be associated with two different vision disorders, high-grade myopia (McClements *et al.*, 2013b) and cone dystrophy (Carroll *et al.*, 2012), and it was demonstrated to cause cone dysfunction in a genetically modified mouse as a consequence of the amino acid sequence, not aberrant splicing (Greenwald, *manuscript in preparation*, and Chapter 2).

Here, experiments performed both in a human subject who was previously reported to have the LIAVA variant expressed in all of his L/M cones (Crognale *et al.*, 2004) and in targeted gene replacement mice that expressed an LIAVA opsin gene that does not require splicing exon 3 are described. Results from these experiments indicate that, indeed, aberrant splicing is likely to be the source of the cone dysfunction observed in humans, as the mice did not exhibit the vision deficits of the human counterparts.

Materials and methods

Human subjects

A male who had previously been reported to have genes encoding LIAVA variants in the first two positions in his X-chromosome opsin gene array, based on the results of real-time quantitative PCR (Crognale *et al.*, 2004), was examined here for cone function using the electroretinogram (ERG). At the time of this study, the subject was 32 years old. ERG data collected from this subject were compared to those of five control subjects (mean age 27 years; age range 22-33 years) who had normal cone function based on visual acuity and color vision tests. None of the control subjects had an LIAVA or an LVAVA opsin variant. Experiments on human subjects were approved by the Institutional Review Board at the University of Washington and were conducted in accordance with the principles embodied in the Declaration of Helsinki.

Mice

We previously reported results for mice that were null for the S-opsin gene (*Opn1sw*$^{-/-}$) and that had the endogenous mouse M-opsin gene (*Opn1mw*) replaced with an engineered L-opsin gene that specified the following amino acids at the polymorphic positions encoded by exons 2, 3, and 4: T65, I111, S116, L153, I171, A174, I178, S180, I230, A233, and M233 (Greenwald, et al *manuscript in preparation*, and Chapter 1). This variant is abbreviated *Opn1lw*$^{\text{LIAIS}}$ and serves as a control normal L-opsin, and the mice are designated *Opn1lw*$^{\text{LIAIS}}$ *Opn1sw*$^{-/-}$. For the studies described here, a line of mice was also created in which the X-chromosome opsin locus differed from the *Opn1lw*$^{\text{LIAIS}}$ locus by two amino acid positions, so that it specified the LIAVA variant. These mice are designated *Opn1lw*$^{\text{LIAVA}}$ *Opn1sw*$^{-/-}$. Examining the L-opsin variants in an S-opsin null background was necessary because mice normally co-express the *Opn1mw* and *Opn1sw* genes in the majority of their cone photoreceptors, which could confound the studies. The *Opn1lw*$^{\text{LIAIS}}$ and *Opn1lw*$^{\text{LIAVA}}$ opsin genes contained only one intron, and that is intron 1. Thus,

any splicing defects caused by exon 3 in the LIAVA gene sequence would not be evident in our experiments.

Electroretinogram: ON-OFF (Long-flash)

Dilation, electrodes, and electrode placement were as described previously for human (Carroll *et al.*, 2000), and dilation, anesthesia, electrodes, and electrode placement were as described previously for mice (Greenwald, *manuscript in preparation*, and Chapter 1). For human subjects, a Roland Consult (Brandenburg, Germany) Q450 Ganzfeld system was modified to hold 10, 1 Watt (W) LEDs that peak at 414 nanometers (nm). The Q450 also had LEDs that peak at 525nm, 594 nm, and 641nm built-in. For mice, a Roland Consult Q400 was modified to hold 26 LEDs that peak 520 nm and 26 LEDs that peak at 365 nm (Nichia NSHU590A).

Custom circuitry controlled the LED intensities with pulse width modulation, which provided a linear intensity response with no shift in peak wavelength. Frame sync pulses from the software controlled the timing of the LEDs, and the light stimulus flashed at approximately 1 Hertz (Hz) with a 50% duty cycle. During the first 500 ms of each cycle (Phase 1), quantal catch increased for the specific photopigment-isolating stimulus (S or M/L), while in the final 500 milliseconds (ms) (Phase 2), the quantal catch decreased. A silent substitution paradigm was used to hold the non-targeted photopigment(s) constant over both phases. ON and OFF responses were generated at the interfaces between the two phases, and the duration of each phase was set so that retinal activity would return to baseline. Additionally, a 20 Hz–100 Hz band-pass filter was used to reject non-retinal signals that can occur during the 1s interval while still allowing the main ERG components to pass.

The technique used to calculate the quantal catch of each photopigment has been described previously (Pauers *et al.*, 2012), with an added estimate for the yellowing of the lens as a function

of age (Pokorny, Smith & Lutze, 1987; Xu, Pokorny & Smith, 1997). For human S-isolating ERGs, having an estimate of how much the lens has yellowed was critical for the accuracy of the S-isolating stimulus. Light intensity values for human M/L cone ERGs were calculated such that M and L cones were modulated together and with the same quantal increase. Assuming M and L cones contribute linearly to the ERG waveform, this method yields equal ERG amplitudes despite variations in cone ratio. For S-isolating conditions, the light intensities were modulated with a larger quantal increase. This increase in quantal modulation was done because, compared to (M+L) cone-isolation, the S cone signal-to-noise ratio is relatively low given that S cones comprise only 6% of the cone photoreceptor population (Hofer *et al.*, 2005).

Subjects (human and mice) were light adapted in standard room lighting, and ERGs were collected under photopic conditions with background lights adjusted to suppress rod activity. For human, the number of stimulation cycles contributing to a single trial was variable in that each trial was terminated when additional cycles did not appreciably change the averaged waveform, as described in Chapter 1. For mice, a single trial was comprised of 20 stimulation cycles. Age-matched mice from each line were tested during the sessions. Retinal function was assessed by the amplitude of the ERG b-wave, which was measured as the absolute voltage change between the a-wave and b-wave peaks. A-, b-, and d-waves in the photopic ERG are considered to be generated by cones/OFF-bipolar, ON-bipolar, and OFF-bipolar cells respectively (Bush & Sieving, 1996). Since S cones do not signal through OFF-bipolar cells, an S cone ERG was considered properly isolated when no d-wave was present in the waveform (Dacey & Packer, 2003).

Immunocytochemistry & image acquisition in mice

Mice were euthanized with a lethal dose of sodium pentobarbital (Nembutal 50mg/mL) at 3 months (n=4 per line) and 16 months (n=5 per line) of age. Tissue was fixed via cardiac perfusion using 4% paraformaldehyde (PFA) in 0.13 M phosphate buffered saline (PBS) pH 7.2-7.4 containing 2 units of heparin per mL PBS followed by 4% PFA plus 1% glutaraldehyde in PBS. The eyes were marked for orientation, dissected, and 100 µm thick sagittal sections were cut so that each specimen contained the dorsal and ventral retina. Only slices obtained from within 100 µm of the optic nerve head were imaged. L-opsin, nuclei, and cone sheaths were labeled by immunocytochemistry using an antibody against L-opsin, DAPI, and peanut agglutinin (PNA), respectively. The absence of S-opsin was confirmed by staining with an antibody against S-opsin. 30x widefield images were acquired form the dorsal retina and L-opsin labeled outer segments were individually counted and measured in length. The outer segment layer was compressed in two of the 16-month-old *Opn1lw*^{LIAVA} mouse retinas, most likely due to the fixation process. While it was possible to count the outer segments, these specimens were not included in the outer segment length measurements. All images, 292.5 µm in width, were taken ~200 µm ventral to the ora serrata. The depth of the z-stack used for measuring outer segment lengths was 19.5 µm deep and a 9.5 µm substack was generated for the outer segment counts. Confocal images were acquired using an Olympus FluoView^{TM} FV1000 confocal microscope with a 20x oil-immersion lens. Z-stacks were combined using Image J software (Schneider *et al.*, 2012) and channel exposure levels were balanced within and across images using Photoshop. More detailed methods are available elsewhere (Greenwald, *manuscript in preparation*, and Chapter 1).

Results

Full-field ERGs were collected in the *OPN1LW*^{LIAVA} subject and in five control subjects. The L cones of the *OPN1LW*^{LIAVA} subject did not generate a detectable ERG in response to full-field stimulation by 525 nm or 641 nm light (**Figure 19**). The timings of the voltage deflections in this subject's waveform were inconsistent with any of the characteristic features (e.g. a-, b-, and d-waves) observed in the averaged 525 nm L/M cone-isolated ERG collected from the controls; instead, large changes in polarization were attributed to blinks and eye movements (nystagmus). In contrast, robust S cone ERGs were generated in the *OPN1LW*^{LIAVA} subject. The temporal profile of the biphasic deflection at light onset was consistent with the characteristic a- and b-waves observed in normal responses (**Figure 20**). The peak of the b-wave occurred with nearly the identical latency after light onset in the *OPN1LW*^{LIAVA} subject (38.5 ms) as for the control subjects (40.7 ms ± 1.1), and the b-wave amplitude in the *OPN1LW*^{LIAVA} subject (2.9 μV) was greater than that of any control subject (1.7 μV ± 0.1).

Figure 19. **Cones containing the LIAVA opsin variant are nonfunctional in human.** Full-field ERGs in response to a 525 nm L/M cone-isolating stimulus were recorded in subjects with normal vision (n=5; black trace), and responses to the same 525 nm stimulus (dark gray trace) and to a 641 nm L cone-isolating stimulus (light gray trace) were recorded from the *OPN1LW*^{LIAVA} subject. Characteristic features of the normal ERG that occur at light onset and light offset (a-, b-, and d-waves are labeled) were not detected in the *OPN1LW*^{LIAVA} subject, indicating an absence of L cone function.

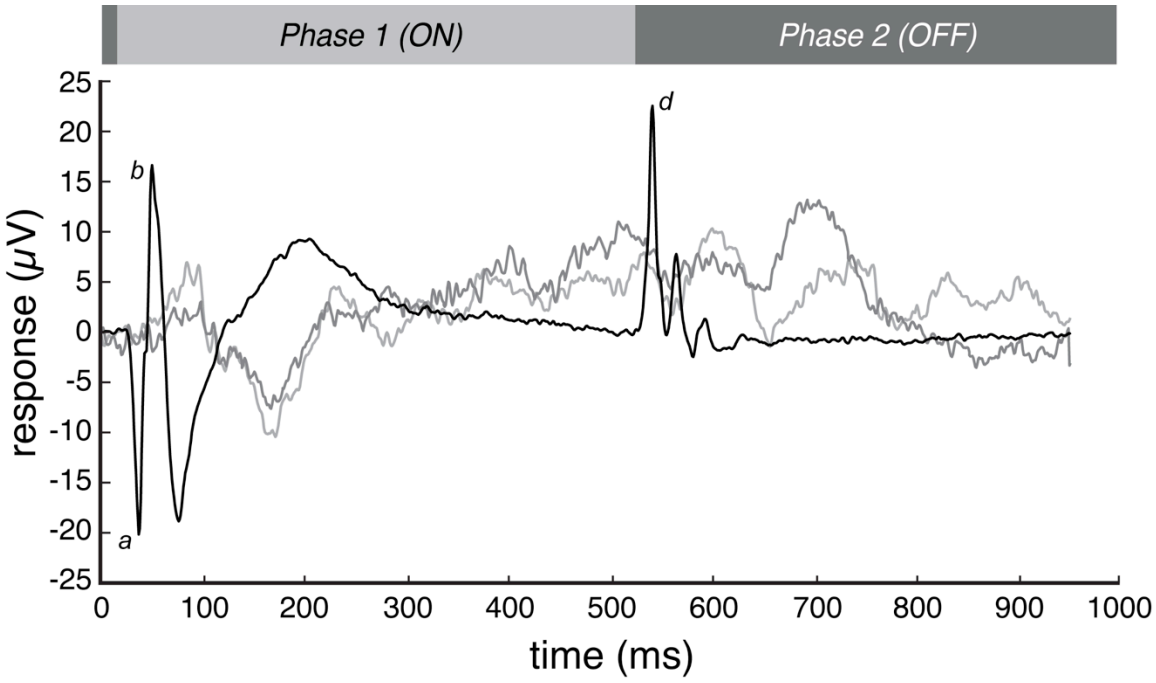
Phase 1 (ON)
Phase 2 (OFF)
a
b
d
response (μV)
time (ms)
25
20
15
10
5
0
-5
-10
-15
-20
-25
0
100
200
300
400
500
600
700
800
900
1000

Figure 20. **S cones function without deficit in the LIAVA retina.** Full-field, S cone-isolated ERGs were recorded from subjects with normal vision (n=5; black trace) and from the *Opn1lw*^{LIAVA} subject (gray trace). The *Opn1lw*^{LIAVA} subject's signal included an unusually strong response at light onset that had a normal temporal profile. The dotted line indicates the synchronicity of the b-waves between the *Opn1lw*^{LIAVA} and control subject's ERGs.

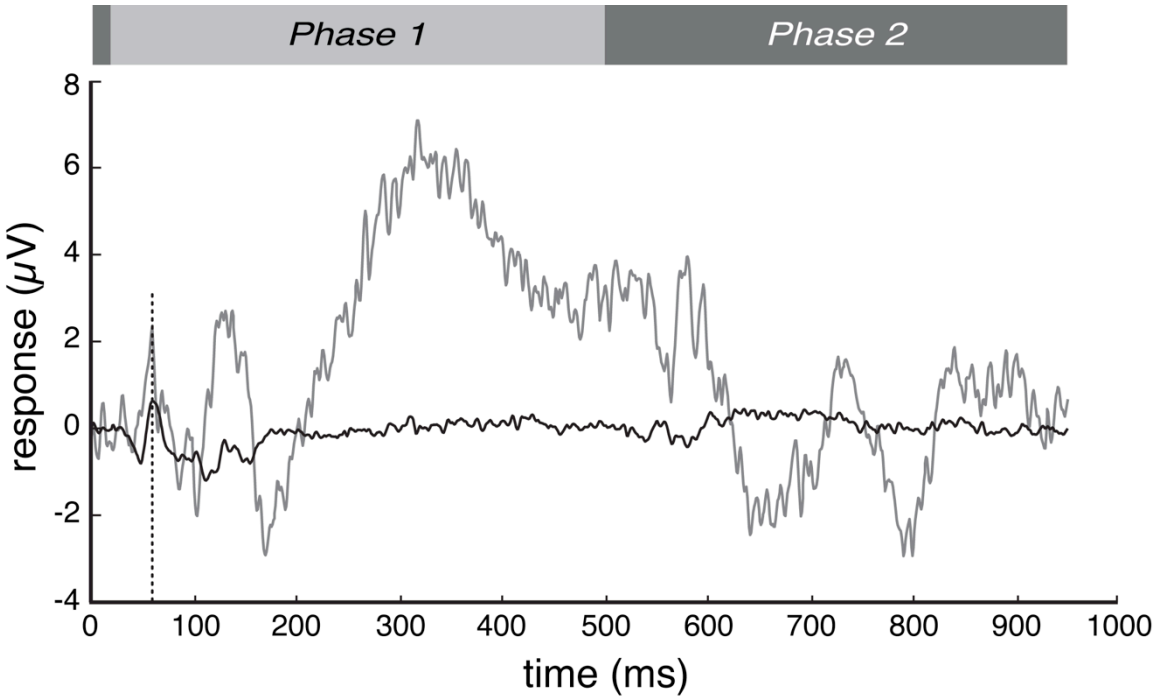
Phase 1
Phase 2
8
6
4
2
0
-2
-4
response (μV)
0
100
200
300
400
500
600
700
800
900
1000
time (ms)

Cone function was measured in the same mice across the first sixteen months of life using the full-field ERG (**Figure 21A**, **Table 5**). The responses to a 520 nm light stimulus (3.0 μW/mm^2 intensity) in young (≤3-months-old) *Opn1lw*^{LIAVA} *Opn1sw*$^{-/-}$ and *Opn1lw*^{LIAIS} *Opn1sw*$^{-/-}$ control mice declined in accordance with the *Opn1sw*$^{-/-}$ background (Greenwald et al., *manuscript in preparation*, and Chapter 1). During this early period, no statistically significant differences were observed between the L cone responses generated by the two mouse lines, although the *Opn1lw*^{LIAVA} *Opn1sw*$^{-/-}$ mice tended to have slightly increased b-wave amplitudes (this trend entirely disappeared by six months). While the responses in the control line remained reasonably stable from the six-month time point through the end of the study, those of the *Opn1lw*^{LIAVA} *Opn1sw*$^{-/-}$ mice continued to decrease steadily. Twelve-month-old *Opn1lw*^{LIAVA} *Opn1sw*$^{-/-}$ mice showed a strong tendency to produce weaker responses (-26.0%; $p = 0.061$) than age-matched controls, and by sixteen months, the b-waves were significantly reduced (-29.7%; $p<0.05$). Moreover, this effect was observed across a broad range of light intensities (**Figure 21B**, **Table 6**). In sixteen-month-old mice, retinal responses across a light intensity series (0.4 μW/mm^2 to 11.8 μW/mm^2) were consistently weaker in the *Opn1lw*^{LIAVA} *Opn1sw*$^{-/-}$ mice (n=7) than the *Opn1lw*^{LIAIS} *Opn1sw*$^{-/-}$ mice (n=10), with statistical significance from 0.8 μW/mm^2 through 6.0 μW/mm^2.

***Figure 21*. Mild loss of cone function in older *Opn1lw*^{LIAVA} *Opn1sw*$^{-/-}$ mice. (A)** Full-field, L cone-isolated ERGs were measured in *Opn1lw*^{LIAIS} *Opn1sw*$^{-/-}$ (black symbols) and *Opn1lw*^{LIAVA} *Opn1sw*$^{-/-}$ (gray symbols) mice across 16 months in response to a 3.0 μW/mm^2 stimulus. Significantly weaker b-wave amplitudes ($p<0.05$) were observed in 16-months-old *Opn1lw*^{LIAVA} *Opn1sw*$^{-/-}$ mice. (**B**) ERGs collected in response to a light intensity series (0.4 μW/mm^2 to 11.8 μW/mm^2) at the 16 month time point were consistently lower in the *Opn1lw*^{LIAVA} *Opn1sw*$^{-/-}$ mice (n=7) than the *Opn1lw*^{LIAIS} *Opn1sw*$^{-/-}$ mice (n=10), with statistical significance ($p<0.05$) from 0.8 μW/mm^2 to 6.0 μW/mm^2. Data were fit with a cumulative normal function and error bars represent the SEM.

A

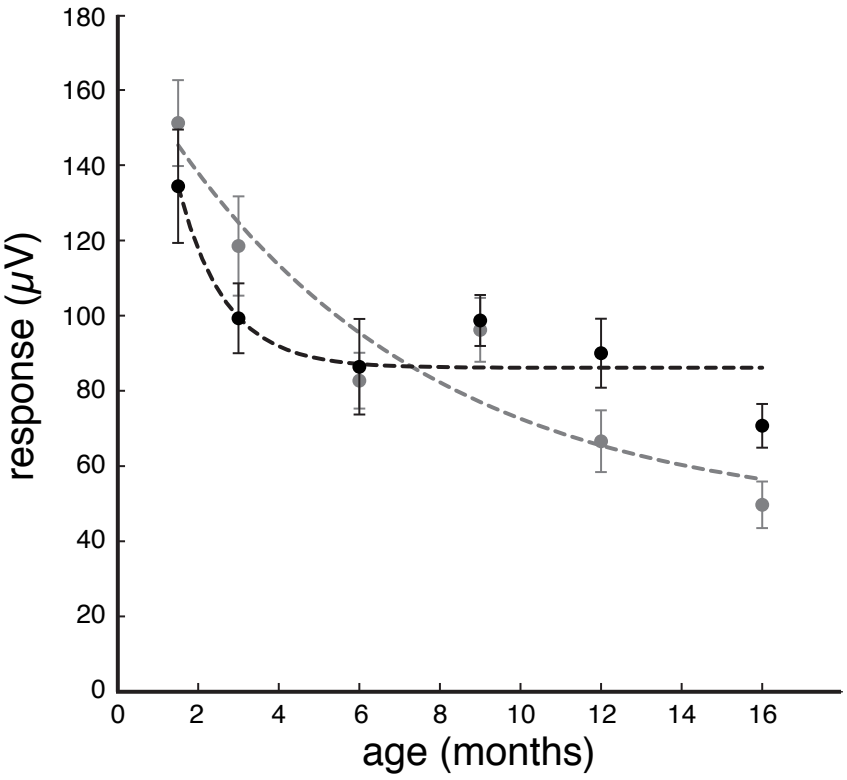
180
160
140
120
100
80
60
40
20
0
response (μV)
0
2
4
6
8
10
12
14
16
age (months)

B

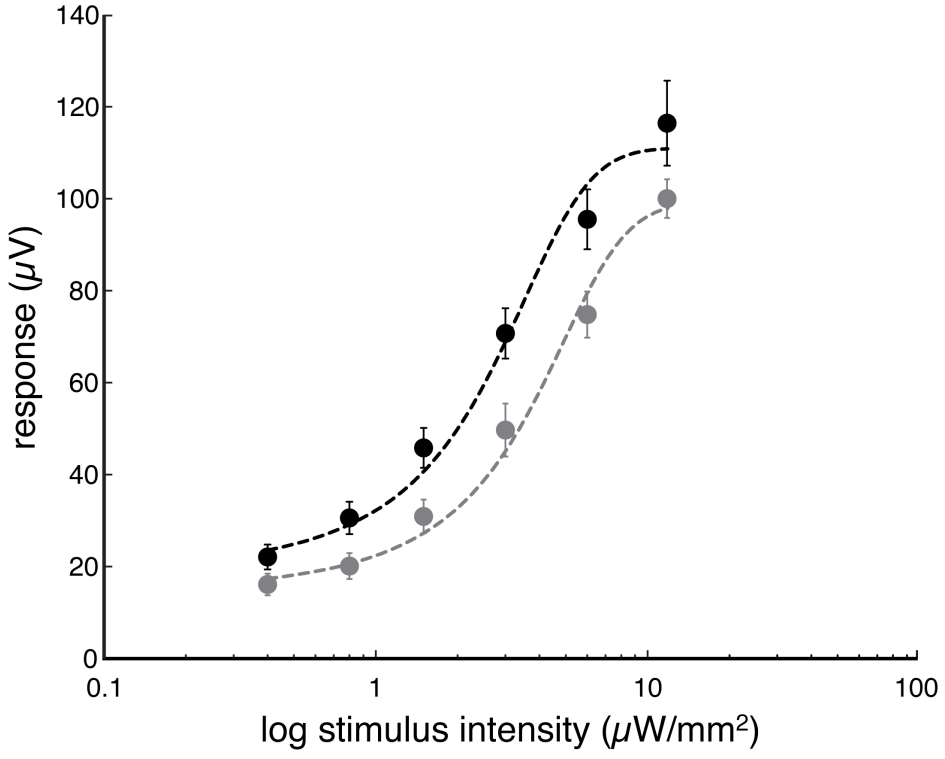
140
120
100
80
60
40
20
0
response (μV)
0.1
1
10
100
log stimulus intensity (μW/mm²)

Table 5. **L cone ERGs collected across 16 months in *Opn1lw*^{LIAVA} and *Opn1lw*^{LIAIS} mice.**

Mouse Line	Age (m)	# of mice	b-wave (μV)	SEM	p-value
Opn1lw^{LIAIS}	1.5	10	134.4	15.1	0.39
Opn1lw^{LIAVA}	1.5	10	151.2	11.4	
Opn1lw^{LIAIS}	3	10	99.3	9.3	0.23
Opn1lw^{LIAVA}	3	10	118.5	13.2	
Opn1lw^{LIAIS}	6	7	86.4	12.7	0.79
Opn1lw^{LIAVA}	6	10	82.7	7.4	
Opn1lw^{LIAIS}	9	10	98.7	6.8	0.81
Opn1lw^{LIAVA}	9	10	96.2	8.5	
Opn1lw^{LIAIS}	12	10	90.0	9.2	0.061
Opn1lw^{LIAVA}	12	10	66.6	8.2	
Opn1lw^{LIAIS}	16	10	70.7	5.8	0.021
Opn1lw^{LIAVA}	16	7	49.7	6.2	

***Table 6*. Intensity response series collected in 16-month-old *Opn1lw*^{LIAVA} and *Opn1lw*^{LIAIS} mice.**

Mouse Line	# of mice	Stimulus (μW/mm^2)	b-wave (μV)	SEM	p-value
Opn1lw^{LIAIS}	10	0.4	22.1	2.71	0.14
Opn1lw^{LIAVA}	7	0.4	16.1	2.35	
Opn1lw^{LIAIS}	10	0.8	30.6	3.52	0.047
Opn1lw^{LIAVA}	7	0.8	20.1	2.82	
Opn1lw^{LIAIS}	10	1.5	45.8	4.34	0.026
Opn1lw^{LIAVA}	7	1.5	30.9	3.64	
Opn1lw^{LIAIS}	10	3.0	70.7	5.47	0.021
Opn1lw^{LIAVA}	7	3.0	49.7	5.77	
Opn1lw^{LIAIS}	10	6.0	95.5	6.52	0.034
Opn1lw^{LIAVA}	7	6.0	74.8	5.02	
Opn1lw^{LIAIS}	10	11.8	116.4	9.25	0.18
Opn1lw^{LIAVA}	7	11.8	100.0	4.20	

For the *Opn1lw*^{LIAIS} *Opn1sw*$^{-/-}$ and *Opn1lw*^{LIAVA} *Opn1sw*$^{-/-}$ mice, cone outer nuclei appeared normal in shape and number, which indicated that a full complement of cones was present in each line. In order to evaluate the structural integrity of these cones, the outer segments were counted and measured in length. Retinal images were acquired using widefield microscopy (30x magnification) within the dorsal region of sagittal sections that had been immunolabeled for L-opsin. Outer segment lengths in three-month-old *Opn1lw*^{LIAVA} *Opn1sw*$^{-/-}$ (n=4) and *Opn1lw*^{LIAIS} *Opn1sw*$^{-/-}$ control mice (n=4) were equivalent, and neither of these measurements were significantly different from control line at sixteen months (n=5). However, the outer segments of sixteen-month-old *Opn1lw*^{LIAVA} *Opn1sw*$^{-/-}$ mice (n=3) were 19.7% ($p<0.01$) shorter than what had been observed in this line at three months and 28.3% ($p<0.01$) shorter than in the age-matched control mice (**Figure 22A**). Correspondingly, the populations of cones with labeled outer segments were equivalent in number for both lines at three months of age (n=4 per line) and in the sixteen-month-old *Opn1lw*^{LIAIS} *Opn1sw*$^{-/-}$ control mice (n=5). In contrast, the number of visible outer segments in sixteen-month-old *Opn1lw*^{LIAVA} *Opn1sw*$^{-/-}$ mice (n=5) was decreased by 19.6% ($p<0.01$) in comparison to what was observed in younger mice of the same line. While the sixteen-month-old *Opn1lw*^{LIAVA} *Opn1sw*$^{-/-}$ mice tended to have ~15% fewer cones with detectable outer segments than the age-matched control mice, the difference was not statistically significant ($p=0.091$) (**Figure 22B**). Representative samples that were used to evaluate the outer segments in Figure 22 were reimaged by confocal microscopy at 20x magnification (**Figure 23**).

***Figure 22*. Cone outer segment length measurements and cone counts.** Immunolabeled sections from 3-month-old (n=4 per line) and 16-month-old (n=5 per line) *Opn1lw*^{LIAIS} *Opn1sw*$^{-/-}$ (black bars) and *Opn1lw*^{LIAVA} *Opn1sw*$^{-/-}$ (gray bars) mice were imaged by widefield microscopy (30x). **(A)** For each specimen, the lengths of L-opsin labeled cone outer segments within a 5.7 mm^2 region of the dorsal retina were measured, and **(B)** the number of the remaining outer segments were counted (unless otherwise noted) in a 2.8 mm^2 subregion. Error bars represent the SEM.

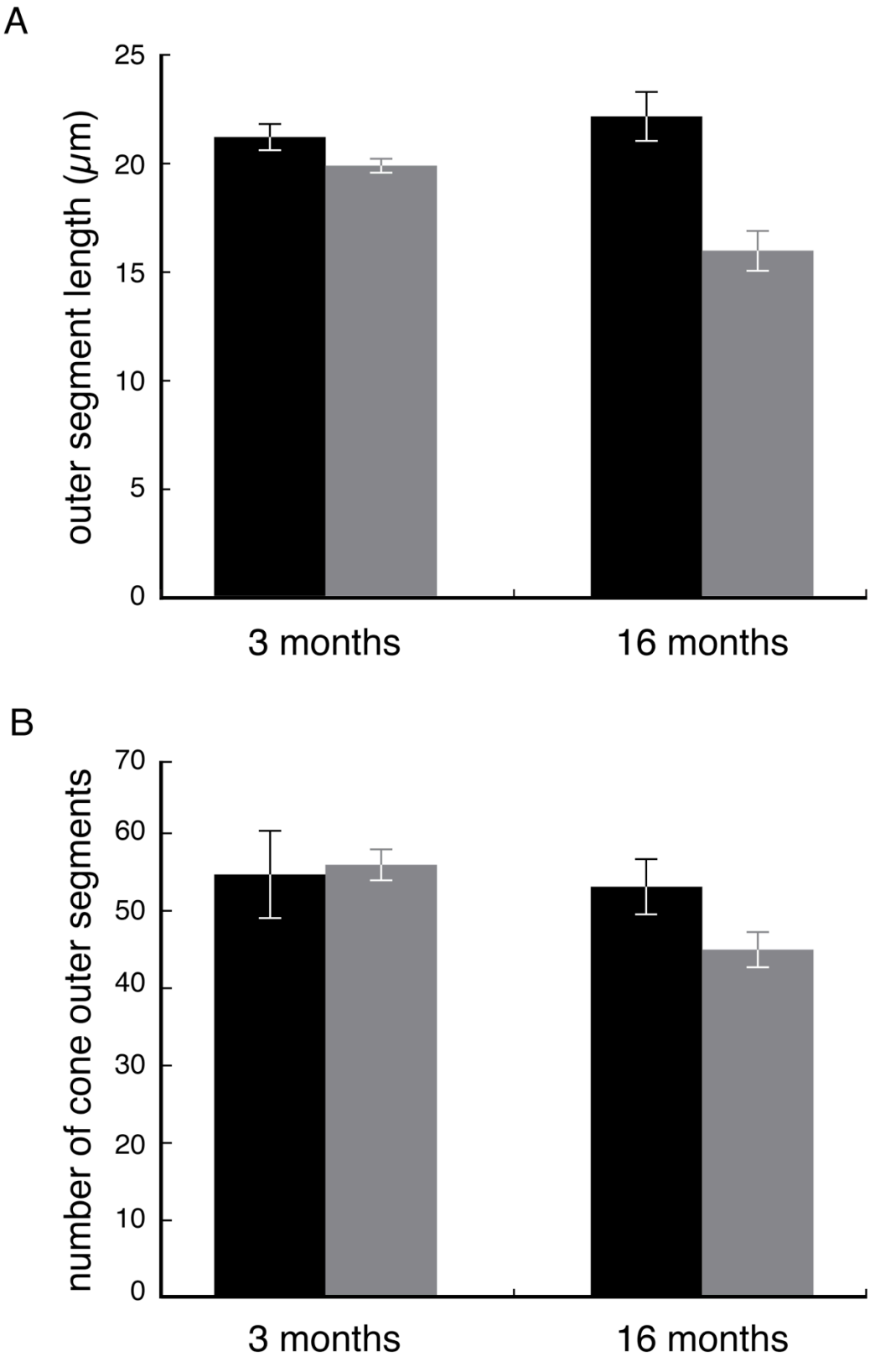
A
outer segment length (μm)
25
20
15
10
5
0
3 months
16 months
B
number of cone outer segments
70
60
50
40
30
20
10
0
3 months
16 months

***Figure 23*. Cone outer segment retraction in older *Opn1lw*^{LIAVA} *Opn1sw*$^{-/-}$ mice.**

Confocal images of sagittal, sections were acquired at the far dorsal retina from *Opn1lw*^{LIAIS} *Opn1sw*$^{-/-}$ (top row) and *Opn1lw*^{LIAVA} *Opn1sw*$^{-/-}$ (bottom row) mice that were sacrificed at 3 months (left column) and 16 months (right column) of age. M-opsin (red), cone sheaths (green/PNA), and nucleic acid (blue/DAPI) were labeled, and representative images are shown. 19.5 μm z-stacks (0.5 μm spacing) were imaged at 20x magnification, and the scale bar represents 100 μm.

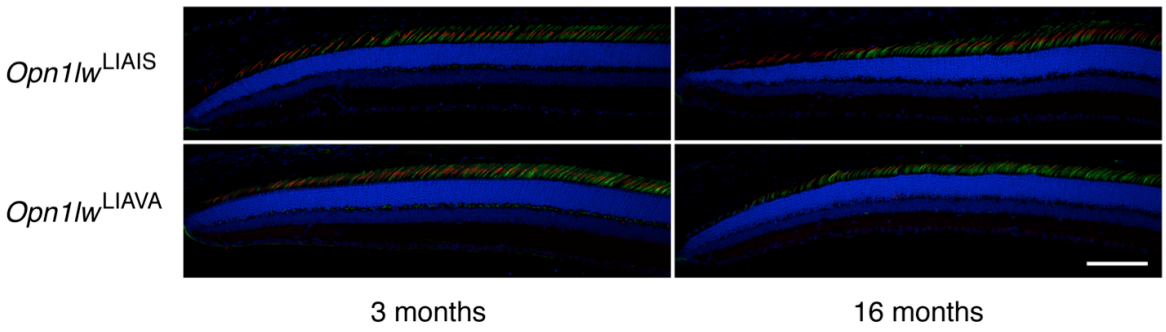
Opn1lw^LIAIS
Opn1lw^LIAVA
3 months
16 months

Discussion

As is evident in the results presented in Figure 19, the effect of the LIAVA opsin variants on cone photoreceptor function in humans is profound, completely ablating the L/M cone ERG. This is consistent with previous reports that males who express both an *OPN1MW*^{LIAVA} gene and a normal *OPN1LW* gene behave as dichromats who have no M cone contribution to vision (Carroll *et al.*, 2004), that males who express both an *OPN1LW*^{LIAVA} gene and a normal *OPN1MW* gene behave as dichromats who have no L cone function (Neitz *et al.*, 2004), and that males who express an LIAVA variant in all of their L/M cones behave as blue cone monochromats (Nathans, Thomas & Hogness, 1986b; Crognale *et al.*, 2004). Remarkably, the complete loss of L/M cone function observed in humans was not recapitulated by the *Opn1lw*^{LIAVA} *Opn1sw*$^{-/-}$ mice. L cone ERGs in these mice did not become significantly weaker than those of the control line until nearly one year of age, and even at the sixteen-month time point, the phenotype was relatively mild. Nonetheless, this reduction in cone response during advanced age was apparent across a wide range of light intensities, and it was coincident with the altered cone morphology. Thus, these results indicate that the LIAVA amino acid combination in the photopigment can only explain a portion of the profound cone defect observed in humans.

Instead, the experiments presented here support that an mRNA splicing error (Ueyama *et al.*, 2012) is ultimately responsible for the majority of the severe disruption observed in LIAVA cones. Ueyama and colleagues report that the codons specifying LIAVA potently interfere with the recognition of exon 3 within the *OPN1LW* and *OPN1MW* pre-mRNA, facilitating aberrant skipping of this exon in the message. By this mechanism, two populations of opsin may be expressed within a single cell: a major class that is truncated and a minor class that is full-length. While the truncated product may be primarily responsible for rendering human cones nonfunctional, data collected from the *Opn1lw*^{LIAVA} *Opn1sw*$^{-/-}$ mouse demonstrated that the full-

length product is also toxic to cones. Based on this finding, a therapeutic approach that forces splicing of the LIAVA variant to include exon 3 would not completely rescue the vision loss.

Another human opsin variant (LVAVA), which differs from LIAVA only at position 171, was shown to cause dysfunction in L/M cones that harbor it and in S cones that are nearby. Likewise, we demonstrate that while the LIAVA variant disrupts L/M cones; however, it does not cause a functional deficit in S cones.

How might the LIAVA and LVAVA variants cause toxicity to the cones that express them? Position 153 lies at the top of helix III and is immediately adjacent to the ERY (glutamic acid, argenine, tyrosine) tri-peptide that is highly conserved in class A GPCRs, including rhodopsin. The ERY tri-peptide corresponds to amino acid positions 150, 151 and 152 in the L and M cone opsins (Kosower, 1988), where the tri-peptide is ERW (glutamic acid, argenine, tryptophan). This tri-peptide is a key component of the hydrogen bond network known as the "ionic lock" (Vogel *et al.*, 2008; Angel *et al.*, 2010). Positions 171, 174 and 178 all lie on the same surface of helix IV, with each one residing a helical turn below the other. Position 180 is also on helix IV where it interacts with the chromophore. Furthermore, key water molecules that have a critical role in the allosteric activation of transducin are an integral part of the structure of rhodopsin (Okada *et al.*, 2004; Angel *et al.*, 2010; Jastrzebska *et al.*, 2011). Experiments using H_2O^{18} exchange, together with radiolysis (Angel *et al.*, 2010; Orban *et al.*, 2010), led to labeling of selected side chain residues within the transmembrane helices of rhodopsin, thereby revealing activation-induced changes in local structural constraints that are thought to be mediated by both water and protein. Angel *et al*. (2010) argue that the disruption and reorganization of multiple close packing interactions, mediated by both amino acid side chains and bound water, interferes with the transmission of information from the chromophore binding site that would ordinarily radiate up helix IV to the ionic lock and to the cytoplasmic surface to promote the activation of

bound transducin. These results implicate the amino acid positions that comprise the deleterious combinations LIAVA and LVAVA in the structural reorganization of tightly bound water. Consequently, the hydrogen bond network in visual pigments that is critical for light activation and activation of transducin becomes disrupted.

Chapter 4

Visual adaptation: An intrinsic feature of the photoreceptor that is rate limited by the class of opsin expressed

Abstract

Visual adaptation adjusts the operating range of the photoreceptors to preserve vision following changes in ambient light. The action of post-bleach decay components of photopigments on the phototransduction cascade has been implicated as underlying the adaptation process in that it causes signaling to persist after the light stimulus is no longer present. Prior studies showing that rods, S cones, and L/M cones adapt at different rates imply that the photopigments play a primary role. The present study directly tested whether S and M photopigments differentially change the light adapted state of the same cone by measuring ERGs in wildtype mice that naturally coexpress both photopigment classes in individual cones. The presentation of short wavelength light was associated with a greatly suppressed the M photopigment response. In S photopigment knockout (*Opn1sw*$^{-/-}$) mice and in human subjects, in which cones only express a single class of photopigment, the effect of short wavelength light exposure did not have a strong effect on the M photopigment response. The experiments described here support the hypothesis that visual adaptation is a feature conferred on the photoreceptor by the class of photopigment that is present.

Introduction

Encountering light levels that, at a given moment, are beyond the processing capabilities of the visual system is a common experience. For instance, we strain our eyes to see when entering a darkened theater on a sunny day, and we are momentarily blinded when exiting the theater into sunshine. Both of these situations occur because there is a significant change in the number of photons entering the eye. Such dramatic shifts in light intensity can cause a discrepancy between the amount of stimulation and the operating range of the visual system. The process of recalibrating the visual system so that the "eyes adjust" to the new environment is referred to as visual adaptation (Reuter, 2011). Visual adaptation is divided into dark adaptation and light adaptation. Dark adaptation is the gradual acclimation to a decrease in ambient light (Barlow, 1964), while light adaptation is a rapid decrease in photoreceptor sensitivity that expands the operating range of the visual system when the ambient light increases (Matthews, 1988).

Since at least the late 1800s, visual adaptation has been understood to occur at the level of the eye. People observed that exposing just one eye of a dark-adapted subject to a bright light decreased the sensitivity of that eye only (Reuter, 2011). Psychophysical studies conducted during the 20th Century elegantly characterized the behavioral experience of visual adaptation and provided evidence that the photoreceptors are at its basis. For instance, Hecht and colleagues' classic experiments parsed the relative contributions of rod versus cone photoreceptors during the time-course of human dark adaptation (Hecht, Haig, & Chase, 1937).

The importance of the opsins in visual adaptation has been recognized since the early 20th Century, although the exact nature of how these proteins contribute has shifted over time. Initially, in experiments that were performed on rods, dark adaptation was thought to result simply from the bleaching of rhodopsin and that the time-course for recovering sensitivity corresponded to rate of photopigment regeneration (Wald, 1955). Moreover, bleaching just a

small portion of rhodopsin was observed to result in a disproportionate increase in visual threshold (Granit, Holmberg, & Zewi, 1938). Later experiments comparing visual sensitivity during dark adaptation to the quantity of regenerated rhodopsin were done in albino rats (Dowling, 1960) and in human subjects (Rushton, 1961). These studies agreed with Granit's observation and determined that visual sensitivity is logarithmically related to the concentration of photopigment. One explanation for this nonlinearity was that large populations of rhodopsin molecules reside within compartments, and that when any molecules are bleached, the entire compartment is rendered nonfunctional until all photopigments are regenerated (Wald, 1954). Although, such compartments do not exist, the concept that the loss of previously activated photopigments directly causes decreased visual sensitivity had credence.

An alternative explanation that has gained traction since the mid-1900s was the idea that constituents of previously activated rhodopsin molecules continue to activate the phototransduction cascade after the light stimulus has ceased. Even in darkness, this residual activation would generate signals in the rod that are physiologically identical to those generated in response to light. This "equivalent background light" would mask the response to an external stimulus unless that response was intense enough to overcome the decrease in photoreceptor sensitivity (Barlow, 1956; Barlow, 1964). In studies focused on rod photoreceptors, the source of this equivalent light was attributed specifically to photopigment decomposition products in post-bleach decay states that are capable of activating the phototransduction cascade (Fain *et al.,* 2001; Grabowski & Pak, 1975; Lamb & Pugh, 2004; Leibrock, Reuter, & Lamb, 1994; Matthews *et al*., 1963; Monod, Changeux, & Jacob, 1963; Pepperberg *et al.*, 1978).

Photopigment decay products have been found to independently and continuously activate the transducin after the light stimulus is no longer present (Leibrock, Reuter & Lamb, 1994; Leibrock, Reuter, & Lamb, 1998). The consequence of this action on the level of intracellular

calcium is thought to play a major role in light adaptation (Matthews, 1988). The activated transducin causes phosphodiesterase (PDE) to hydrolyze cyclic guanosine monophosphate (cGMP) to GMP, and this decrease in cGMP causes the close of cyclic nucleotide-gated (CNG) cation channels. Prolonged closure of CNG cation channels results in a decrease in intracellular calcium. With less calcium present to inhibit rhodopsin kinase, metarhodopsin molecules are phosphorylated, bound by arrestin, and thereby deactivated (Detwiler, 1996; Burns & Baylor, 2001; Lamb & Pugh, 2004). In the meantime, the low calcium concentration stimulates guanylyl cyclase activity via a reaction with guanylyl cyclase activating protein (GCAP). In turn, the cGMP content increases, which opens the CNG cations channels, and the circulating current returns (Detwiler, 1996; Pugh, Nikonov & Lamb, 1999). However, the degree to which this calcium feedback loop impacts visual adaptation remains unclear (Nakatani, 1988; Pugh, Nikonov & Lamb, 1999). The regeneration of the native photopigment and the associated removal of equivalent light may be rate-limited by the delivery of the 11-cis retinal to the naked opsins (Lamb & Pugh, 2004).

In short, visual adaptation likely requires terminating the phototransduction cascade following quantal events by inactivating the catalytic photoproducts. However, there is evidence that these processes have differing kinetics in rods versus cones, in that cone photoproducts are inactivated faster (Firsov, Golobokova, & Govardovskii, 2007). This difference in photopigment decay and regeneration is thought to be determined by the opsin, itself. For instance, the decay of chicken cone meta-III can be substantially slowed to the rate of rod meta III by substituting two amino acid residues (Kuwayama *et al.*, 2005). Cones being able to adapt faster than rods is beneficial because it is typical for ambient light levels rapidly change in photopic conditions. The fact that rhodopsin and the cone opsins have different inactivation kinetics implies that visual adaptation is a feature conferred on the photoreceptor by the class of opsin that is present, as oppose to it being an intrinsic feature of the photoreceptor.

Definitively determining whether the opsin protein mediates the rate of human visual adaptation has been challenging. One reason is that, since individual photoreceptors always contain only one class of opsin in nearly all animals, directly comparing the effects of any two opsin types is difficult. However, mice are unique in that the majority of their cones naturally coexpress both M-opsin and S-opsin simultaneously (Szél *et al.*, 1993; Röhlich, van Veen, Szél, 1994; Applebury *et al.*, 2000), and this provides the opportunity to examine the role of visual adaptation, *in vivo*.

The kinetics of human and macaque S cone adaptation are both well-documented to be considerably slower than for than M or L cones (Norren & Padmos, 1974). If the slow kinetics of the S cone are due to S photopigment inactivation being sluggish, then in the wildtype mouse, exposure to S photopigment activating light should globally light adapt the cone and consequently decrease sensitivity to M photopigment stimulating light. In the present study, responses to M and S photopigment-isolating stimuli were separately recorded by eletroretinogram (ERG) in wildtype mice, and the results were compared to S-opsin knockout mice (*Opn1sw*$^{-/-}$) (Greenwald et al., *in preparation*, and Chapter 1). While the *Opn1sw*$^{-/-}$ mouse served as a negative control in this study, it was of particular interest because visual adaptation should be similar to that of man. To determine whether the knockout mouse appropriately models human vision in this case, the results were compared to those of human subjects.

Materials and methods

Mice

The *Opn1sw*$^{-/-}$ mice were generated by standard homologous recombination techniques so that exons 1 through 4 of the *Opn1sw* gene on chromosome 6 were deleted. Successful knockout was validated by direct sequencing of genomic DNA of founder mice, and the genotypes of mice used in this study were confirmed as wildtype or *Opn1sw*$^{-/-}$ by polymerase chain reaction assays. The details of these methods have been described previously (Greenwald et al., *in preparation*, and Chapter 1). All experiments using animals conformed to the principles regarding the care and use of animals adopted by the American Physiological Society and the Society for Neuroscience and were approved by the Animal Care and Use Committee at the University of Washington.

Human Subjects

Human subjects (n=4; mean age=28 years with a range of 27 to 33) had normal color vision, as assessed by form identification in HRR and Dvorine psuedoisochromatic plates, Rayleigh matching using the standard Nagel-type anomaloscope, and the Farnsworth D-15 color arrangement test. Blood samples were taken for *OPN1MW* and *OPN1LW* gene sequencing and no subject had an opsin variant that would be predictive of L or M cone dysfunction. Experiments were approved by the Institutional Review Board at the University of Washington and conducted in accordance with the principles embodied in the Declaration of Helsinki.

Electroretinogram: ON-OFF (Long-flash)

The effects on visual adaptation by S and M photopigment coexpression in cone photoreceptors were investigated in human subjects, wildtype mice, and *Opn1sw*$^{-/-}$ mice using the ON-OFF ERG. Dilation, electrodes, and electrode placement were as described previously for human (Carroll, McMahon, Neitz, & Neitz, 2000), and dilation, anesthesia, electrodes, and electrode placement were as described previously for mice (Greenwald et al., *in preparation*, and Chapter 1). For

human subjects, a Roland Consult (Brandenburg, Germany) Q450 Ganzfeld system was modified to hold 10, 1W LEDs that peak at 414 nm. The Q450 also had LEDs that peak at 525 nm, 594 nm, and 641 nm built-in. For mice, a Roland Consult Q400 was modified to hold 26 LEDs that peak 520 nm and 26 LEDs that peak at 365 nm (Nichia NSHU590A).

Custom circuitry controlled the LED intensities with pulse width modulation, which provided a linear intensity response with no shift in peak wavelength. Frame sync pulses from the software controlled the timing of the LEDs, and the light stimulus flashed at approximately 1 Hz with a 50% duty cycle. During the first 500 ms of each cycle (Phase 1), quantal catch increased for the specific photopigment-isolating stimulus (S or M/L), while in the final 500 ms (Phase 2), the quantal catch decreased. A silent substitution paradigm was used to hold the non-targeted photopigment(s) constant over both phases. ON and OFF responses were generated at the interfaces between the two phases, and the duration of each phase was set so that retinal activity would return to baseline. Additionally, a 20 Hz–100 Hz band-pass filter was used to reject non-retinal signals that can occur during the 1s interval while still allowing the main ERG components to pass.

The technique used to calculate the quantal catch of each photopigment has been described previously (Pauers, Kuchenbecker, Neitz, & Neitz, 2012), with an added estimate for the yellowing of the lens as a function of age (Pokorny, Smith, & Lutze, 1987). For human S-isolating ERGs, having an estimate of how much the lens has yellowed was paramount for the accuracy of the S-isolating stimulus. Light intensity values for human M/L cone ERGs were calculated such that M and L cones were modulated together and with the same quantal increase. Assuming M and L cones contribute linearly to the ERG waveform, this method yields equal ERG amplitudes despite variations in cone ratio. For S-isolating conditions, the light intensities were modulated with a larger quantal increase. This increase in quantal modulation

was done because, compared to (M+L) cone-isolation, the S cone signal-to-noise ratio is relatively low given that S cones comprise only 6% of the cone photoreceptor population (Hofer, Carroll, Neitz, Neitz, & Williams, 2005).

Human subjects and mice were light adapted in standard room lighting, and ERGs were then collected under photopic conditions with background lights adjusted to suppress rod activity. For mice, unless otherwise noted, a single trial was comprised of 20 stimulation cycles. For human, the number of stimulation cycles contributing to a single trial was variable in that each trial was terminated when additional cycles did not appreciably change the averaged waveform. Exclusion criteria for individual ERG traces included 60 Hz electronic interference and artifacts from large eye movements/blinks. For mouse ERGs, all waveforms represent the average of 20 stimulation cycles. Exclusion criteria included 60 Hz electronic interference and large breathing artifacts. Age-matched mice from each line were tested during the sessions. Retinal function was assessed by the amplitude of the ERG b-wave, which was measured as the absolute voltage change between the a-wave and b-wave peaks. A-, b-, and d-waves in the photopic ERG are considered to be generated by cones/OFF-bipolar, ON-bipolar and OFF-bipolar cells respectively (Bush & Sieving, 1996). Since S cones do not signal through OFF-bipolar cells, an S cone ERG was considered properly isolated when no d-wave was present in the waveform (Dacey & Packer, 2003).

Results

Retinal responses to an M photopigment-isolating stimulus (520 nm, 11.8 μW/mm^2) were measured by full-field ERG immediately before and after a 10 second exposure to an S photopigment-stimulation light (365 nm, 10.0 μW/mm^2) in wildtype and *Opn1sw*$^{-/-}$ mice. Data were collected at seven time points spanning the first twenty-one months of life. For wildtype mice, M photopigment responses to the test stimulus following S photopigment activation were ~40% lower than the responses to the reference stimulus that were presented prior to S photopigment activation, whereas only ~7% suppression was observed in *Opn1sw*$^{-/-}$ mice (**Figure 24**, **Table 7**). In addition, M photopigment responses were collected across an intensity response series (0.4 μW/mm^2 to 11.8 μW/mm^2) before and after the 365 nm light exposure. The reduction in sensitivity to the 520 nm light following the short wavelength light stimulus scaled logarithmically with stimulus intensity for wildtype mice, but the ~7% suppression observed *Opn1sw*$^{-/-}$ mice was roughly constant for all intensities. Data shown is from the nine-month time point (**Figure 25**).

***Figure 24*. M photopigment mediated responses in *Opn1sw*$^{-/-}$ mice were greatly suppressed after exposure to short wavelength light.** M photopigment responses to 520 nm light were suppressed following exposure to 10 seconds of 365 nm S photopigment activating light. ERG data acquired across sixteen months are summarized as the average percent *decrease* in b-wave amplitude from wildtype mice (black symbols) and *Opn1sw*$^{-/-}$ mice (gray symbols). Error bars represent standard error of the mean (SEM).

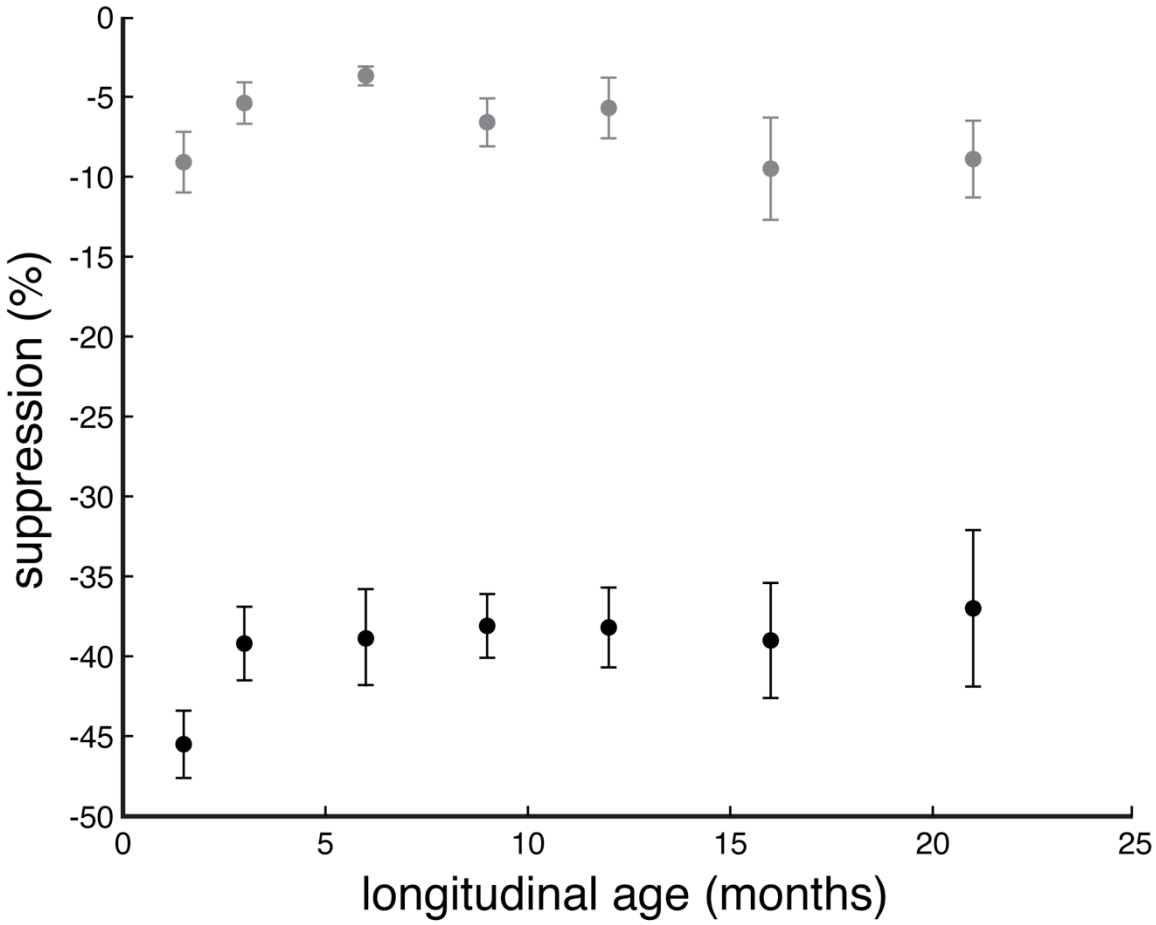
0
-5
-10
-15
-20
-25
-30
-35
-40
-45
-50
suppression (%)
0
5
10
15
20
25
longitudinal age (months)

***Table 7*. M photopigment mediated responses in *Opn1sw*$^{-/-}$ mice were greatly suppressed after exposure to short wavelength light.** Comparisons of M photopigment responses measured immediately before (pre-S) and after (post-S) 365 nm light exposure in wildtype and *Opn1sw*$^{-/-}$ mice across 21 months of life.

Mouse Line	Age (m)	# of mice	M response Pre-S (μV)	SEM (Pre-S)	M response Post-S (μV)	SEM (Post-S)	Percent Suppression	SEM (Suppr)	p-Value (paired)
Wildtype	1.5	9	284.8	32.3	154.2	17.3	45.5	2.1	6.1×10^{-5}
Opn1sw$^{-/-}$	1.5	10	300.9	26.2	273.1	23.2	9.1	1.9	1.0×10^{-3}
Wildtype	3	9	233.9	15.9	143.3	13.8	39.2	2.3	8.8×10^{-7}
Opn1sw$^{-/-}$	3	10	193.2	12.7	183.2	13.0	5.4	1.3	3.7×10^{-3}
Wildtype	6	9	202.9	15.0	124.8	10.5	38.3	3.0	1.6×10^{-5}
Opn1sw$^{-/-}$	6	10	158.3	14.7	152.9	14.8	3.7	0.6	4.8×10^{-5}
Wildtype	9	10	190.5	9.0	118.7	8.4	38.1	2.0	2.6×10^{-8}
Opn1sw$^{-/-}$	9	10	100.6	8.3	94.3	8.5	6.6	1.5	3.4×10^{-3}
Wildtype	12	10	176.0	12.5	110.0	11.5	38.2	2.5	7.0×10^{-8}
Opn1sw$^{-/-}$	12	10	122.4	12.1	115.0	10.9	5.7	1.9	0.026
Wildtype	16	8	165.2	18.6	104.3	15.7	39.0	3.2	3.3×10^{-6}
Opn1sw$^{-/-}$	16	10	47.0	6.3	43.1	6.2	9.5	3.6	0.010
Wildtype	21	7	103.2	11.2	63.0	5.9	37.0	4.9	3.3×10^{-6}
Opn1sw$^{-/-}$	21	8	61.6	7.8	57.5	7.7	8.9	2.4	0.069

Figure 25. **M photopigment response suppression following short wavelength light exposure in mice is logarithmic.** M photopigment mediated intensity response functions were collected immediately before and after a ten second exposure to 365 nm light (10.0 μW/mm^2) in the 9-month-old wildtype (black symbols, n=10) and age-matched *Opn1sw*$^{-/-}$ mice (gray symbols, n=10). The suppression, shown by a *loss* of response on the Y-axis, scaled logarithmically with the intensity of the 520 nm light the wildtype mice. Data for the *Opn1sw*$^{-/-}$ mice were fit with a linear function. Error bars represent SEM.

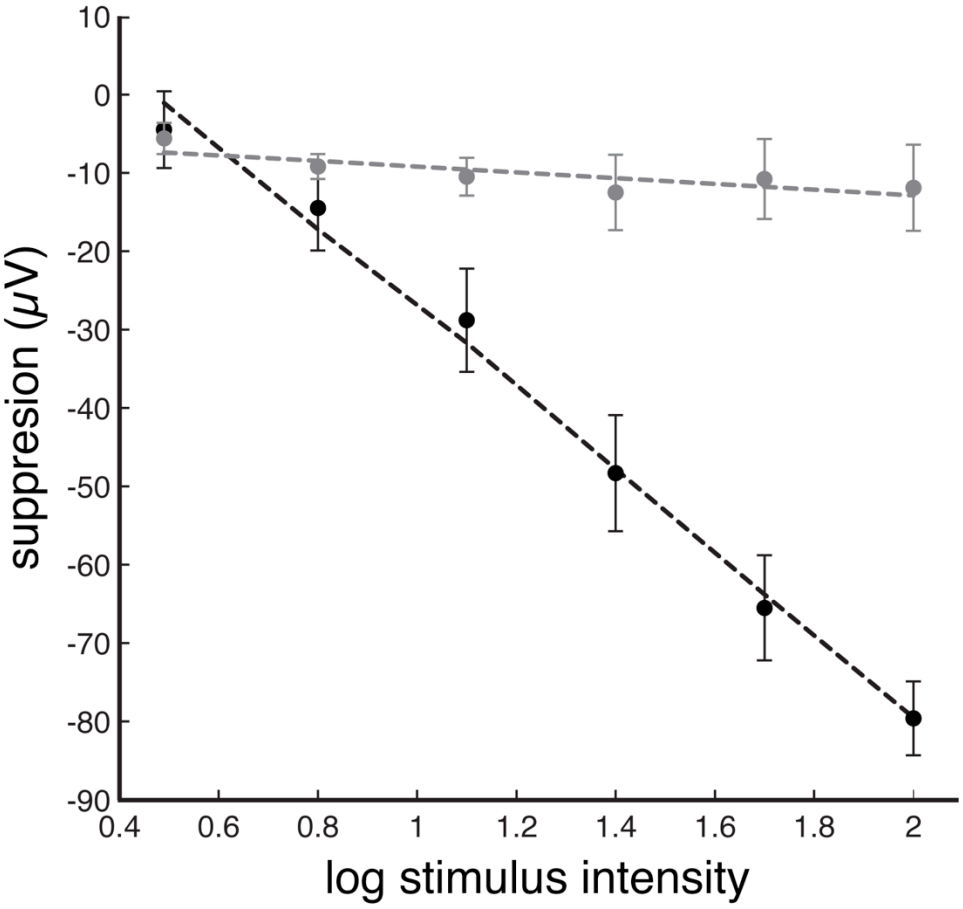
10
0
-10
-20
-30
-40
-50
-60
-70
-80
-90
suppresion (μV)
0.4
0.6
0.8
1
1.2
1.4
1.6
1.8
2
log stimulus intensity

Since the M photopigment ERGs were obtained a few seconds after the presentation of the 365 nm light, the suppression appeared to be the result of a prolonged light adaptation of cones in response to the short wavelength light exposure. If so, this time course of recovery must differ from that of M/L cones, which has previously been shown to occur more quickly. To investigate the relative time courses of recovery after exposure to S photopigment vs. M photopigment stimuli, ERG light responses were collected from wildtype mice (n=5) that had not been exposed to the 365 nm stimulus. A 1 Hz 520 nm stimulus was presented continuously for 33 seconds and measurements of responses to single flashes were made after cycles 1, 3, 13, and 33. After the 33 seconds, response were probed with single flashes at 43, 63, ad 93 seconds. The ERG after the 33rd cycle was decreased by 7.2%±3.2 (paired t-test, $p<0.05$) in comparison to the baseline response after cycle 1, and the responses remained stably suppressed throughout the single flash trials (**Figure 26**).

Next, the same mice were then presented with the S photopigment stimulating light according to the same schedule and the ERGs were measured as before. In contrast to the effect of the 520 nm light, the ERG after the 33rd cycle of 365 nm light was decreased by 53.7% ± 2.2 (paired t-test, $p<0.0005$) in comparison to the 1st cycle (Figure 26). The recovery was, thus, slower from 365 nm flashes, but the response did return to baseline within 10 seconds of stimulation ceasing. However, even the after the response to the 365 nm light stimulation had recovered almost completely, M photopigment sensitivity was still decreased by ~40% (data not shown), as observed in the previous experiments.

***Figure 26*. S-opsin inactivation is slow compared to M-opsin inactivation.** Retinal responses to M photopigment and S photopigment-isolating stimuli were measured using the 1 Hz On-Off ERG in wildtype mice (n=5). The entire M photopigment isolating condition (black symbols) was carried out first, followed by the S photopigment-isolating condition (gray symbols). In each condition, the first 33 stimulation cycles were presented continuously (denoted by lines) with measurements taken after cycles 1, 3, 13, and 33. Single flash measurements were then taken at 43, 63, and 93 seconds.

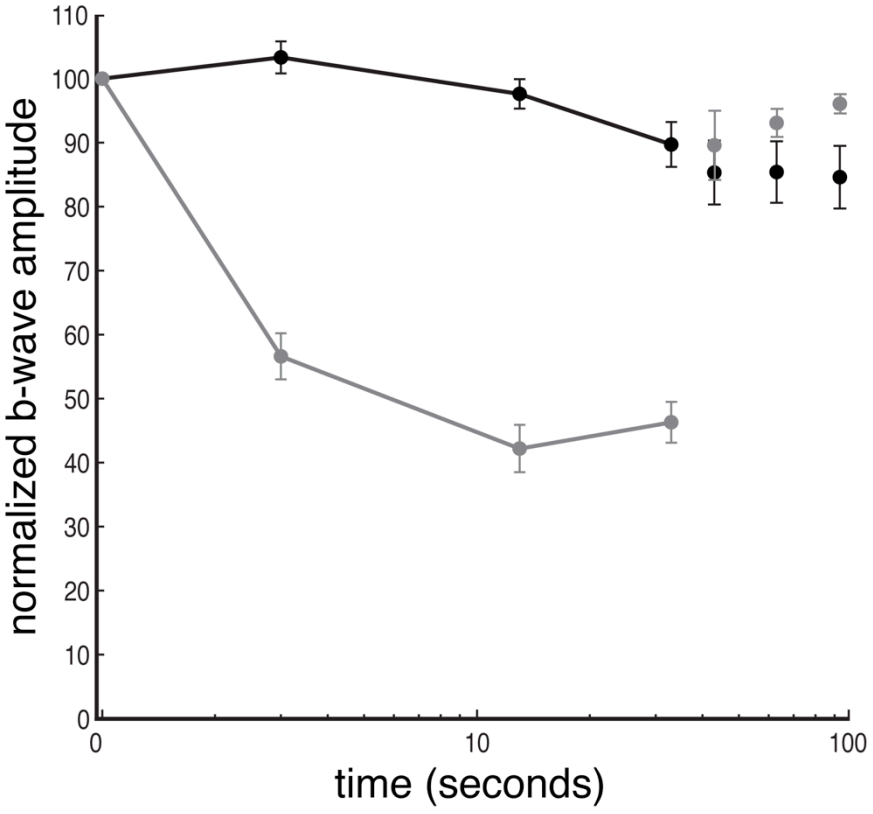
normalized b-wave amplitude
110
100
90
80
70
60
50
40
30
20
10
0
0
10
100
time (seconds)

In order determine whether the M photopigment response would return to baseline within a short period of time, an additional intensity response function was acquired fifteen minutes after the presentation of the 365 nm light in both mouse lines (n=4 per line). At fifteen minutes post-short wavelength exposure, the M photopigment response in the wildtype mouse had not fully recovered. For instance, at the 11.8 $\mu W/mm^2$ intensity, the M photopigment response immediately following 365 nm light stimulation was decreased by 38.9%±3.9 ($p<0.001$) compared to baseline, and the response after 15 minutes still showed a reduction of 31.9%±2.4 (paired t-test, $p<0.001$). Under the identical conditions, the M photopigment ERGs from the *Opn1sw*$^{-/-}$ mice were initially suppressed by 9.3%±2.5 (paired t-test, $p<0.05$), but after fifteen minutes, the responses were statistically equivalent to baseline (**Figure 27**).

Finally, retinal responses in four human subjects were measured using the full-field ERG. As in the mouse experiments, M photopigment responses to a 525 nm light were recorded immediately before and after a 10 second exposure to a human S photopigment activating light (414 nm). M cone sensitivity was not modulated by previous activation of the S cones in these subjects (paired t-test, $p>0.35$). The averaged ERGs from the four subjects are shown in **Figure 28**, where all pre-S data were normalized according to Subject 1's b-wave amplitude and the scale factor for each subject was applied to post-S data. Raw data is presented in **Table 8**.

Figure 27. **Recovery of the M photopigment response is slow in the wildtype mouse.** Responses to three M photopigment-isolated intensity response series (520 nm stimulus presented at intensities ranging from 0.4 μW/mm^2 to 11.8 μW/mm^2) were collected from four wildtype mice (**top panel**) and four *Opn1sw*$^{-/-}$ mice (**bottom panel**). The first series was presented immediately prior to 10 seconds of 365 nm light exposure (dark, solid traces), the second series was presented immediately after the short wavelength light exposure (lighter, evenly dashed traces), and the third series was presented fifteen minutes after the short wavelength light exposure (lightest, dotted trace). After fifteen minutes, sensitivity to M photopigment-isolating light had not recovered in the wildtype mice.

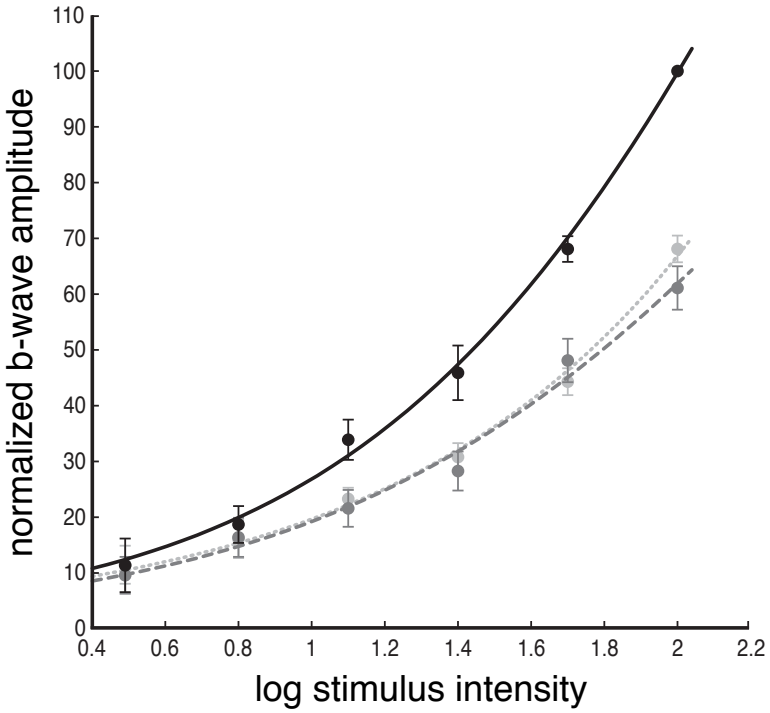
normalized b-wave amplitude
log stimulus intensity
0
10
20
30
40
50
60
70
80
90
100
110
0.4
0.6
0.8
1
1.2
1.4
1.6
1.8
2
2.2

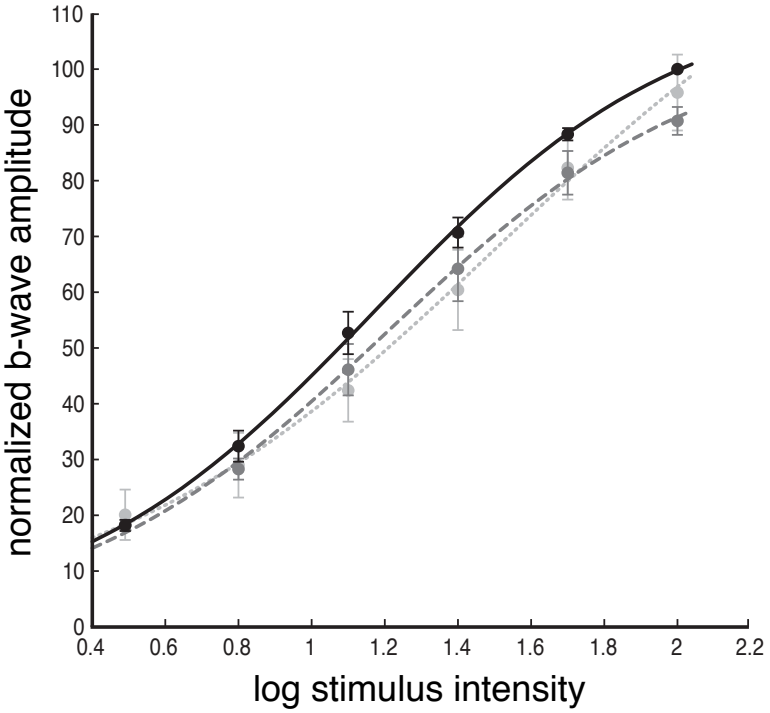
normalized b-wave amplitude
log stimulus intensity
0
10
20
30
40
50
60
70
80
90
100
110
0.4
0.6
0.8
1
1.2
1.4
1.6
1.8
2
2.2

Figure 28. **Human M cone response is not modulated by exposure to short wavelength light.** Responses to an M photopigment stimulus (525 nm) measured in four subjects immediately before (black trace) and after (gray trace) 10 seconds of exposure to an S photopigment stimulus (414 nm) were the same. All pre-S data were normalized to Subject 1's b-wave, and the scale factor for each subject was applied to the post-S data. Error bar represents the SEM.

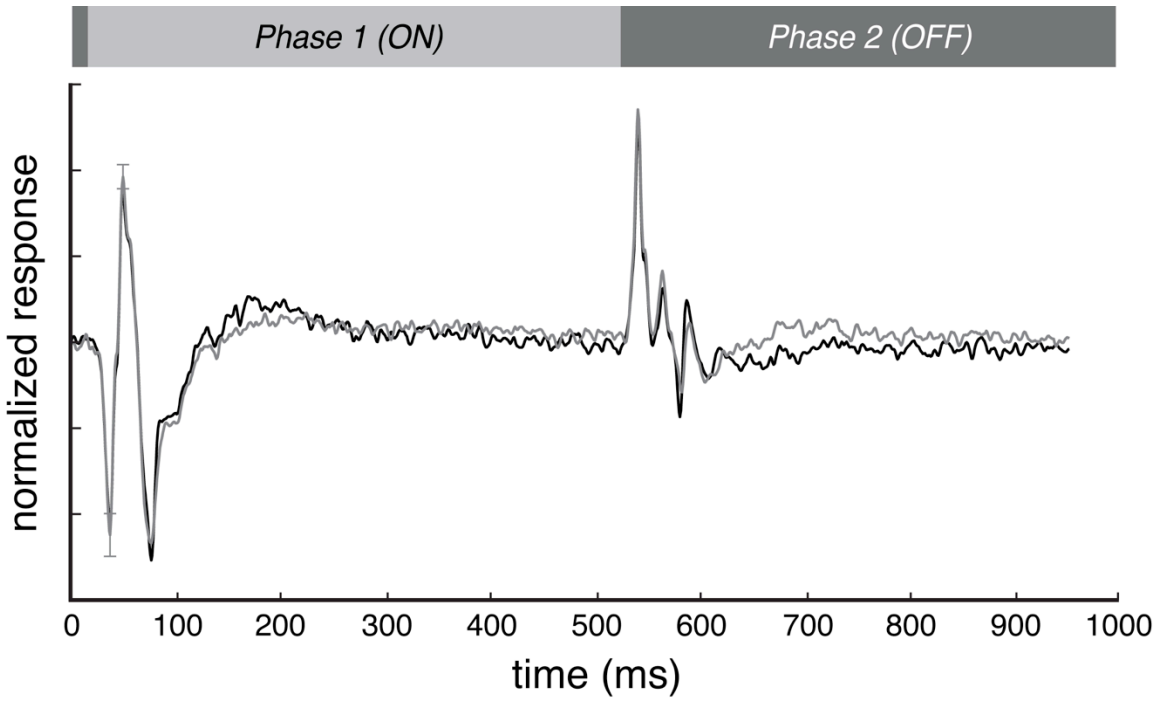
Phase 1 (ON)
Phase 2 (OFF)
normalized response
0
100
200
300
400
500
600
700
800
900
1000
time (ms)

Table 8. **Human M cone response is not modulated by exposure to short wavelength light.** Comparisons of M/L cone responses immediately before (pre-S) and after (post-S) 414 nm light exposure in four human subjects.

	Sex	Age	M/L response Pre-S (μV)	M/L response Post-S (μV)	Change (μV)	Change (%)
Subject 1	F	27	57.6	58.0	0.4	0.7
Subject 2	M	34	42.3	47.3	5.0	10.6
Subject 3	F	23	41.5	41.6	0.1	0.2
Subject 4	M	31	35.5	35.1	-0.4	-1.1
Average			**44.2**	**45.5**	**1.3**	**2.6**
SEM			*4.7*	*4.9*	*1.3*	*2.7*

Discussion

Historically, two competing hypotheses have been proposed to explain dark adaptation. 1) The photochemical hypothesis: The process of dark adaptation is controlled by the concentration of a substance in the receptors. 2) The equivalent-background hypothesis: The effect of a given state of adaptation following bleaching is identical to that produced by some stabilized background of light with the same spatial configuration as the bleaching field. More specifically, a circulating current persists in the photoreceptors after the stimulating light has been extinguished that cannot be distinguished from the effects of activated opsin. This "dark light" is thought to be generated by continued activation of transducin by components of formerly bleached photopigment. While the photopigment is recovering in the dark, the photoreceptor behaves as it would in the presence of a background light: the light response is accelerated and reduced in size so as to extend the range of intensities over which the photoreceptors operate. After being exposed to an actual background light, it takes some time for the magnitude of the light response to recover to the dark adapted state.

Although many experiments on rod vision favor the equivalent background hypothesis, considerably less is known about light adaptation in cones. Because the majority of cones in the mouse retina contain both S and M photopigments, separating the role of bleaching in light adaption compared to dampening of the signal from a reduction in response produced by dark light is possible. Moreover, since S cones are known to dark adapt more slowly than M cones (Norren & Padmos, 1974), previously activated S-opsin should dampen retinal responses to M photopigment activating stimuli even when none of the M photopigment is bleached. Here, to test this prediction, ERGs were measured in response to an M photopigment-isolating stimulus in wildtype mice, both before and after ten seconds of exposure to an S photopigment activating light. Consistent with the prediction, a 10 second presentation of an S photopigment activating light suppressed the subsequent M photopigment responses to an 11.8 $\mu W/mm^2$ light by ~40%,

independent of age. These results in wildtype mice were compared to those of *Opn1sw*$^{-/-}$ mice and human subjects in which each cone expressed no more than a single class of photopigment. Individual cones in the *Opn1sw*$^{-/-}$ mice exclusively expressed the M photopigment and those of the human subjects only contained either the M or L photopigment. In comparison to the wildtype mice, the *Opn1sw*$^{-/-}$ mice showed a small decrease in the M photopigment response after exposure to the S photopigment activating stimulus and the humans subjects' M photopigment responses were unaffected. Thus, as predicted, the presentation of short-wavelength light had little impact on the M photopigment response in either *Opn1sw*$^{-/-}$ mice or human subjects.

The desensitization observed in the wildtype mouse line scaled logarithmically with the intensity of the M photopigment stimulation test light. This indicates that the threshold for generating a retinal response to an external stimulus is not so much raised in the photoreceptors, but rather that the dynamic range of the response amplitude is compressed in a manner consistent with the functional role of light adaptation extending the operating range of the cone photoreceptors. While cones do not saturate even when the background illumination is increased by 6-7 log units (Perlman, 1998), a high intensity stimulus will drive a response that is limited by the reduced gain of the system.

The adaptation state of a cone and the time-course of recovery is determined by the class(es) of opsin present. As has been proposed for rhodopsin, it is reasoned here that bleached S photopigments, being slow to regenerate, create "dark light" by protractedly activating the phototransduction cascade and consequently reducing the cone response. Together, the data collected from mouse and human show that exposure to short wavelength light greatly suppresses the M-response only when cones contain both S and M photopigments. This suggests that light adaptation is a feature conferred on the photoreceptor by the complement of photopigment that is present.

References

Angel, T., Gupta, S., Jastrzebska, B., Palczewski, K. & Chance, M. (2010). Structural waters define a functional channel mediateing activation of the GPCR, rhodopsin. *Proc. Natl. Acad. Sci. USA* 106, 14367-14372.

Applebury, M.L., Antoch, M.P., Baxter, L.C., Chun, L.L.Y., Kalk, J.D., Farhangfar, F., Kage, K., Krzystolik, M.G., Lyass, L.A. & Robbins, J.T. (2000). The murine cone photoreceptor: A single cone type expresses both S and M opsins with retinal spatial patterning. Neuron 27, 513-523.

Asenjo, A.B., Rim, J. & Oprian, D.D. (1994). Molecular determinants of human red/green color discrimination. Neuron 12, 1131-1138.

Barlow, H. B. (1956). Retinal noise and absolute threshold. *J Opt Soc Am, 46*(8), 634-639.

Barlow, H. B. (1964). Dark-adaptation: a new hypothesis. *Vision Res, 4*(1), 47-58.

Burns, M. E., & Baylor, D. A. (2001). Activation, deactivation, and adaptation in vertebrate photoreceptor cells. *Annu Rev Neurosci, 24*, 779-805.

Bush, R.A. & Sieving, P.A. (1996). Inner retinal contributions to the primate photopic fast flicker electroretinogram. *J Opt Soc Am A Opt Image Sci Vis* 13, 557-565.

Carroll, J., Dubra, A., Gardner, J.C., Mizrahi-Meissonnier, L., Cooper, R.F., Dubis, A.M., Nordgren, R., Genead, M., Connor, T.B., Jr., Stepien, K.E., Sharon, D., Hunt, D.M., Banin, E., Hardcastle, A.J., Moore, A.T., Williams, D.R., Fishman, G., Neitz, J., Neitz, M. & Michaelides, M. (2012). The effect of cone opsin mutations on retinal structure and the integrity of the photoreceptor mosaic. Invest Ophthalmol Vis Sci 53, 8006-8015.

Carroll, J., McMahon, C., Neitz, M. & Neitz, J. (2000). Flicker-photometric electroretinogram estimates of L : M cone photoreceptor ratio in men with photopigment spectra derived from genetics. *Journal of the Optical Society of America A* 17, 499-509.

Carroll, J., Neitz, M., Hofer, H., Neitz, J. & Williams, D.R. (2004). Functional photoreceptor loss revealed with adaptive optics: An alternate cause of color blindness. Proceedings of the National Academy of Sciences of the United States of America 101, 8461-8466.

Crognale, M.A., Fry, M., Highsmith, J., Haegerstrom-Portnoy, G., Neitz, J., Neitz, M. & Webster, M.A. (2004). Characterization of a novel form of X-linked incomplete achromatopsia. Visual Neuroscience 21, 197-204.

Dacey, D.M. & Packer, O.S. (2003). Colour coding in the primate retina: diverse cell types and cone-specific circuitry. *Current Opinion in Neurobiology* 13, 421-427.

Daniele, L. L., Insinna, C., Chance, R., Wang, J., Nikonov, S. S., & Pugh, E. N. (2011). A mouse M-opsin monochromat: retinal cone photoreceptors have increased M-opsin expression when S-opsin is knocked out. *Vision Res, 51*(4), 447-458.

Detwiler, P. B., & Gray-Keller, M. P. (1996). The mechanisms of vertebrate light adaptation: speeded recovery versus slowed activation. *Curr Opin Neurobiol, 6*(4), 440-444.

Dowling, J. E. (1960). Chemistry of visual adaptation in the rat. *Nature, 188*, 114-118.

Drummond-Borg, M., Deeb, S.S. & Motulsky, A.G. (1989). Molecular patterns of X-chromosome-linked color genes among 134 men of European ancestry. *Proceedings of the National Academy of Sciences of the United States of America* 86, 983-987.

Fain, G. L., Matthews, H. R., Cornwall, M. C., & Koutalos, Y. (2001). Adaptation in vertebrate photoreceptors. *Physiol Rev, 81*(1), 117-151.

Firsov, M. L., Golobokova, E. Y., & Govardovskii, V. I. (2007). Two-stage quenching of cone phototransduction cascade (Vol. 21, pp. 55-59). Sensory Systems.

Fliesler, S.J., & Basinger, S.F. (1985). Tunicamycin blocks the incorporation of opsin into retinal rod outer segment membranes. *Proceedings of the National Academy of Sciences of the United States of America.* 82(4), 1116-1120.

Grabowski, S. R., & Pak, W. L. (1975). Intracellular recordings of rod responses during dark-adaptation. *J Physiol, 247*(2), 363-391.

Granit, R., Holmberg, T., & Zewi, M. (1938). On the mode of action of visual purple on the rod cell. *J Physiol, 94*(3), 430-440.

Green, D.G. (1972). Visual acuity in the blue cone monochromat. *J. Physiology* 222, 419-426.

Haim, M., Fledelius, H.C. & Skarsholm. (1988). X-linked myopia in Danish family. *Acta Ophthalmologica Copenhagen* 66, 450-456.

Haverkamp, S., Wassle, H., Duebel, J., Kuner, T., Augustine, G.J., Feng, G. & Euler, T. (2005). The primordial, blue-cone color system of the mouse retina. Journal of Neuroscience 25, 5438-5445.

Hecht, S., Haig, C., & Chase, A. M. (1937). The influence of light adaptation on subsequent dark adapation of the eye. *J Gen Physiol, 20*(6), 831-850.

Hofer, H., Carroll, J., Neitz, J., Neitz, M. & Williams, D.R. (2005). Organization of the human trichromatic cone mosaic. *Journal of Neuroscience* 25, 9669-9679.

Jastrzebska, B., Palczewski, K. & Golczak, M. (2011). Role of bulk water in hydrolysis of the rhodopsin chromophore. *J Biol Chem* 286, 18930-18937.

Kainz, P. M., Neitz, M., & Neitz, J. (1997). Molecular detection of female carriers of protan color vision defects. *Investigative Ophthalmology & Visual Science (Supplement), 38*, S1015.

Kosower, E.M. (1988). Assignment of groups responsible for the "opsin shift" and light absorption of rhodopsin and red, green, and blue iodopsins (cone pigments). *Proceedings of the National Academy of Sciences of the United States of America* 85, 1076-1080.

Kuwayama, S., Imai, H., Morizumi, T., & Shichida, Y. (2005). Amino acid residues responsible for the meta-III decay rates in rod and cone visual pigments. *Biochemistry, 44*(6), 2208-2215.

Lamb, T. D., & Pugh, E. N. (2004). Dark adaptation and the retinoid cycle of vision. *Prog Retin Eye Res, 23*(3), 307-380.

Leibrock, C. S., Reuter, T., & Lamb, T. D. (1994). Dark adaptation of toad rod photoreceptors following small bleaches. *Vision Res, 34*(21), 2787-2800.

Leibrock, C. S., Reuter, T., & Lamb, T. D. (1998). Molecular basis of dark adaptation in rod photoreceptors. *Eye (Lond), 12 (Pt 3b)*, 511-520.

Lem, J., Krasnoperova, N. V., Calvert, P. D., Kosaras, B., Cameron, D. A., Nicolò, M., Makino, C. L., & Sidman, R. L. (1999). Morphological, physiological, and biochemical changes in rhodopsin knockout mice. *Proceedings of the National Academy of Sciences of the United States of America* 96, 736-741.

Matthews, H. R., Murphy, R. L., Fain, G. L., & Lamb, T. D. (1988). Photoreceptor light adaptation is mediated by cytoplasmic calcium concentration. *Nature, 334*(6177), 67-69.

Matthews, R.G., Hubbard, R., Brown, P.K., & Wald, G. (1963). Tautomeric forms of metarhodopsin. *J Gen Physiol, 47*, 215-240.

McClements, M., Davies, W.I., Michaelides, M., Carroll, J., Rha, J., Mollon, J.D., Neitz, M., Maclaren, R.E., Moore, A.T. & Hunt, D.M. (2013a). X-linked cone dystrophy and colour vision deficiency arising from a missense mutation in a hybrid L/M cone opsin gene. *Vision Res*.

McClements, M., Davies, W.I., Michaelides, M., Young, T., Neitz, M., Maclaren, R.E., Moore, A.T. & Hunt, D.M. (2013b). Variations in opsin coding sequences cause X-linked cone dysfunction syndrome with myopia and dichromacy. Invest Ophthalmol Vis Sci.

Merbs, S.L. & Nathans, J. (1993). Role of hydroxyl-bearing amino acids in differentially tuning the absorption spectra of the human red and green cone pigments. Photochemistry and Photobiology 58, 706-710.

Mizrahi-Meissonnier, L., Merin, S., Banin, E. & Sharon, D. (2010). Variable retinal phenotypes caused by mutations in the X-linked photopigment gene array. Investigative Ophthalmology and Visual Science 51, 3884-3892.

Monod, J., Changeux, J.P., & Jacob, F. (1963). Allosteric proteins and cellular control systems. *J Mol Biol, 6*, 306-329.

Nakatani, K., & Yau, K. W. (1988). Calcium and light adaptation in retinal rods and cones. *Nature, 334*(6177), 69-71.

Nathans, J., Piantanida, T.P., Eddy, R.L., Shows, T.B. & Hogness, D.S. (1986a). Molecular genetics of inherited variation in human color vision. *Science* 232, 203-210.
Nathans, J., Thomas, D. & Hogness, D.S. (1986b). Molecular genetics of human color vision: the genes encoding blue, green, and red pigments. *Science* 232, 193-202.

Neitz, J. & Neitz, M. (2011). The Genetics of Normal and Defective Color Vision. *Vision Research* 51, 633-651.

Neitz, J., Neitz, M. & Jacobs, G.H. (1989). Analysis of fusion gene and encoded photopigment of colour-blind humans. Nature 342, 679-682.

Neitz, M., Neitz, J. & Jacobs, G.H. (1991). Spectral tuning of pigments underlying red-green color vision. Science 252, 971-974.

Neitz, M., Neitz, J., & Jacobs, G. H. (1995). Genetic basis of photopigment variations in human dichromats. *Vision Research, 35*, 2095-2103.

Neitz, J., Neitz, M. & Kainz, P.M. (1996). Visual pigment gene structure and the severity of human color vision defects. *Science* 274, 801-804.

Neitz, M., Carroll, J., Renner, A., Knau, H., Werner, J.S. & Neitz, J. (2004). Variety of genotypes in males diagnosed as dichromatic on a conventional clinical anomaloscope. Visual Neuroscience 21, 205-216.

Norren, D. V., & Padmos, P. (1974). Dark adaptation of separate cone systems studied with psychophysics and electroretinography. *Vision Res, 14*(8), 677-686.

Okada, T., Sugihara, M., Bondar, A.N., Elstner, M., Entel, P. & Buss, V. (2004). The retinal conformation and its environment in rhodopsin in light of a new 2.2 angstrom crystal structure. *J. Mo. Biol.* 342, 571-583.

Orban, T., Gupta, S., Palczewski, K. & Chance, M. (2010). Visualizing water molecules in transmembrane proteins using radiolytic labeling methods. *Biochemistry* 49, 827-834.

Papermaster, D.S., & Dreyer, W.J. (1974). Rhodopsin content in the outer segment membranes of bovine and frog retinal rods. *Biochemistry.* 13(11), 2438-2444.

Pauers, M., Kuchenbecker, J., Neitz, M. & Neitz, J.. (2012). Changes in the colour of light cue circadian activity. *Animal Behavior* 83, 1143-1151.

Pepperberg, D. R., Brown, P. K., Lurie, M., & Dowling, J. E. (1978). Visual pigment and photoreceptor sensitivity in the isolated skate retina. *J Gen Physiol, 71*(4), 369-396.

Perlman, I. & Normann, RA. (1998). Light adaptation and sensitivity controlling mechanisms in vertebrate photoreceptors. Prog. Retin Eye Res. 17(4), 523-563.

Pokorny, J., Smith, V.C. & Lutze, M. (1987). Aging of the human lens. *Applied Optics* 26, 1437-1440.

Pugh, E. N., Nikonov, S., & Lamb, T. D. (1999). Molecular mechanisms of vertebrate photoreceptor light adaptation. *Curr Opin Neurobiol, 9*(4), 410-418.

Radhakrishna, U., Lysle, R., Raval, R., Blouin, J.L., Singh, R., Patel, J.V.U.C., Solanki, J.V., Morris, M.A., Himabindu, V., Vattalarao, S., Uppala, R. & Antonarakis, S.E. (2005). The 'X-linked" severe form of myopia locus at Xq28 (MYP1): Narrowing of the critical region and exclusion of twelve known genes localized in the interval. *Investigative Ophthalmology & Visual Science* supplement (abstract #3814).

Ratnamala, U., Lyle, R., Rawal, R., Singh, R., Vishnupriyz, S., Himabindu, P., Rao, V., Aggarwal, S., Paluru, P., Bartoloni, L., Young, T., Paoloni-Giacobina, A., Morris, M., Nath, S., Antonarakis, S. & Radhakrishna, U. (2011). Refinement of the X-linked nonsyndromic high-grade myopia locus MYP1 on Xq28 and exclusion of 13 known positional candidate genes by direct sequencing. *Invest Ophthalmol Vis Sci* 52, 6814-6819.

Reuter, T. (2011). Fifty years of dark adaptation 1961-2011. *Vision Res, 51*(21-22), 2243-2262.

Röhlich, P., van Veen, T. & Szél, Á. (1994). Two different visual pigments in one retinal cone cell. Neuron 13, 1159-1166.

Rushton, W. A. (1961). Dark-adaptation and the regeneration of rhodopsin. *J Physiol, 156*, 166-178.

Schneider, C.A., Rasband, W.S. & Eliceiri, K.W. (2012). NIH Image to ImageJ: 25 years of image analysis. *Nat Methods* 9, 671-675.

Schwartz, M., Haim, M. & Skarsholm, D. (1990). X-linked myopia: Bornholm eye disease. Linkage to DNA markers on the distal part of Xq. *Clinical Genetics* 38, 281-286.

Smallwood, P.M., Olveczky, B.P., Williams, G.L., Jacobs, G.H., Reese, B.E., Meister, M. & Nathans, J. (2003). Genetically engineered mice with an additional class of cone photoreceptors: implications for the evolution of color vision. *Proceedings of the National Academy of Sciences of the United States of America* 100, 11706-11711.

Szél, Á., Röhlich, P., Mieziewska, K., Aguirre, G. & van Veen, T. (1993). Spatial and temporal differences between the expression of short- and middle-wave sensitive cone pigments in the mouse retina: A developmental study. The Journal of Comparative Neurology 331, 564-577.

Ueyama, H., Muraki-Oda, S., Yamade, S., Tanabe, S., Yamashita, T., Shichida, Y. & Ogita, H. (2012). Unique haplotype in exon 3 of cone opsin mRNA affects splicing of its precursor, leading to congenital color vision defect. *Biochem Biophys Res Commun* 424, 152-157.

Verrelli, B. C., & Tishkoff, S. A. (2004). Signatures of selection and gene conversion associated with human color vision variation. *American Journal of Human Genetics, 75*, 363-375.

Vogel, R., Mahalingam, M., Ludeke, S., Huber, T., Siebert, F. & Sakmar, T. (2008). Functional role of the "ionic lock"--an interhelical hydrogen-bond network in family A heptahelical receptors. *J. Mol BIoil* 380, 648-655.

Wagner-Schuman, M., Neitz, J., Rha, J., Williams, D. R., Neitz, M., & Carroll, J. (2010). Color-deficient cone mosaics associated with Xq28 opsin mutations: a stop codon versus gene deletions. *Vision Research, 50*, 2396-2402.

Wald, G. (1954). On the mechanism of the visual threshold and visual adaptation. *Science, 119*(3104), 887-892.

Wald, G. (1955). The photoreceptor process in vision. *Am J Ophthalmol, 40*(5 Part 2), 18-41.

Wald, G., Brown, P.K., Gibbons, I.R. (1963). The problem of visual excitation. *Journal of the Optical Society of America.* 53, 20-35.

Williams, G.A. & Jacobs, G.H. (2007). Cone-based vision in the aging mouse. *Vision Res* 47, 2037-2046.

Winderickx, J., Battisti, L., Hibibya, Y., Motulsky, A.G. & Deeb, S.S. (1993). Haplotype diversity in the human red and green opsin genes: evidence for frequent sequence exchange in exon 3. *Human Molecular Genetics* 2, 1413-1421.

Winderickx, J., Battisti, L., Motulsky, A.G. & Deeb, S.S. (1992). Selective expression of human X chromosome-linked green opsin genes. *Proceedings of the National Academy of Sciences of the United States of America* 89, 9710-9714.

Xu, J., Pokorny, J. & Smith, V.C. (1997). Optical density of the human lens. *Journal of the Optical Society of America A* 14, 953-960.

Yamaguchi, T., Motulsky, A.G. & Deeb, S.S. (1997). Visual pigment gene structure and expression in the human retinae. *Human Molecular Genetics* 6, 981-990.

Young, T.L., Deeb, S.S., Ronan, S.M., Dewan, A.T., Alvear, A.B., Scavello, G.S., Paluru, P.C., Brott, M.S., Hayashi, T., Holleschau, A.M., Benegas, N., Schwartz, M., Atwood, L.D., Oetting, W.S., Rosenberg, T., Motulsky, A.M. & King, R.A. (2004). X-linked high myopia associated with cone dysfunction. *Archives of Ophthalmology* 122, 897-908.